Winter 2002

# Nitric oxide reduction by non-thermal plasma and catalysis

Zhongyuan Chen
*University of New Hampshire, Durham*

# INFORMATION TO USERS

This manuscript has been reproduced from the microfilm master. UMI films the text directly from the original or copy submitted. Thus, some thesis and dissertation copies are in typewriter face, while others may be from any type of computer printer.

**The quality of this reproduction is dependent upon the quality of the copy submitted.** Broken or indistinct print, colored or poor quality illustrations and photographs, print bleedthrough, substandard margins, and improper alignment can adversely affect reproduction.

In the unlikely event that the author did not send UMI a complete manuscript and there are missing pages, these will be noted. Also, if unauthorized copyright material had to be removed, a note will indicate the deletion.

Oversize materials (e.g., maps, drawings, charts) are reproduced by sectioning the original, beginning at the upper left-hand corner and continuing from left to right in equal sections with small overlaps.

ProQuest Information and Learning
300 North Zeeb Road, Ann Arbor, MI 48106-1346 USA
800-521-0600

# NITRIC OXIDE REDUCTION BY NON-THERMAL PLASMA AND CATALYSIS

BY

ZONGYUAN CHEN

B.S. Tsinghua University, China, 1986
M.S. Tsinghua University, China, 1991

DISSERTATION

Submitted to the University of New Hampshire
in Partial Fulfillment of
the Requirement for the Degree of

Doctor of Philosophy

in

Engineering: Chemical

December, 2002

ProQuest Information and Learning Company
300 North Zeeb Road
P.O. Box 1346
Ann Arbor, MI 48106-1346

This dissertation has been examined and approved.

Virendra K. Mathur

Dissertation Director, Dr. Virendra K. Mathur
Professor of Chemical Engineering

Stephen S.T. Fan

Dr. Stephen S.T. Fan, Professor of Chemical Engineering

Gupta

Dr. Nivedita Gupta, Assistant Professor of Chemical Engineering

Joseph Paterno

Dr. Joseph Paterno, Affiliate Professor

Christopher R McLarnon

Dr. Christopher R. McLarnon, Director of Research and Development, Powerspan Corporation

Dec 11th, 2002

Date

Dedicated to my parents and wife

whose expectation, encouragement and support made this work possible.

## ACKNOWLEDGEMENTS

I would like to express my deepest gratitude and thanks to Professor V.K. Mathur for his guidance, experience and inspiration in directing the work presented in this dissertation. Thanks are also due to Professors Stephen S.T. Fan, Nivedita Gupta, Joseph Paterno and Dr. Christopher R. McLarnon for examining and improving this dissertation.

I would like to thank Dr. Christopher R. McLarnon and Ms. Claire Golden for their valuable advice and assistance to my experimental work of this study. Special thanks are owed to Professor Sterling A. Tomellini for his help in instrumentation. Thanks are also due to senior student James R. Carleton who helped conduct the dielectric constant measurement of barrier materials. Thanks also go to Mr. Jonathan Newell, who gave me a great amount of assistance in the assembly and maintenance of my apparatus. I would also like to express my appreciation to Ms. Nancy Littlefield for the administrative work done to support the completion of this study.

Finally, I would like to acknowledge to the Department of Chemical Engineering, UNH, whose financial support has been of great assistance.

## TABLE OF CONTENTS

## LIST OF TABLES

## LIST OF FIGURES

## ABSTRACT

NITRIC OXIDE REDUCTION BY NON-THERMAL PLASMA AND CATALYSIS

by

Zongyuan Chen

University of New Hampshire, December 2002

Combustion of fossil fuels produces millions of tons of air pollutants such as $NO_x$ and $SO_2$. The high cost and operating difficulties of prevailing selective catalytic reduction(SCR) process are driving R&D efforts towards alternative technologies and modifications to the SCR technology. Non-thermal plasma technique has been found to be one of the most promising technologies for $NO_x$ removal.

In the present study, a non-thermal plasma technique in the form of dielectric barrier discharge(DBD) has been extensively investigated for the removal of $NO_x$. The main variables including electrical parameters, chemical compounds and flow conditions are identified and studied in terms of their effects on $NO/NO_x$ conversions. Significant increases in $NO/NO_x$ conversions of 90% and 40% are observed in the presence of both $O_2$ and $H_2O$ than in the presence of either $O_2$ or $H_2O$ alone. Addition of 1000 ppm ethylene to the $NO/O_2/CO_2/N_2$ mixture almost promotes 100% NO oxidation to $NO_2$. The chemistry of plasma reactions is discussed. The DBD system is found to be effective for NO oxidization into $NO_2$ and $HNO_3$. Kinetics studies have also been made for $NO\text{-}O_2$ reaction under plasma conditions. A rate equation has been proposed, $-d[NO]/dt = k_p$

$[NO]^{1/2}[O_2]^{1/2}$ with $k_p$=0.0143exp(-1865/$E_d$) showing that a reaction can be initiated at much lower activation energy under plasma conditions.

A hybrid plasma-catalyst(P-C) system has been developed to achieve the synergy. $\gamma$-$Al_2O_3$ and laboratory-prepared tungsten catalysts have been used in the hybrid P-C experiments. The improvement in $NO_x$ removal by the P-C system is about 15% compared to by the SCR alone when 1000-3000 ppm of methane or ethylene is added to the inlet gas stream. There is no formation of $N_2O$(greenhouse gas) in the P-C system when inlet gas contains moisture or ethylene. DBD reactor design parameters have also been investigated in terms of $SO_2$ oxidation to $SO_3$ with respect to reactor geometry, dielectric material and thickness.

The DBD technique has the great potential to replace the prevailing combined SCR and flue gas disulfurization(FGD) processes both technically and economically. The P-C system has the potential to be used for the removal of $NO_x$ from diesel engine exhausts.

# CHAPTER I

## INTRODUCTION

The U.S. Environmental Protection Agency's (EPA) most recent evaluation of status and trends of national air quality shows that the emissions of nitrogen oxides ($NO_x$) have increased almost 20% between 1970 and 2000 (EPA 2001a). The emissions of other principal pollutants (volatile organic compounds, $SO_2$, particulate matter, CO and Pb) have decreased significantly in the same period. Of the six tracked pollutants, improvement of ground-level ozone has been the least. Much of this ozone trend is due to increased emissions of $NO_x$, which have been well identified as a major contributor to acid rain and haze. These emissions pose potentially serious environmental and public health impacts. The growth in emissions from non-road engines, diesel vehicles and power plants accounts for most of the increase in $NO_x$ emissions.

Both natural and anthropogenic (man-made) processes contribute to the $NO_x$ levels. Anthropogenic emissions outweigh natural contributions such as lightning and the chemical transformation of nitrous oxide ($N_2O$) in the stratosphere. Therefore, emissions of $NO_x$ are generally referred to as anthropogenic processes. It is estimated that the total emissions of $NO_x$ in the United States for 1998 and 2000 are about 24.454 and 25.115 million tons, respectively. European Environmental Agency (EEA) reports that the total emissions of $NO_x$ for 1998 are about 14.3 million tons in the 18 EEA member countries (15 EU Member States and Liechtenstein, Switzerland and Iceland) and 13 PHARE

Central and Eastern European countries (EEA 1999). $NO_x$ emissions in China increased from 8.4 million tons in 1990 to 11.18 million tons in 1998 (Hao and others 2001).

The amounts of emissions of $NO_x$ associated with fuel combustion in the United States are given in Table 1.1 (EPA 2000). The total amount of emissions of $NO_x$ from the combustion of fossil fuel is 23.234 million tons, accounting for 95% of total anthropogenic emissions for 1998. Power plants contribute about one quarter of the total emissions of $NO_x$. Since the wide application of three-way converters to the automobile exhaust systems in 1980s, $NO_x$ emissions from gasoline-engine automobiles have been significantly reduced. However, the $NO_x$ emissions from on-road vehicles still account for one third of the total partly because of no control for the diesel engine exhausts. Diesel engines contribute 23.6% of the total emissions of $NO_x$. The emissions from power plants have long been the focus of regulation due to stationary nature and large unit scale in comparison with mobile and small unit-scale sources such as automobiles, trains and ships.

**Table 1.1**

**Emissions of $NO_x$ for Energy Production in U.S. (1998)**

| Emissions of $NO_x$ | Fuel combustion, electrical power plants | Fuel combustion, industrial | Fuel combustion, others | On-road vehicles | Non-road engines and vehicles | Total |
|---|---|---|---|---|---|---|
| Amounts, million tons | 6.103 | 2.969 | 1.117 | 7.765 | 5.280 | 23.234 |
| Percent, % | 26.3 | 12.8 | 4.8 | 33.4 | 22.7 | 100 |

## Regulation of $NO_x$ and $SO_2$ Emissions

The regulation of $NO_x$ emissions in U.S. has come with the passage of The Clean Air Act Amendments (CAAAs) of 1970 and the centralization of all administrative functions by EPA. The 1970 CAAAs initially defined the first six criteria pollutants including nitrogen dioxide and sulfur dioxide. The National Ambient Air Quality Standards (NAAQSs) were established corresponding to the Amendments. However, the great progress and impact about $NO_x$ and $SO_2$ regulation had not been seen until the 1990 CAAAs were adopted. The 1990 CAAAs are the most substantive regulations thus far containing 11 major divisions referred to Title I through XI. $NO_x$ emissions are regulated both under Title I to reduce ground level ozone concentration and Title IV to reduce acid deposition. Title II calls for reductions in motor vehicle $NO_x$ emissions. Emission limits for new vehicles constitute the majority of reductions from vehicles.

Under the 1990 CAAAs, the EPA's Acid Rain Program is being implemented in two phases: the first phase for $SO_2$ began in 1995 and for $NO_x$ began in 1996. It targeted the largest and highest-emitting coal-fired power plants. The second phase for both pollutants began in 2000 and sets restrictions on the first phase plants as well as smaller coal, gas, and oil-fired plants (EPA 2001a). The goal of the second phase is to reduce emissions by over 2 million tons per year beginning in the year 2000.

The global greenhouse effect and world-wide regulation to limit carbon dioxide emissions are calling for improved fuel economy and lower emissions of carbon dioxide that will increase the demand for diesel engines. As mentioned earlier, $NO_x$ emissions by diesel engines (on-road and non-road) are responsible for one quarter of the total $NO_x$ emissions in U.S. Regulations on $NO_x$ emissions of diesel engines are represented by Tier

1-3 emissions standards. Tier 3 for engines above 50 horsepower (hp) and Tier 2 for engines below 50 hp were adopted in a 1998 rulemaking, but do not begin to take effect until the middle of this decade (EPA 2001b). The 2004 model of heavy-duty diesel trucks will be required to meet new highway emission standards.

## $NO_x$ Reduction Technologies

The increasingly restrict regulations on $NO_x$ emissions have driven electrical power producers and diesel engine manufacturers to seek for any potential and state-of-art $NO_x$ reduction techniques. In general, pollution reduction techniques fall into two categories: pollutant prevention and pollutant abatement. Since $NO_x$ is formed in the combustion processes, $NO_x$ reduction techniques are divided into combustion modification (prevention) and post-combustion control (abatement). Prevention of pollutant formation is an ideal way to eradicate pollution problems. Adopting either of these two approaches or their combination, however, depends on the maximization of benefit to meet the emission standards. In other words, a combustion technique is not necessarily better than a post-combustion technique. Usually, a combustion technique is developed to reduce $NO_x$ to some degree while a post-combustion technique is needed to finally meet the emission standards. For example, installation of low $NO_x$ burners (combustion) in a coal-fired unit may decrease $NO_x$ generation from 337 ppm to 225 ppm and a catalytic reactor (post-combustion) may be selected to further reduce the $NO_x$ level.

Combustion techniques are aimed at suppressing $NO_x$ formation. According to Zeldovich's free radical chain mechanism, a fraction of oxygen molecules ($O_2$) dissociate to form atomic oxygen radicals at the high temperature zones of the flame in a

combustion process. These oxygen radicals then react with nitrogen molecules ($N_2$) forming nitric oxide (NO), the primary $NO_x$ constituent. Nitrogen dioxide ($NO_2$), the other $NO_x$ constituent, is formed from NO in the flame region. On the other hand, there is ample evidence that fuel nitrogen contributes to the total $NO_x$ formation especially when coal or oil is burned. The $NO_x$ formation rate has a strong exponential relationship to temperature. Therefore, high temperatures result in high $NO_x$ formation rates.

Any changes to combustion system that can lower the peak temperatures, the duration of time at these peak temperatures, or the partial pressures of dissociated oxygen can lower $NO_x$ emissions. The combustion reduction methods for coal or oil-burned units include fuel switching, air staging, water injection, low-$NO_x$ burners, flue gas recirculation, reduced air preheat and low $NO_x$ concentric firing systems. The methods for diesel engines include charge air cooling, fuel injection rate shaping and multiple injections, injection timing retard, exhaust gas recirculation and so on (EPA 2001b).

Substantial reductions in $NO_x$ emissions, often over 50%, can be achieved through individual or joint application of combustion reduction methods. However, thermodynamics and kinetics of $NO_x$ formation pose a limit to the degree which a combustion control method can reach in reducing $NO_x$ formation when the energy output of a combustion system is maintained. This is challenging the new combustion system building as emission regulations become more stringent in near future. For those existing stationary combustion systems, the retrofitting cost is usually prohibitive. Thus, post-combustion control methods become necessary because of the technical limit of combustion methods and/or economical optimization.

Actually, two post-combustion techniques have found wide commercial applications in reducing $NO_x$ from mobile and stationary $NO_x$ sources. They are three-way catalyst system for exhaust from gasoline engines and selective catalytic reduction (SCR) system for flue gases from utility boilers. The three-way catalyst system is exclusively used for the exhaust gas containing significant amounts of hydrocarbons (HCs) and carbon monoxide (CO) with no oxygen from rich burn combustors. In the absence of oxygen, HCs and CO react with $NO_x$ over catalysts to form $N_2$, $CO_2$ and water. Unfortunately, there is no commercial system available for lean burn diesel engines. The commercial SCR process is to selectively promote the reduction of $NO_x$ to $N_2$ over proprietary catalysts when ammonia ($NH_3$) is injected into boiler flue gases. This can give $NO_x$ removal rates of 80% or better with acceptable $NH_3$ slip.

First patented in U.S. but successfully developed and commercially used in Japan and Germany, SCR technique has recently found its applications in U.S. power plants to reduce $NO_x$ emissions. The first six commercial SCR installations established in mid 1990s on coal-fired utility boilers, a capacity of 2 GWe in comparison with total capacity of 340 GWe in U.S. based on 1996 data. Economical evaluation was made against a new 250-MWe power plant for a 30-year project life. For a 60% removal of $NO_x$ from inlet 0.35 lb/$10^6$Btu, the capital cost is \$54/kW, with a levelized cost of \$2500 per ton of $NO_x$ removed. The capital cost increases to \$66 /kW for a 90% removal of $NO_x$. It means an additional capital cost of 16.5 million dollars to remove $NO_x$ for a new 250-MWe power plant (DOE 1997). The cost for retrofitting SCR system to an existing power plant could be significantly higher. A SCR system is being retrofitted to a 332-MWe unit in H.A. Wagner Plant at a cost of 35 million dollars (CPS 2001).

In addition to the prohibitive cost of SCR systems, there are technical problems to be solved in order to smoothen SCR application in U.S. New SCR catalysts are demanding especially for resistance to poisoning by trace metal species present in high-sulfur U.S. coals. The optimum operating temperature for the SCR process using titanium and vanadium oxide catalysts is about 650-750 °F. Therefore, catalysts are required to have high activity even at relatively low temperatures. $NH_3$ slip is the unreacted $NH_3$ out of the SCR reactor. It is essential to control $NH_3$ slip to less than 5 ppm in order to limit the formation of $(NH_4)_2SO_4$ and $NH_4HSO_4$ and minimize the plugging and corrosion of downstream equipment.

The only other commercially available technology for $NO_x$ removal is selective noncatalytic reduction (SNCR). Ammonia or urea is injected into the upper furnace to reduce $NO_x$ into $N_2$ without a catalyst. Thus, SNCR has a considerably lower cost than SCR. However, the disadvantages of SNCR include low effectiveness of 30-40% $NO_x$ removal from uncontrolled level, higher ammonia slip and limit to smaller boilers due to difficulties in achieving uniform distribution of ammonia or urea.

Technical limitations and particularly prohibitive costs of existing commercially available $NO_x$ control techniques have driven a wide exploration of new alternative techniques for post-combustion $NO_x$ removal. SCR with lean $NO_x$ catalysts and lean $NO_x$ trap are the two focuses for diesel exhaust abatement. Lean $NO_x$ catalysts are presently under development. Those kinds of catalysts require near-zero sulfur fuels (less than 5 ppm). However, the limit of 30 ppm sulfur content in fuels proposed by EPA has already caused strong opposite responses by petroleum industry. The lean $NO_x$ trap is a two-stage device that converts NO to $NO_2$ in the first stage and then reduces $NO_2$ into $N_2$ with the

aid of injected hydrocarbons in the second stage. An adsorption and recirculation technique for stationary diesel engines was demonstrated by Sorbent Technologies Corp. A highly efficient sorbent bed adsorbs the $NO_x$ and then is periodically regenerated to produce a high concentration $NO_x$ stream. The high concentration $NO_x$ stream is returned to the engine air intake system and $NO_x$ is chemically reduced to $N_2$ and $O_2$ in the combustion process.

One of the most promising classes of new technologies is non-thermal plasma that has been investigated for air pollution abatement during past couple of decades. The principle is that energetic electrons initiate a series of reactions associated with $NO_x$ removal under the plasma conditions. Two primary types of non-thermal plasmas are e-beam irradiation and electrical discharge. An e-beam irradiation process includes the generation of high-energy e-beam and its application to gas streams. The high-energy electrons collide with gas molecules and produce non-thermal plasma. Electrical discharge is a direct way to produce non-thermal plasma by applying a high voltage to a gas space and incurring gas breakdowns. The gas breakdowns generate electrons that are accelerated by electric field forming non-thermal plasma. The electrical discharges can be realized in several ways depending on the types of voltage applied and reactor specification. Glow discharge, corona discharge and dielectric barrier discharge (DBD) are of importance in dealing with air pollution. Great efforts have recently been made by Powerspan Corp., New Durham, NH in commercialization of DBD technique for a simultaneous removal of $NO_x$ and $SO_2$ (McLarnon and Jones 2000; McLarnon 2002). Their pilot plant work using a slipstream from a utility boiler has been found to be

attractive both technically and economically. The latest trend is to couple DBD and SCR techniques, called plasma-aided catalysis system (Penetrante and others 1998).

## Proposed Study

The research and development of non-thermal plasma DBD technology have been directed to addressing two major issues, i.e., $NO_x$ and $SO_2$ control of flue gases from coal-fired power plants and $NO_x$ control of exhausts from diesel-engine vehicles (truck, train, ship, etc.). DBD technology has a great potential to simultaneously convert $NO_x$ and $SO_2$ into compounds such as $NO_2$ and $SO_3$ that can be easily scrubbed. There is still a lot of fundamental work to be done before this technology finds its commercial applications in power industry. $NO_x$ control for diesel-engine vehicles calls for an on-board process which should be compact, reliable and able to effectively reduce $NO_x$ into $N_2$. A hybrid plasma-catalyst system may lead to such an on-board process. The conversion of $NO_x$ to $N_2$ is important for $NO_x$ removal from diesel-engine vehicles where $NO_2$ from a plasma DBD reactor alone would not easy to remove because of the difficulties in installing a wet scrubber. This requires extensive R&D work in both DBD and catalysis.

The objectives of this study are (i) to identify important parameters governing the operation of the DBD to gain a better understanding of DBD process for the removal of $NO_x$ and $SO_2$ from flue gases, and (ii) to investigate the synergetic effect of a hybrid plasma-catalyst system on the conversion of $NO_x$ into $N_2$. The hybrid plasma-catalyst system consists of a plasma reactor followed by a catalytic reactor. This combination is to investigate an improvement in $NO_x$ removal as compared to plasma and catalytic reactors,

individually. These objectives are achieved through conducting a systematic experimental investigation as well as theoretical analysis. There are four main tasks.

The first task is to modify the existing DBD system and conduct experiments with respect to electrical parameters and chemical compounds. Inlet gas humidifying unit, outlet gas cooling unit and tubing heating to prevent water vapor from condensing are the major modifications. Electric frequency and energy density are the main electrical parameters. Temperature and residence time (by varying total flow rate) are investigated in terms of their effects on $NO_x$ conversion. Oxygen, water vapor and $CO_2$ are individually and jointly studied. Emphasis is placed on the introduction of reducing agents such as CO, $CH_4$ and $C_2H_4$ to the simulated gas stream regarding their effects on $NO_x$ conversion. The work has been extended to investigate the $NO_x$ reaction kinetics. Appendix A is a published paper presenting part of this work under the first task.

The second task is to build a SCR reactor and prepare lab-made catalysts for running the SCR reactor to make a comparative study with P-C system. Catalysts with different amounts of $WO_3$ loading on $\gamma$-$Al_2O_3$ are prepared. The main experimental parameters included catalysts, temperature, water vapor concentration and reducing agents (NO, $CH_4$ and $C_2H_4$).

The third task is to couple the DBD and SCR forming a plasma-aided catalysis system. Comparative experiments are conducted to investigate the synergic effect with respect to different reducing agents added. Experiments are also conducted to study the potential formation of nitrous oxide ($N_2O$), one of the six greenhouse gases listed in the Kyoto Protocol.

The investigation of DBD reactor design parameters is the fourth task. The study is focused on the effects of reactor geometry, barrier materials and barrier thickness on $SO_2$ conversion. A brief cost estimates and comparison are made based on literature information regarding removal of $NO_x$ and $SO_2$ from coal-fired utility boilers.

An additional task is to explore the application of DBD to the conversion of $CH_4$ and $CO_2$ into value-added products. Both gases are among the six greenhouse gases listed in the Kyoto Protocol. This work is exploratory in nature. Some of the results are in agreement with results reported by other workers during the same time period (Gesser 1998; Zhou 1998). The experiments and results are presented in Appendix B.

# CHAPTER II

# LITERATURE REVIEW

This chapter is divided into five sections. The first section is focused on the $NO_x$ removal with non-thermal plasma especially dielectric barrier discharge (DBD). The second covers selective catalytic reduction (SCR) of $NO_x$. Literature on hybrid plasma-catalyst system for $NO_x$ removal is reviewed in the third section. The fourth section highlights DBD reactor design parameters. The last section is devoted to the prospective applications of DBD technique in promoting reactions of gaseous compounds such as $CO_2$ and $CH_4$.

## Section I $NO_x$ Removal with Non-Thermal Plasma

Non-thermal plasma can be defined as a gas consisting of electrons, ions and neutral particles in which the electrons have a much higher energy than the neutral gas particles. Therefore, non-thermal plasma is also called non-equilibrium plasma due to the significant temperature or kinetic energy difference between the electrons and neutral particles. The energetic electrons collide with molecules in the gas, resulting in excitation, ionization, electron multiplication, and formation of atoms and metastable compounds. The active atoms and metastable compounds subsequently collide with molecules and reactions may occur. It is expected that some gaseous pollutants such as $NO_x$ and $SO_2$ could participate in the reactions and be converted into conventionally

treatable or environmentally benign substances. This is the chemistry basis on which non-thermal plasma is used to remediate air pollution. Non-thermal plasma can be generated and maintained by either electron-beam (e-beam) irradiation or electrical discharge.

E-Beam Technique

An e-beam irradiation process includes the generation of high-energy e-beam and its application to gas streams. The e-beam is generated and accelerated in a vacuum region and then injected through a thin foil window and into an atmospheric-pressure processing chamber. The high-energy electrons collide with gas molecules in the chamber and produce non-thermal plasma.

Considerable efforts have been made to investigate the application of e-beam in the treatment of combustion flue gases (Person and Ham 1988; Matzing 1991; Maezawa and Izutsu 1993; Frank 1993; Frank and Hirano 1993). The initial work was performed by Ebara Corporation in Japan in 1970 and 1971. Since then both laboratory- and pilot-scale experiments have been conducted extensively in Japan and United States. For combustion flue gases, nitric and sulfuric acids are formed from NO, $SO_2$, $O_2$ and $H_2O$ by e-beam irradiation. Ammonia or lime is injected to the gas stream to react with the acids forming dry solid products that can be collected by following electrostatic precipitators or fabric filters. Helfritch (1993) uses lime in his e-beam process and reports that $NO_x$ removal is strongly dependent on radiation dose and $SO_2$ concentration. $NO_x$ removal in the range of 80 - 90% can be achieved at 1.5 and 2.0 Mrad, respectively. Energy consumption is thought to be one of the most critical factors that hinder the commercialization of e-beam technique. E-beam approach consumes about six times less

energy than electrical discharge method (Penetrante 1997). This advantage is tempered, however, by the high capital investment of a conventional MeV-type e-beam accelerator as well as x-ray hazard.

Electrical Discharge

Electrical discharge is a direct way to produce non-thermal plasma by applying a high voltage to a gas space and incurring gas breakdowns. The gas breakdowns generate electrons that are accelerated by electric field forming non-thermal plasma.

The electrical discharges can be realized in several ways depending on the types of voltage applied and reactor specification. Glow discharge, corona discharge and dielectric barrier discharge (DBD) are of importance in dealing with air pollution. The glow discharge is generated between flat electrodes encapsulated in a tube and characterized by its low pressure typically smaller than 10 mbar that limits the glow discharge application (Eliasson Kogelschatz 1991a; 1991b). The corona discharge can be realized at atmospheric pressure by using inhomogeneous electrode geometries such as pointed electrode to a plane or a thin wire to a cylinder. A pulsed corona is referred to the corona discharge generated by a pulsed voltage. The DBD technique can be traced back to the Siemens Ozonator in 1857. Ozone is generated by discharge in the annular gap between two coaxial glass tubes at atmospheric pressure. The two glass tubes serve as dielectric barrier. The DBD integrates the large volume homogeneous excitation of the glow discharge with the high pressure of the corona discharge. The DBD is also called silent discharge or barrier discharge. The two popular discharges for air pollution control are pulsed corona and DBD.

Pulsed Corona. Clements *et al.* (1989) used a wire-to-cylinder reactor to produce pulsed corona for a combined removal of $SO_2$, $NO_x$ and fly ash. The electrode configuration (wire-to-cylinder or similarly wire-to-plate) and performance of the reactor make it attractive to be retrofitted to an existing ESP or baghouse. A pilot-scale pulsed discharge system was developed for the removal of NO, $SO_2$ and $NH_3$ from flue gas (Veldhuizen 1998). The NO conversion was strongly increased by the addition of $SO_2$ or $NH_3$. The best result for initial concentrations of 300 ppm is 80% NO removal and 95% $SO_2$ removal with $NH_3$ slip of 3 ppm. Mok *et al.* (1998) evaluated the energy utilization efficiencies for $SO_2$ and NO removal by pulsed corona. They found that shortening pulse width is very important to the increase in energy utilization efficiency and the energy efficiencies for $SO_2$ and NO removal were maximized at the pulse-forming capacitance five times larger than the reactor capacitance. In a positive-pulsed corona discharge reactor, byproducts generated from propene addition were identified to be ethane and formaldehyde of negligibly small amounts (Mok and others 2000). By comparing several types of electrical discharge reactors, Penetrante (1997) reported that pulsed corona has the same energy efficiency as DBD.

DBD Technique. DBD technique has attracted much more attention because of its most important characteristic, i.e., DBD can be provided in a much simpler way than other alternatives such as glow discharge, pulsed corona or e-beam. DBD technique is marked for its unprecedented flexibility in reactor fabrication and operation, easy scale-up from laboratory experiments to large industrial units, and efficient low-cost power supply (Kogelschatz and others 1997). These advantages greatly facilitate the

investigation of $NO_x$ removal via DBD at laboratory scale. Considerable efforts have been made on $NO_x$ removal with DBD techniques.

Investigation of the electrical discharge-initiated reaction of nitrogen oxides was first undertaken by S.S. Joshi at the University College, London (Joshi 1927; 1929a; 1929b). Joshi studied the decomposition of nitrous oxide ($N_2O$) in a Siemens Ozonator at 6,000-12,000 voltes and 150 Hz. An excellent experimental system was set up by Visvanathan(1952; 1953) to investigate the decomposition of nitric oxide. The reaction vessel consists of an all-glass Siemens Ozonator. A batch process was used to obtain different residence times for gas exposure to discharge. Pure NO was prepared as feed gas. The time for a complete decomposition of NO changed from 2 to 188 minutes when the initial pressure of NO was increased from 2 to 31.5 cm(Hg). It was found that $NO_2$ was formed as an intermediate product, while $N_2$ and $O_2$ are the final products. The study of nitrogen oxides and $SO_2$ aimed at controlling air pollution, however, has been substantially conducted after the US federal government first enacted the Air Pollution Control Act of 1955 and the Britain government enacted the English Clean Air Act in 1956.

Since then, particularly in 1980s and 1990s, considerable work has been conducted for controlling $NO_x$ and $SO_2$ using electrical discharge techniques. Henis (1976) passed an NO-$N_2$ gas stream through a barrier discharge with low conductivity catalyst materials in the gas space between coaxial electrodes. He found that a higher NO removal was achieved for packing non-conducting catalyst materials in the barrier discharge reactor than for unpacking. The maximum NO decomposition was reported to be 79.6% for packing zirconium silicate at inlet 1500 ppm NO, compared with the NO removal of 18% for no packing under same space velocity and power input. In addition,

1% $O_2$ /1% CO / 12% $CO_2$/balance $N_2$ mixtures were also used as the background gas to investigate total NO removal over different types of packing materials. The total NO removal was found to be 43.9% for packing zirconium silicate at a lower power input of 50 w (compared with 80 w for the maximum NO decomposition of 79.6% mentioned above).

Reduction of $NO_x$ by electrical discharge in a tubular reactor has been conducted in the Department of Chemical Engineering, University of New Hampshire since 1987. The earlier investigation was focused on reactor design parameters, effect of electrical parameters and packing materials on $NO_x$ conversion (McLarnon 1989; McLarnon and others 1990; McLarnon and Mathur 1991; Mathur and others 1992). Breault *et al.*(1993) employed a tubular reactor with fibrous dielectric packing to convert $NO_x$ into $N_2$ and $O_2$ in the absence of water vapor and oxygen. Quartz or ceramic covering the inner electrode (steel rod) served as barrier material. Greater than 99% removal of $NO_x$ from the flue gas was achieved. A series of chemical reactions were proposed. McLarnon (1996) conducted a series of experiments on both DBD bench-top apparatus and process development system and reported effects of electrical parameters (voltage, frequency and power), reactor size and other chemical compounds such as $O_2$ and $H_2O$ on NO/$NO_x$ conversions.

NO-$N_2$ mixture was used to investigate the energy consumption for NO removal by chemical reduction (Penetrante and others 1995). Penetrante *et al.* reported that the specific energy consumptions (eV per NO molecule reduced) were all similar for a pulsed corona, pulsed barrier discharge and pulsed barrier discharge with dielectric pellet packing reactors. The specific energy consumption was around 240 eV per NO molecule

reduced. This corresponded to a specific energy consumption of about 240 eV per nitrogen atom produced when $N_2$ was dissociated by electrical discharge.

An extensive study was conducted over both bench-top apparatus and process development system (McLarnon and Mathur 2000). The reactors were each made of a pair of coaxial cylinders. The parameters investigated included applied voltage, frequency, specific energy (kJ/mole-$NO_x$ inlet), packing, chemical composition of the gas stream, residence time, electrode spacing, temperature, gas turbulence, etc. Both simulated gas and flue gas from burning natural gas were used in the study. Most data were acquired over the bench-top DBD reactor packed with glass wool. It was reported that glass wool packing did not improve $NO/NO_x$ conversions while it helped stabilize electrical discharge. The residence time in the reactor did not affect $NO_x$ conversion. The change in residence time was realized by changing the length of the inner electrode, thereby changing the volume of discharge region. This actually significantly changed the capacitance of the reactor and affected the discharge. It may be better to change the flow rate for different residence times. The experimental results showed that decreasing space gap between the electrodes would increase $NO_x$ conversion for a given specific energy.

Schluep and Rosocha (2000) used dry NO mixtures with $N_2$, $N_2/O_2$ or $N_2$/Ar to study $NO_x$ removal via a rectangular-planar DBD reactor. A NO destruction efficiency of exceeding 99% was reported for the inlet NO-$N_2$ or NO-$N_2$-Ar mixture. The addition of Ar significantly enhanced $NO_x$ removal. The authors assumed that excited-state argon species were formed and might affect the NO and $NO_x$ conversions. Moreover, the mean electron energy in an $Ar/N_2$ mixture is higher than that in a $N_2/O_2$ mixture, which would produce reductive N-atoms more efficiently.

In a computational investigation over a DBD reactor, Dorai *et al.* (2000) used a base gas mixture that contained $N_2/O_2/H_2O/CO_2$ of 79/8/6/7 with 400 ppm CO, 260 ppm NO, 133 ppm $H_2$, 500 ppm propene and 175 ppm of propane. It was a kind of simulated diesel exhaust gas. The $NO_x$ chemistry in the DBD reactor is mainly driven by oxidation processes that convert NO into $NO_2$.

## Section II Selective Catalytic Reduction of $NO_x$

Selective catalytic reduction (SCR) technology had been used extensively in Japan and West Germany to eliminate 80-90% $NO_x$ emissions from utility boilers and industrial furnace stacks in 1980s (Hardison 1991). In the past decade, this technology has been further developed and used in the U.S. Although many improvements aimed at lowering the cost of SCR systems and expanding their range of industrial application have been achieved, both fixed investment and operating cost are still high.

The commercial practice in US power industry for $NO_x$ reduction has been recently involved in developing new SCR catalysts. These SCR catalysts are generally oxides of titanium, vanadium and, in some cases, tungsten (DOE 1997). Many researchers in this area believe that SCR technology can be modified and applied to control of NO from diesel exhausts. Development of an inexpensive catalyst with high performance has also been intensively conducted.

### $\gamma$-$Al_2O_3$ as a Support

Sadhankar and Lynch (1997) investigated the kinetic behavior of NO reduction by CO over a $Pt/Al_2O_3$ catalyst. A high-conversion steady state was obtained starting with a net

oxidizing feed composition ($[NO]_0 > [CO]_0$), and a low-conversion steady state was obtained for a net reducing initial feed composition.

Kudla *et al.* 's (1996) study was focused on increasing the acidity of γ- $Al_2O_3$ through the addition of $WO_3$ and increasing the resulting catalytic activity. It was found that $WO_3$-modified alumina compositions has higher $NO_x$ removal activity under lean-burn conditions than the unmodified γ-$Al_2O_3$. Maximum $NO_x$ conversion (50-60%) occurred at a 1 wt% loading of $WO_3$ on γ-$Al_2O_3$ at 580 °C. Yan *et al.*(1997) reported that the effectiveness of $Co/Al_2O_3$ in the SCR process depends strongly on Co loading, calcination temperature, and source of alumina.

Bethke and Kung (1997) reported that higher conversions of NO to $N_2$ were obtained over 2 wt% $Ag/Al_2O_3$ than over 6 wt% $Ag/Al_2O_3$. Meunier *et al.*(1999) found that the γ-$Al_2O_3$ and the low-loading silver material exhibited high NO conversion to $N_2$ whereas the high-loading sample predominantly yielded to $N_2O$. The promoting effect of low loadings of silver on alumina on the activity for $N_2$ production was attributed to the higher rate of formation of inorganic ad-$NO_x$ species (e.g., nitrates).

Kung *et al.* (1999) reported the catalytic properties of highly active Sn/γ-$Al_2O_3$ for lean $NO_x$ reduction. The activity depended on the Sn loading. For a 10 wt% $Sn/Al_2O_3$ at 475-500 °C, 58% conversion of 1000 ppm NO to $N_2$ was obtained in the presence of 10% water and 15% $O_2$, at a space velocity of 30,000 $h^{-1}$. Park *et al.* (1999) found that an unusual feature of $SnO_2/Al_2O_3$ is the independence of maximum NO conversion over a wide range of Sn contents (1 to 10 wt% Sn). Sn is present in the +4 oxidation state irrespective of Sn loadings. Sirdeshpande and Lighty (2000) reported a copper oxide process that could

simultaneously remove $SO_2$ and $NO_x$. This process needs regeneration using $H_2$ or $CH_4$. A reactor model was also presented for SCR of NO by $NH_3$ over $CuO/\gamma\text{-}Al_2O_3$.

Almusaiteer *et al.*(2000) have examined the $Rh^+(CO)_2$ reactivity and its role in $CO_2$ formation over $Rh/Al_2O_3$. Sodium promotion enhances the performance of $Rh/\gamma\text{-}Al_2O_3$ catalysts in the reduction of NO by propene (Macleod and others 2000). Pronounced activity enhancement is accompanied by marked improvement in nitrogen selectivity. Na also strongly suppresses CO and HCN formation. By examining the influence of various parameters over a large range of initial metal dispersion, Denton *et al.* (2000) found that only the Pt dispersion is of key importance. The dispersion does not clearly affect the selectivity.

Diffusional effects and intrinsic kinetics for NO reduction by CO over $Pt\text{-}Rh/\gamma\text{-}Al_2O_3$ monolithic catalysts were investigated by Kyriacopoulou *et al.* (1994). A first-order kinetic rate expression with respect to NO concentration, which includes an inhibition term of second order, was found to fit the experimental data via a model which also accounts for internal transport resistances.

The presence of partially reduced molybdenum oxide improved the NO dissociation to $N_2$ on a Pd-Mo catalyst. Schmal *et al.* (1999) suggested a model that shows $Mo^{+\delta}$ is a promoter in the catalytic cycle for NO reduction by CO. Their activity studies showed that the Pd8Mo catalyst is much more active and more selective to $N_2$ than the monometallic catalyst. The $Pd\text{-}20Mo/Al_2O_3$ catalyst showed better activity and selectivity for $N_2$ formation during the CO-NO reaction (Baldanza and others 2000).

The behavior of a series of palladium and palladium-copper catalysts supported on ceria/alumina for the $CO+NO+O_2$ reaction has been analyzed (Fernandez-Garcia and others

2000). The addition of copper to a palladium system leads to beneficial effects related to alloy formation in which both CO and NO elimination are enhanced. Haneda *et al.* (2000) reported that $Ga_2O_3$-$Al_2O_3$ prepared by the sol-gel method exhibited excellent activity for NO reduction, compared with $Al_2O_3$, $Ga_2O_3$, and impregnated $Ga_2O_3/Al_2O_3$.

ZSM-5 as Support

Overexchanged Fe/ZSM-5 catalysts have been found to be highly active and remarkably stable for the SCR reaction in the presence of $H_2O$. The reaction intermediates in the SCR of $NO_x$ over Fe/ZSM-5 with alkanes were investigated (Chen and others 1999). Long and Yang (1999a) found that, for Fe-ZSM-5 catalysts, the SCR activity decreased with increasing Si/Al ratio in the zeolites. As the Fe-exchange level in the Fe-ZSM-5 catalysts was increased from 58 to 252%, NO conversion increased at lower temperatures(e.g., 300°C). Compared with the commercial vanadia catalyst, based on the first-order rate constants, the Fe-ZSM-5 catalyst was five times more active at 400 °C.

Pd-H-ZSM-5 (Pd/Al= 0.048) has been used by Lobree *et al.* (1999) to investigate the SCR mechanism. It was found that prior to reaction most of the Pd in Pd-H-ZSM-5 is present as $Pd^{2+}$ cations. Reduction of $Pd^{2+}$ cations is significantly suppressed when $O_2$ is added to the feed of NO and $CH_4$. Li and Flytzani-Stephanopoulos(1999) reported on the promotion of Ag-ZSM-5 by cerium for the SCR of NO by methane. The major functions of cerium are to catalyze the oxidation of NO to $NO_2$, suppress the $CH_4$ combustion, and stabilize silver in dispersed $Ag^+$ state. By comparing CoZSM-5 with CuZSM-5 in the SCR of $NO_x$ by methane, Desai *et al.* (1999) exposed why CoZSM-5 selectively reduces $NO_x$ with methane. Higher concentrations of metal oxides will lower the selectivity toward $N_2$.

Cu-ZSM-5 does not appear to possess either the necessary high activity or stability under actual exhaust conditions. However, Millar *et al.* (1999) investigated its mechanism for providing a logical approach to future $NO_x$ reduction catalyst development. Samarium was used as a promoter in Cu-ZSM-5 catalysts (Parvulescu and others 2000). The authors suggested that (i) either that samarium blocked exchange sites where copper would be trapped in a non-active form, thereby directing the implantation of copper to favorable sites; (ii) or that samarium, in close association with active copper, would adjust the oxido-reduction properties of active copper (possibly the Cu(I)–to–Cu(II) ratio), thus facilitating NO decomposition.

$TiO_2$ as Support

Kamata *et al.* (1999) made the measurements on the reaction rate for the SCR of NO by $NH_3$ over a $V_2O_5$ $(WO_3)/TiO_2$ commercial catalyst. The addition of $WO_3$ and $MoO_3$ is expected to improve the thermal stability and retard the oxidation of $SO_2$ to $SO_3$. Among the preparation methods for copper catalysts, the sol-gel technique offers some advantages. $CuO\text{-}SiO_2$ sol-gel catalysts were prepared and their characterization was achieved by Diaz *et al.* (1999). 0.5% $Rh/TiO_2$ was prepared by Kondarides *et al.* (2000) to investigate the activity that is hindered by accumulation of surface oxygen, originating from NO decomposition and/or gas-phase oxygen in the feed.

Long and Yang (1999b; 2000) reported that Fe-exchanged $TiO_2$-pillared clay catalysts showed very high activities in the reduction of $NO_x$ by $NH_3$ in the presence of excess oxygen. $H_2O$ and $SO_2$ further increased the activity at high temperature(i.e., above 300 °C). This kind of catalysts were about twice as active as the commercial $V_2O_5$-

$WO_3/TiO_2$ catalysts in the presence of $H_2O$ and $SO_2$. Subbotina *et al.* (1999) for the first time reported that photocatalytic reduction of NO by CO over a $MoO_3/SiO_2$ catalyst (2.5wt% of Mo). $N_2$ and $CO_2$ are found to be the major reaction products, and the selectivity of the photoreduction is close to 100%.

## Section III Hybrid Plasma-Catalyst System for $NO_x$ Removal

Recently, a combination of non-thermal plasma and catalysis for the reduction of $NO_x$ to $N_2$ has attracted attention. The approach is aimed at obtaining a higher $NO_x$ conversion to $N_2$ effectively and economically than when each of the techniques is used alone. A significant advantage is claimed that plasma helps convert NO into $NO_2$ which is then more easily reduced to $N_2$ by a conversional catalytic process (Penetrante and others 1998).

In the presence of $O_2$, one of the dominant reactions is that plasma oxidizes NO to $NO_2$. Penetrante *et al.*(1998) reported that hydrocarbons play three important functions in the plasma: lowering the energy cost for oxidation of NO to $NO_2$, minimizing the formation of acid products and preventing the oxidation of $SO_2$ to $SO_3$. A simulated gas mixture consisting of NO (or $NO_2$) was passed through a catalyst bed at 450 °C, resulting in 44% conversion of NO to $N_2$ (88% of $NO_2$ was converted to $N_2$ ). However, the simulated gas used for catalysis test excludes the two main components, $H_2O$ and $CO_2$ present in large amount in real diesel engine exhausts. This might leave the conclusions open to question. The main test result for diesel engine exhaust is only combined effect of plasma and catalysis(54% $NO_x$ conversion to $N_2$). No result for either plasma or SCR used alone is available for comparison. $\gamma$-$Al_2O_3$ served as catalyst.

The hybrid technique called plasma-assisted catalysis(PAC) is being developed in cooperation with Cummins Engine Company (Penetrante 2000). It is reported that the PAC process already has proven efficacy for relatively small diesel engines. No detailed result is available.

The combination of DBD and SCR can be realized by packing catalyst into DBD reactor(one-stage configuration) or put the SCR reactor downstream of the DBD reactor (two-stage configuration). It is reported that the same De-$NO_x$ results are achieved over the two set-ups (Penetrante and others 1998). However, Balmer *et al.* (1998) reported that 76% and 44-56% of the $NO_x$ are reduced to $N_2$ for single stage and two-stage configurations, respectively and energy efficiency is about ten times higher in the two-stage configuration. The results also showed that $N_2$ from $NO_x$ reduction can be measured if background $N_2$ is replaced with helium. The parallel plate reactor without the catalyst did not reduce NO but simply converted it to $NO_2$. Although the product distribution (NO and $NO_x$) appears to be similar, the predominant chemical mechanisms for He and $N_2$ individually as a carrier gas are probably different. $N_2$ as a product of $NO_x$ reduction is replaced with He, favoring the $NO_x$ reduction to $N_2$. This might leave the conclusions open to question.

Hoard and Balmer (1998) developed a plate-type plasma device followed by a catalytic reactor. Two proprietary catalysts, Cu-ZSM and "A" were used at a relatively low temperature of 180 °C. It was concluded that plasma without a catalyst did not give real $NO_x$ reduction. Instead, it produced a variety of species which could be reconverted to $NO_x$ by Cu-ZSM catalyst. At energy deposition of 30 J/L, a $NO_x$ conversion of 53%

was reported with plasma device followed by catalyst "A". It less than doubled the conversion of 29% when plasma used alone.

Koshkarian *et al.* (1998) also reported that conversion of NO to $NO_2$ was dominant reaction in the plasma reactor. $HNO_3$ and $N_2O$ were detected, 8-15 ppm and 5-10 ppm, respectively. The oxidation catalyst reconverted species back to $NO_x$. For engine test, a greater formation of $HNO_2$ and $HNO_3$ was observed. Formaldehyde, acetaldehyde (combined 20-50 ppm) and ozone (5-8 ppm) were also detected. The low reduction (less than 10% conversion to $N_2$) may be mainly due to poor performance of the catalyst used. Result about $SO_2$ effect is unavailable from the paper.

Oda *et al.*(1998) showed that $NO_x$ concentration was not decreased by using only pulsed voltage application because NO was oxidized into $NO_2$. Hydrocarbon additives, especially double-bone structure hydrocarbons significantly promoted $NO_x$ conversion into $N_2$. Catalyst effect was not significant in this experiment. When the catalyst temperature is at room temperature, high $NO_x$ removal performance is obtained compared with that of the higher temperature. Two unusual results reported in the paper: catalyst Cu-ZSM-5 helps $NO_x$ removal and works better at room temperature than at higher temperature. It is against Hoard and Balmer's (1998) finding that Cu-ZSM reconverts species back to $NO_x$. There may be a flaw in the conclusion that Catalyst Cu-ZSM-5 works better at room temperature. It is most likely that Cu-ZSM-5 reconverts species back to $NO_x$ less at room temperature than at higher temperature.

## Section IV Dielectric Barrier Discharge (DBD) Reactor Design Parameters

Reactor design is an essential part of the overall R&D work of DBD. Although DBD technology was first used by Siemens in 1857 for the generation of ozone and since

then commercial ozonators have been available, developments of DBD reactors for treating gas pollutants have encountered various problems including scale-up, energy efficiency, manufacturing and operating costs, and treatment efficiency. Most efforts have been devoted towards studying operating parameters such as pollutants and their concentrations, gas mixing, voltage, frequency, etc. Little attention has been paid to reactor design parameters including geometry, size, dielectric barrier materials and catalytic packing.

The objective of this literature review is to provide information on reactor design parameters and experimental operating conditions particularly with respect to DBD plasma. Presented in Table 2.1 are main parameters of DBD reactor design used by some researchers in their experiments. For dimension and other details, the readers may refer to the original papers.

Manley(1944) used two types of geometry, plate and tubular to investigate ozonator discharge. In the plate reactor, a pair of window glass plates were used as barrier materials. In the tubular reactor, only the central high-voltage electrode was covered with a glass tube. An excellent experimental system was set up by Visvanathan(1952) to investigate decomposition of nitric oxide. The reaction vessel consisted of an all-glass Siemens Ozonator. NaCl solution served as electrodes and dielectric materials were glass. Water was used to cool the reaction vessel.

A reactor was described in Henis' (1976) patent for the removal of nitrogen oxides from gases. The reactor is typically tubular. Dielectric materials can be glass or quartz. The final products are nitrogen and oxygen. Packing materials including ceramic spheres, metal oxides, molecular sieve, etc. were tested. Gap spacing was recommended

to be 2-8 mm. The temperatures generally range from ambient to 100 °C. Dhali and Sardja (1991) reported an investigation on plasma-assisted oxidation of $SO_2$ to $SO_3$. A coaxial dielectric barrier discharge reactor is used. Only outer grounded electrode is interiorly covered with glass.

**Table 2.1**

**Summary of Main Parameters of DBD Reactors**

| Reference | Geometry, i.d.xL cm or LxW | Barrier Material | Gas Spacing (mm) | Voltage (kV) | Frequency (Hz) | Temperature (°C) |
|---|---|---|---|---|---|---|
| (Manley 1944) | Planar 86x56 cm | Glass | 1.84-3.70 | 20 (peak) | 60-410 | 26-39 |
| | Tubular 7.9x86 cm | Glass | 2.15 | | | |
| (Visvanathan 1952) | Tubular 3.2x65 cm | Glass | 2 | 5 (rms) | 100 | room temp. |
| (Henis 1976) | Tubular 1.7x33 | Glass Quartz | 2-8 | 75 (peak) | n/a | 100 (mostly) |
| (Dhali and Sardja 1991) | Tubular 3.6x20 | Glass | 15.5 | 24 (peak) | 60 | room temp. |
| (Rosocha and others 1993) | Planar 71x18 | Glass | 3.3 | 25-35 (peak) | 10-3500 | room temp. |
| (Breault and others 1993) | Tubular 25.4x | Ceramic | n/a | 10-20 | 60-400 | 150-176 |
| (Pashaie and others 1994) | Tubular 3.5x5 | Glass | 3.3-15.2 | 20 (peak) | 400 | room temp. |
| (McLarnon 1996) | Tubular 2.5x31 | Quartz | 6-8 | 7-35 (peak) | 60-1000 | room temp. |
| | Tubular 2.9x122 | Quartz | 11 | | | |
| (Schluep and Rosocha 2000) | Planar, 31x18 cm | Pyrex | 2 | 9-11 | 1000-2000 | n/a |

Rosocha *et al.*(1993) used a flat silent discharge plasma (SDP) cell for destruction of aliphatic hydrocarbons, CFCs, TCE and $CCl_4$. The SDP cell consisted of glass plate and water pool that served as HV electrode. It is a planar BD reactor. Breault *et al.*(1993) employed a tubular reactor with fibrous dielectric packing to convert $NO_x$ into $N_2$ and $O_2$ in the absence of water vapor and oxygen. Quartz or ceramic covering the inner electrode (steel rod) served as barrier material. The ID of the outer stainless steel tube is 25.4 mm. The experimental investigation of the electrical characteristics of a coaxial dielectric barrier discharge is reported (Pashaie and others 1994). Glass serves as dielectric material adjacent to the outer electrode (SS wire mesh). By varying the inner SS electrode diameter, Pashaie *et al.* found that the ratio of the inner to outer electrode radius has a strong influence on the discharge onset voltage and generation of radicals.

A bench-scale apparatus and a process development unit were used to remove $NO_x$ (McLarnon 1996). Experimental studies of scale-up were conducted. The reactor is typically tubular. The annular space is packed with glass wool. It was found that the packing did not increase $NO_x$ conversion although it helped stabilize discharge. The process development reactor consisted of seven 1.22 m long each stainless steel tubes with an ID of 28.6 mm arranged in series. Schluep and Rosocha (2000) used a flat plate DBD reactor with 31 cm long and 18 cm wide. The spacing gap of 2 mm is relatively small. A high frequency of 1000-2000 Hz was employed.

## Section V Other Prospective Applications of DBD

Efforts have also been made to use dielectric barrier discharge (DBD) technique for remediation of toxic gas streams in addition to $NO_x$. It is believed that DBD-

generated oxidizing radicals would convert the toxins into treatable or exhaustible substances. The oxidation of chlorobenzene, trichloroethylene, formaldehyde, etc. by DBD techniques were investigated by several workers (Snyder and Anderson 1998; Evans and others 1993; Storch and Kushner 1993).

Rosocha *et al.*(1993) used a flat silent discharge plasma (SDP) cell for destruction of aliphatic hydrocarbons, CFCs, TCE and $CCl_4$. Destruction of 80% or greater was observed. Some of reaction products such as phosgene ($COCl_2$) were identified. A mathematical model was also presented.

In a cylindrical DBD reactor, the effect of electrical, chemical and hydrodynamic parameters on the decomposition of R-12, R-22 and R-50 were investigated (Golden 1997; Golden and Mathur 1997). The majority of experimental work was performed with pure $N_2$ as the carrier gas. However, it is observed that addition of a very small amount of $O_2$ in the inlet stream, on the order of 0.1% by volume, considerably improved percent conversion over pure $N_2$ as the carrier gas. A gas chromatograph was used for freons and methane analyses.

Another important investigation is to reform two greenhouse gases, i.e., $CO_2$ and $CH_4$ over a DBD reactor, resulting in formation of high-value products such as $H_2$, CO or hydrocarbons. Literature review conducted so far shows that studies on methane dissociation over barrier discharge in cylindrical reactors have been conducted by several workers. Golden(1997) reported a methane conversion of 22% by passing 125 ppm methane in nitrogen through a BDR at 18,385 V(rms)and 400 Hz. The products were not identified. Nikravech *et al.* (1994) applied 90 kV (1-60 Hz) to a DBD reactor and reported conversions up to 25% and 40% for pure $CO_2$ and $CH_4$, respectively.

Gesser *et al.*(1998) investigated the conversion of a $CH_4$/ $CO_2$ (1:1)mixture to $H_2$ and CO at ambient temperature in a DBD reactor. Conversions of up to 50% were achieved at 13 kV and 25 mA. Motret *et al.* (1997) also reported that DBD processing of $CH_4$ and $CO_2$ mixture could lead to the formation of synthesis gas CO and $H_2$. Using a mixture of $CH_4/CO_2$ (80/20), Zhou *et al.* (1998) reported that conversions of $CH_4$ and $CO_2$ were 64% and 54%, respectively. They also found that the amount of syngas produced strongly depends on the electric energy input.

Larkin *et al.* (2001) used a DBD reactor operated at 7 kV and 26-178 w of AC power to conduct the partial oxidation of methane. They found that the organic liquid oxygenates formed from the partial oxidation of methane were principally methanol, formaldehyde, methyl formate, and formic acid.

Catalysts have also been added to DBD reactors aimed at improving product selectivity of methane and $CO_2$ reactions. Eliasson and Kogelschatz (2000) presented a direct higher hydrocarbon formation from methane and carbon dioxide using DBD with zeolite catalysts. The products include alkanes, alkenes, oxygenates, and syngas. Kraus *et al.* (2001) placed ceramic foams in the annular gap of a DBD reactor to study $CO_2$ reforming of methane. Nickel and rhodium coatings on the ceramic foams were investigated regarding their effect on the plasma chemistry.

# CHAPTER III

# THEORIES OF NON-THERMAL PLASMA, CATALYSIS AND HYBRID PLASMA-CATALYST SYSTEM

The theories of non-thermal plasma, catalysis and hybrid plasma-catalyst (P-C) systems are discussed in this chapter with an emphasis on $NO_x$ reactions. This chapter consists of three sections. The first section is focused on generation of non-thermal plasma especially dielectric barrier discharge (DBD) and its effect on chemical reactions. The theories of selective catalytic reduction (SCR) are discussed in the second section. Hybrid plasma-catalyst sytem is relatively new and its theoretical exploration is still in the preliminary stage. Several key issues about P-C system are highlighted in the last section.

## Section I $NO_x$ Reactions in Non-Thermal Plasma

Non-thermal plasma can be defined as a gas consisting of electrons, ions and neutral particles in which the electrons have a much higher energy than the neutral gas particles. Therefore, non-thermal plasma is also called non-equilibrium plasma due to the significant temperature or kinetic energy difference between the electrons and neutral particles. The temperature of gas can be in the range of room temperature. The energetic electrons collide with molecules in the gas, resulting in excitation, ionization, electron multiplication, and the formation of atoms and metastable compounds. The active atoms and metastable compounds subsequently collide with molecules and reactions may occur. It is expected that some gaseous pollutants such as $NO_x$ and $SO_2$ could participate in the

reactions and be converted into conventionally treatable or environmentally benign substances. Non-thermal plasma can be generated and maintained by either electron-beam (e-beam) irradiation or electrical discharge.

E-Beam Technique

An e-beam irradiation process includes the generation of high-energy e-beam and its application to gas streams. The e-beam is generated and accelerated in a vacuum region and then injected through a thin foil window and into an atmospheric-pressure processing chamber. The high-energy electrons in the range of 300-800 keV collide with gas molecules in the chamber and produce non-thermal plasma. Positive ions such as $N_2^+$, $O_2^+$, $N^+$ and $O^+$ are considered to be important irradiation products in the chemical processing of $NO_x$ and $SO_2$ (Matzing 1991). These positive ions undergo fast charge transfer reactions, leading to formation of radicals. This contributes to the major radical source and in particular the significant OH source in the electron beam dry scrubbing (EBDS) process. The concentrations of radicals formed are high enough to oxidize $NO_x$ and $SO_2$ traces.

Electrical Discharge

Electrical discharge is a direct way to produce non-thermal plasma by applying a high voltage to a gas space and incurring gas breakdowns. The gas breakdowns generate electrons that are accelerated by electric field forming non-thermal plasma.

The electrical discharges can be realized in several ways depending on the types of voltage applied and reactor specification. Glow discharge, corona discharge and

dielectric barrier discharge (DBD) are of importance in dealing with air pollution. The glow discharge is generated between flat electrodes encapsulated in a tube and characterized by its low pressure typically smaller than 10 mbar that limits the glow discharge application (Eliasson and Kogelschatz 1991a; 1991b). The corona discharge can be realized at atmospheric pressure by using inhomogeneous electrode geometries such as pointed electrode to a plane or a thin wire to a cylinder. A pulsed corona is referred to the corona discharge generated by a pulsed voltage. The DBD technique can be traced back to the Siemens Ozonator in 1857. The ozone is generated by discharge in the annular gap between two coaxial glass tubes at atmospheric pressure. The two glass tubes serve as dielectric barrier. The DBD integrates the large volume homogeneous excitation of the glow discharge with the high pressure of the corona discharge. The DBD is also called silent discharge or barrier discharge. The two popular discharges for air pollution control are pulsed corona and DBD. Table 3.1 shows the characteristics of several non-thermal discharges (Eliasson and Kogelschatz 1991a; 1991b). The item of degree of ionization in the table is the ratio of the number density of charged species to the number density of neutral species in the gas.

**Table 3.1**

**Characteristics of Non-Thermal Discharges**

| Parameter | Glow Discharge | Corona Discharge | Barrier Discharge |
|---|---|---|---|
| Pressure (Bar) | $< 10^{-2}$ | 1 | 1 |
| Electric Field (kV/cm) | 0.01 | 0.5 – 50, variable | 0.1 - 100 |
| Reduced Field (Td) | 50 | 2- 200, variable | 1 - 500 |
| Electron Energy (eV) | 0.5 - 2 | 5, variable | 1 - 10 |
| Electron Density ($cm^{-3}$) | $10^{8} – 10^{11}$ | $10^{13}$, variable | $10^{14}$ |
| Degree of Ionization | $10^{-6} – 10^{-5}$ | small, variable | $10^{-4}$ |

Dielectric Barrier Discharge

The classical DBD configurations are planar or cylindrical with at least one electrode covered with dielectric materials such as glass, quartz and ceramics. In order to initiate and maintain an electrical discharge process, a high voltage is applied across two electrodes separated by dielectric materials and gas gap. The voltage applied should be high enough to establish a high electric field that causes gas breakdown, i.e., electrical discharge. The discharge-generated ions traverse the space in a pulse and accumulate on the surface of the dielectric materials. These accumulated space charges generate a reverse electric field that finally makes the discharge terminate. The short duration and limited charge transport and energy dissipation result in little gas heating. The electron temperature reaches thousands degree K while the background gas can be in the range of room temperature.

The most important property of DBDs coming with gas breakdown is a large number of independent current filaments of nanosecond duration, i.e., microdischarges. A considerable amount of such microdischarges were observed at a frequency of twice the frequency of voltage applied (Kogelschatz 1999). Eliason and Kogelschatz (1991a) discerned three separate stages during the life cycle of such a filament: the electrical breakdown; transport of charge across the gas; and the excitation of the atoms and molecules initiating the reaction kinetics. The durations of these three stages are of different orders of magnitudes. The local breakdown usually finishes within nanoseconds. The current transport takes typically 1-100 ns. The chemical process can last from nanoseconds to seconds depending on species involved. A great advantage of the DBD over many other discharge types is that one can vary the average energy of the electrons

generated by adjusting the product (n·d) of gas density (n) and gap width (d). In general, the lower the product (n·d), the higher mean electron energy. The electron energy inside the conductive filament is of a few eV.

Chemical Reactions of $NO_x$ in DBD

Chemical reactions of NOx in DBD have been studied in the past two decades. Because of the complicated chemistry of DBD plasma reactions, our knowledge of reactions of $NO_x$ in DBD is still limited and partially based on speculation.

Gentile and Kushner (1995) establish a model for $N_2/O_2/H_2O/N_xO_y$ gas mixture. There are 42 electron-impact processes considered. The plasma chemistry model contains 56 species and 331 reactions and uses the rate coefficients obtained from solving Boltzmann's equation. The primary radicals N, O, OH and H are produced by electron-impact dissociation of the feed gas. The six major end products are assumed: $N_2$, $NO_2$, $H_2O$, $N_2O_5$, $HNO_2$ and $HNO_3$. Two main remediation pathways for removal of NO are:

Reduction: $NO + N \rightarrow N_2 + O$ (3.1)

Oxidation: $NO + O \rightarrow NO_2$ (3.2)

$NO_2 + OH \rightarrow HNO_3$ (3.3)

Electron-impact dissociations:

$e + N_2 \rightarrow N + N + e$ (3.4)

$e + H_2O \rightarrow H + OH + e$ (3.5)

$e + O_2 \rightarrow O + O + e$ (3.6)

$e + O_2 \rightarrow O + O(^1D) + e$ (3.7)

Where, $O(^1D)$ is metastable excited oxygen atom. Second radicals $HO_2$, $NO_3$ and $O_3$ also help in the remediation of $N_xO_y$. They are produced by the following reactions:

$$H + O_2 + M \rightarrow HO_2 + M \quad (3.8)$$

$$O + OH + M \rightarrow HO_2 + M \quad (3.9)$$

$$NO_2 + O + M \rightarrow NO_3 + M \quad (3.9)$$

$$NO_2 + O_3 \rightarrow NO_3 + O_2 \quad (3.11)$$

$$O + O_2 + N_2 \rightarrow O_3 + N_2 \quad (3.12)$$

where M is a third collision partner ($O_2$, $O_3$, $N_2$).

## Section II Selective Catalytic Reduction of $NO_x$

Selective catalytic reduction (SCR) of NOx using ammonia ($NH_3$) or urea as the reducing agent has been commercially used in American power plants. As the name SCR implies, this technique selectively realizes the reduction of $NO_x$ to $N_2$ over proprietary catalysts. The initial SCR technique using $NH_3$ was patented by Englehard Corporation in 1957. Unfortunately, the catalysts based on platinum or platinum group metals were proved unsuccessful and other base metal catalysts were found of low activity. The later development of vanadium/titanium catalysts in Japan has been successful. Considerable efforts have also been made in Germany to develop SCR catalysts. Siemens has become the major SCR catalyst supplier in American market (US DOE and SCS 1997). Tungsten trioxide($WO_3$) and molybdenum trioxide ($MoO_3$) are also major components of the SCR catalysts. Since most SCR catalysts are proprietary and the complexity of SCR mechanism is very challenging, little detailed knowledge is available about the mechanism of individual catalysts.

The research and development of SCR technique are still undergoing along two main approaches, i.e., developing new catalysts and fining different reducing agents rather than $NH_3$. New specific catalysts are in demand especially for resistance to poisoning by trace metal species present in high-sulfur U.S. coals. Addition of new reducing agents such as hydrocarbons have been investigated to prevent plugging and corrosion of equipment due to reactions between $SO_2$, $SO_3$, $H_2O$ and $NH_3$.

SCR of $NO_x$ by Ammonia or Urea

The basic reactions are as follows:

$$4NO + 4\,NH_3 + O_2 \rightarrow 4\,N_2 + 6\,H_2O \quad (3.13)$$

$$2NO_2 + 4\,NH_3 + O_2 \rightarrow 3\,N_2 + 6\,H_2O \quad (3.14)$$

$$6\,NO + 2(NH_2)_2CO \rightarrow 5\,N_2 + 4H_2O + 2\,CO_2 \quad (3.15)$$

Side reactions:

$$SO_2 + \tfrac{1}{2}\,O_2 \rightarrow SO_3 \quad (3.16)$$

$$2\,NH_3 + SO_3 + H_2O \rightarrow (NH_4)_2SO_4 \quad (3.17)$$

$$NH_3 + SO_3 + H_2O \rightarrow NH_4HSO_4 \quad (3.18)$$

The optimum operating temperature for the SCR process using titanium and vanadium oxide catalysts is about 650-750 °F. Therefore, catalysts are required to have high activity even at relatively low temperatures. $NH_3$ slip is the unreacted $NH_3$ out of the SCR reactor. It is essential to control $NH_3$ slip to less 5 ppm to limit the formation of $(NH_4)_2SO_4$ and $NH_4HSO_4$ and minimize the plugging and corrosion of downstream equipment.

The performance of a SCR process depends on the type of catalyst, the effective surface area of the catalyst, gas residence time, temperature, and the amount of ammonia injected. The kinetics of the SCR reaction is based on the assumption that the reaction is first order with respect to $NO_x$ or $NH_3$. The removal efficiency ($\eta$) of an SCR reactor is defined as the amount of $NO_x$ removed divided by the amount of inlet $NO_x$. It can be expressed in terms of the space velocity (SV) and the molar ratio (m) of ammonia to $NO_x$ (Cho 1994):

$$\eta = m\,(1 - e^{-k/SV}) \tag{3.19}$$

The SCR process can be better represented by a modified Langmuir-Hinshelwood relationship:

$$k/SV = -\ln(1 - x/r) + \ln[(1-x)/(1-x/r)]/KN_o(1-r) \tag{3.20}$$

Where x = fractional conversion of $NO_x$ ( as $\eta$ in equation 3.19)

r = molar ratio of $NH_3$ to $NO_x$ at reactor inlet (as m in equation 3.20)

K = adsorption coefficient of $NO_x$ on the catalyst

$N_o$= $NO_x$ concentration at reactor inlet

SCR of Lean-Burn $NO_x$ by Hydrocarbons

Development of catalysts for lean-burn diesel engines (high excess oxygen and less or no CO, HC present in the exhaust) has attracted attention in the past decade. Different forms of base and noble metal exchanged zeolites, as well as noble metals supported on $\gamma$-$Al_2O_3$ or $TiO_2$ have been extensively investigated for reduction of NO in the exhausts of lean burn diesel engines (Amiridis 1996).

The earlier development and mechanism exploration of lean-burn catalysts were derived from the SCR by ammonia for flue gas as discussed above and the three-way catalysis. The three-way catalysis provides an ideal mode to abate NO with the aid of the reducing compounds, i.e., CO and hydrocarbons (HCs) already present in the exhaust from gasoline engines. Platinum group metals (Pt, Pd and Rh) serve as catalysts for stoichiometric reduction of NO by CO and HCs as follows:

$$2\,NO + 2\,CO \rightarrow 2\,CO_2 + N_2 \qquad (3.21)$$

$$NO + HCs \rightarrow N_2 + CO_2 + H_2O \qquad (3.22)$$

These catalysts are designed exclusively for the rich-burn conditions where there are high enough amounts of CO and HCs while oxygen content is very low. However, lean-burn exhausts do not contain enough amounts of CO and HCs. They instead include a large excess of oxygen up to 10%, high $H_2O$ content of 10-14% and 25-50 ppm sulfur dioxide. In addition, the exhaust temperature can be as high as 973 K. Accordingly, a commercially acceptable lean-burn catalyst should have high activity, broad temperature window of operability, good hydrothermal stability and resistance to poisoning by $SO_2$. (Amiridis 1996).

Ammonia is excluded from the candidate pool of reducing agents because it requires stoichiometric control of reaction, storage and transportation. It is projected that HCs can be either generated from controlling engine combustion or directly converted from fuels fed to engines. The most popular HC used for laboratory studies of lean-burn catalysts is propylene ($C_3H_6$). $CH_4$ also receives some attention due to its abundance and it could be one of the main products converted from diesel fuels.

A comparative study over barium-promoted copper chromite catalysts with various hydrocarbons provided the following findings (Ault and Ayen 1971). For a given NO conversion, an increase in carbon number in hydrocarbons results in a decrease in the required temperature. For a given NO conversion and a given carbon number, the required temperature decreases with degree of saturation. Accordingly, propylene ($C_3H_6$) requires a lower temperature than methane. Ethylene ($C_2H_4$) needs a lower temperature than methane.

Therefore, a new class of lean-burn catalysts is in demand to have the potential to carry out SCR of NO by HCs represented by $C_3H_6$ under excess oxygen conditions:

$$NO + HCs + O_2 \rightarrow N_2 + CO_2 + H_2O \qquad (3.23)$$

Numerous ion exchanged zeolites including Cu-, Fe-, Pt-, Co-, Ga-, Ce-, and H-exchanged zeolites and $\gamma$-$Al_2O_3$ as well as noble metals supported on it have been found to be active for reaction (3.23). Several other catalyst groups including supported transition base metals, mixed metal oxides and pillared clay have also been found to be active. Ion exchanged zeolites and $\gamma$-$Al_2O_3$ supported catalysts have become the two dominant series for SCR systems of lean-burn NO by HCs.

The zeolites, all containing intracrystalline pores and apertures, have dimensions approximately equal to those of many of the molecules converted in a catalytic processes (Gates 1992). ZSM-5, a member of the zeolites family, has been extensively studied for SCR of NO. The average channel size of ZSM-5 is around 0.55 nm, about the same molecular dimension of isoparaffins. Thus, it is large enough to allow small gas molecules such as NO, $NO_2$, $C_2H_6$ and $CO_2$ to pass. ZSM-5 has a relatively high Si/Al ratio (10 or greater), showing relatively high stability of the crystal framework. It is

known that the Si/Al ratio in zeolites affects their acidity-basicity as well as cation exchange capacity related to ion exchange for preparing catalysts.

The mechanisms for SCR of NO by HCs have not been clearly understood although considerable efforts have been made for exploring different mechanisms over various developing lean-burn catalysts. Two important factors have been linked to the activity of ion exchanged zeolites for the SCR of NO by HCs. They are catalyst acidity and the presence of a metal cation associated with reduction and oxidation cycles. A mechanism proposed by Iwanoto and Mizuno is reviewed in the literature (Amiridis 1996). The mechanism involves the formation of an oxygenated intermediate. The intermediate then selectively reduces NO in the presence of excess $O_2$ over Cu-ZSM-5 catalysts forming $CO_2$, $N_2$ and $H_2O$ as final products. This intermediate is believed to be generated from partial oxidation of the HCs.

Alumina ( $\gamma$-$Al_2O_3$) is one of the most active single-metal oxides for the SCR of NO by propene. It can be further promoted with a wide range of metal oxides including cobalt, copper, silver, stannum and wolfram (tungsten). The supported noble metal catalysts, particularly those containing platinum, are active for the SCR of NO by HCs at relatively low temperature in the presence of high water content. The mechanism of SCR reaction by propene over $Pt/Al_2O_3$ could be that the surface of the platinum is kept reduced and a decomposition-type process carries out on the noble metal, leading to the formation of significant amount of $N_2O$ and $N_2$ as well (Meunier 1999).

Another example is given about the exploration of mechanism for $Ag/\gamma$-$Al_2O_3$ catalysts (Meunier 1999). Meunier *et al.* reported that the $\gamma$-$Al_2O_3$ and the low-loading $Ag/\gamma$-$Al_2O_3$ catalysts exhibited high conversions to $N_2$. A mechanism involving the

formation of organo-nitrite species followed by their decomposition/oxidation was suggested to be the main route for the formation of $NO_2$. The promoting role of low Ag loading was attributed to the higher rate of formation of inorganic ad-$NO_x$ species. These inorganic ad-$NO_x$ species further react with the reductant or a derived species to form various organo-$NO_x$ compounds, part of which react with NO or $NO_2$ to yield $N_2$.

## Section III Hybrid Plasma-Catalyst System

$NO_x$ control for diesel-engine vehicles calls for an on-board process which should be compact, reliable and able to effectively reduce $NO_x$ into $N_2$. A hybrid plasma-catalyst system may lead to such an on-board process. The conversion of $NO_x$ to $N_2$ is important for $NO_x$ removal from diesel-engine vehicles where $NO_2$ from a plasma DBD reactor alone is not easy to remove because of the difficulties in installing a wet scrubber.

The physical combination of non-thermal plasma and catalytic reactors forming a hybrid Plasma-catalyst (P-C) system can be achieved with two types of configurations. One is referred to two-stage system consisting of a plasma reactor and catalytic reactor connected in series. The other is called one-stage system with the plasma reactor space packed with a catalyst. The literature information is not very clear on whether there is any scientific benefit in keeping plasma and catalyst in one-stage configuration.

According to Penetrante *et al.* (1998), the plasma-assisted catalytic reduction of $NO_x$ could be described in two steps. In the presence of a hydrocarbon such as propylene, the plasma effectively oxidized NO into $NO_2$:

$$\text{Plasma: } NO + HC + O_2 \rightarrow NO_2 + \text{HC-products} \qquad (3.24)$$

where HC refers to a hydrocarbon and HC-products refers to partially oxidized hydrocarbons. Next step was that $NO_2$ was selectively reduced by the HCs over the catalyst $\gamma$-$Al_2O_3$:

$$\text{Catalyst: } NO_2 + HC \rightarrow N_2 + CO_2 + H_2O \tag{3.25}$$

It was concluded that the plasma oxidation process was partial and it did not further oxidize $NO_2$ to nitric acid. With the aid of HC, the plasma oxidation process was selective. This means only NO was oxidized to $NO_2$ while $SO_2$ oxidation to $SO_3$ was suppressed.

Catalysts used in a P-C system are not limited to $\gamma$-$Al_2O_3$. R&D work of a P-C system should be focused on investigation of plasma reactions and catalytic reactions and development of suitable catalysts corresponding to HCs added to the gas stream.

# CHAPTER IV

# EXPERIMENTAL APPARATUS AND PROCEDURE

The present study includes non-thermal plasma processing of pollutant gases, selective catalytic reduction (SCR) of $NO_x$ and hybrid plasma-catalyst system. The apparatus was set up by designing and adding a catalytic reactor to the existing plasma system. The experimental apparatus used in the present study consists of four sections. They are high-voltage power supply, reactors, gas supply and analytical instrumentation sections as shown in order from top to bottom in Figure 4.1.

## Bench-Scale Dielectric Barrier Discharge Reactor and Catalytic Reactor

Shown in the center of Figure 4.1 are the schematic diagrams of the dielectric barrier discharge (DBD) reactor and the catalytic reactor. The piping system allows the two reactors to be operated either individually or in series with the catalytic reactor on the downstream of the DBD reactor. This gives three experimental modes including DBD reaction only, catalytic reaction only, and hybrid plasma-catalytic reaction.

### Dielectric Barrier Discharge Reactor

The geometry of the DBD reactor is cylindrical. Two concentric stainless steel tubes serve as the electrodes as well as the pressure boundary as shown in Figure 4.2. A high voltage is applied across the two electrodes to initiate discharges with the outer electrode

grounded for safety. The outer diameter (OD) of the central electrode is 3 mm. The inner diameter (ID) of the outer electrode is 23 mm.

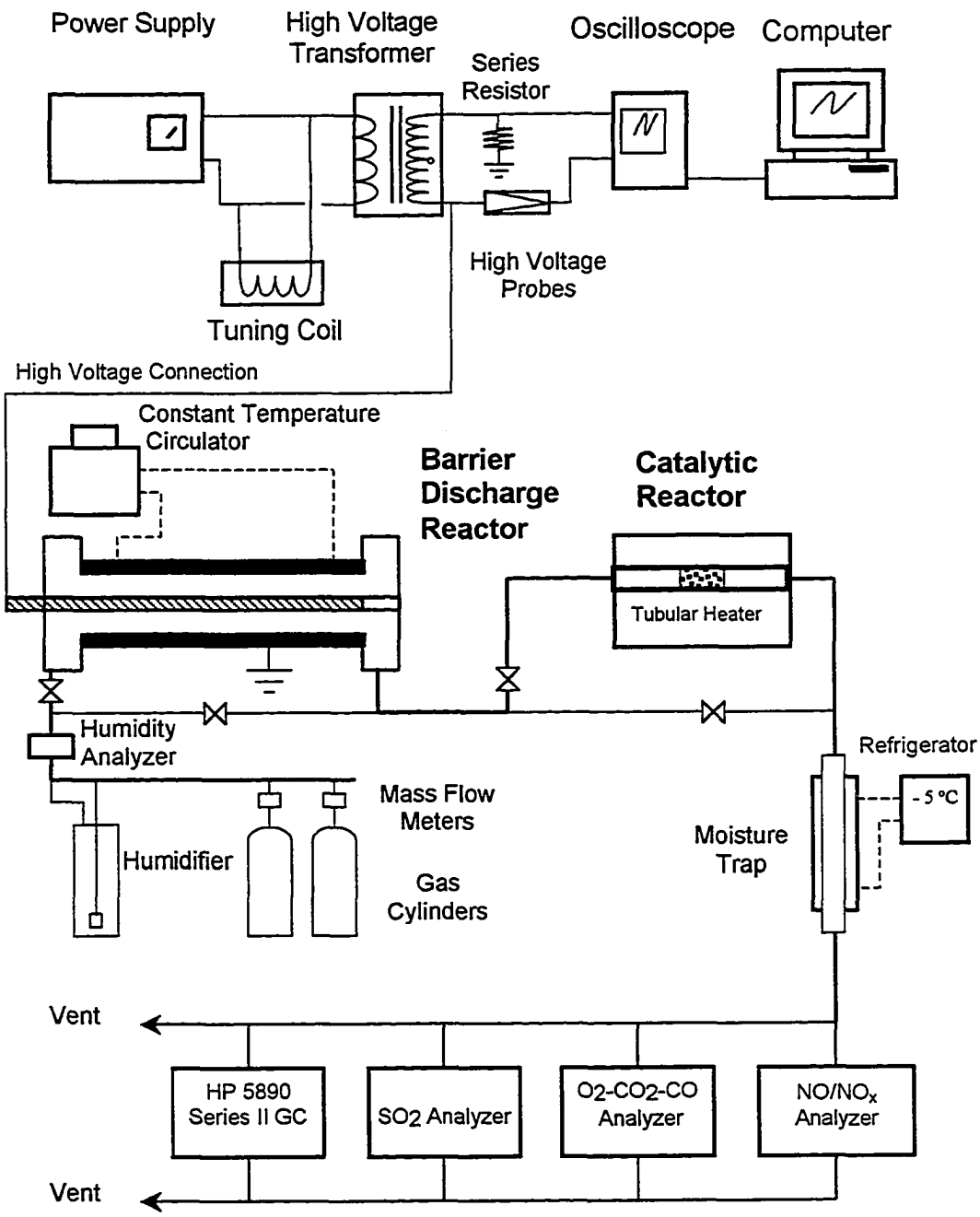


**Figure 4.1 Schematic Diagram of Bench-Top System**

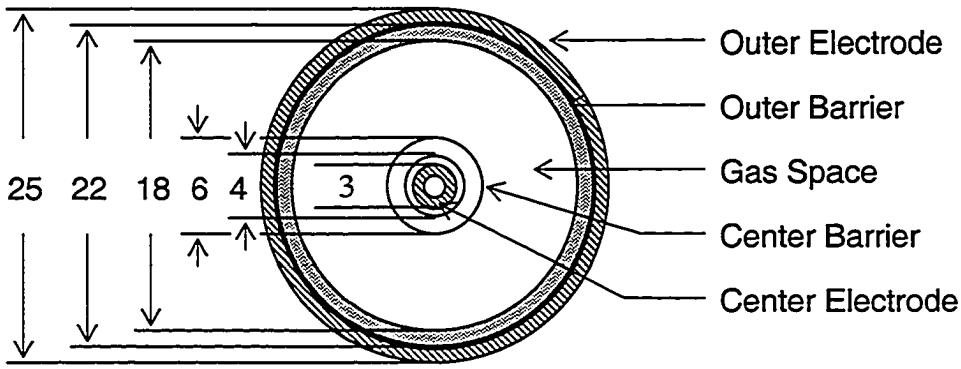


(a) Concentric Cylinder Electrodes – End View (dimension: mm)

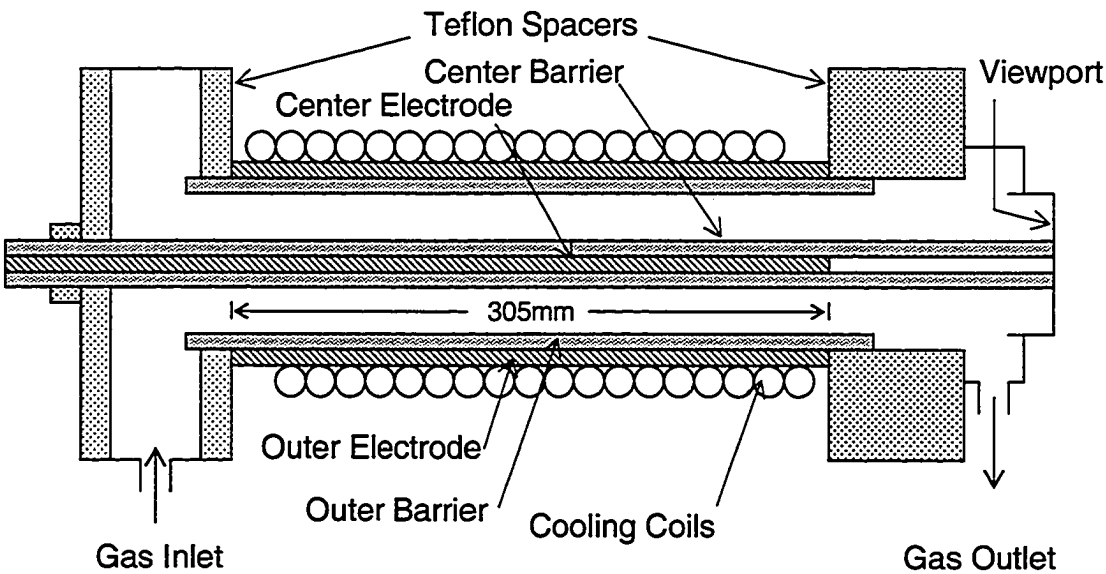


(b) Dielectric Barrier Discharge Reactor

**Figure 4.2 Bench-Top Dielectric Barrier Discharge Reactor**

In order to generate the microdischarges along the length of the electrodes as discussed in Chapter III, at least one piece of dielectric barrier is needed to cover either central or outer electrode. Quartz is selected as the dielectric barrier because of its outstanding dielectric strength, low dielectric loss, high volume resistivity, and good temperature stability as well as high resistance to chemicals. The properties of quartz are listed in Table 4.1. The properties of vycor are also listed for comparison. Quartz and vycor have the same dielectric constant of 3.8. Either material can be used as a barrier to create microdischarges.

**Table 4.1**

**Properties of Dielectric Barrier Materials**

| | | **Quartz** | **Vycor** |
|---|---|---|---|
| Composition | | >99.9% $SiO_2$ | 96% $SiO_2$ |
| Thermal Expansion (m/m-°C) | | $5.5x10^{-7}$ | $8x10^{-7}$ |
| Density ($g/cm^3$) | | 3.6 | 3.5 |
| $Log_{10}$ Volume Resistivity | | | |
| | 25 °C | >17 | 17 |
| | 250 °C | 11.8 | 9.7 |
| | 350 °C | 10.2 | 8.1 |
| Dielectric Properties | | | |
| At 1 MHz, 20 °C | | | |
| | Power Factor | 0.001 | 0.005 |
| | Dielectric Constant | 3.8 | 3.8 |
| | Loss Factor | 0.0038 | 0.19 |
| | Strength (V/m) | $1.67x10^{-7}$ | |
| Dissipation Factor (1MHz) | | 0.0002 | 0.0005 |

In the present study, two quartz tubes are concentrically placed adjacent between the central and outer electrodes as shown in Figure 4.2. The ID and OD of the central quartz tube are 4 and 6 mm, respectively. The ID and OD of the outer quartz tube are 18 and 22 mm, respectively. The annulus between the pair of quartz tubes is gas space where gas

stream is passed through and dielectric barrier discharge occurs. The gap spacing is 6 mm. Most experiments of the present study are conducted with the annular space unpacked. Dielectric packing material glass wool is used in some cases to stabilize discharge.

The effective length of the DBD reaction space is the length along which both electrodes function and generate microdischarges. It is 305 mm (12") as shown in Figure 4.2(b). The reactor volume is 69 $cm^3$ and the residence time is 3.8 seconds when the total flow rate of a gas stream is 1000 $mm^3$(STP)/min Two chambers are attached each to both ends of the concentric electrodes with high electrical insulation material Teflon placed between preventing discharge from occurring outside the discharge region and hurting human. The two chambers also serve as a mixing and stabilizing container for inlet gas and a mixing container for outlet gas, respectively. A view port is installed in the outlet chamber of the reactor in line with the central electrode to observe the discharge.

The DBD reactor was designed to run mostly at room temperature and atmospheric pressure. Copper tube fed with water from a constant temperature bath is wrapped over outer surface of the outer electrode, providing a limited temperature control of the DBD reactor. In addition, the entire reactor could be held in an electrical heating jacket that could be heated up to 100 °C to prevent condensation in the inlet and outlet chambers. However, it was recommended that the experiments should be run below 100 °C because of the softening of the insulation material Teflon and other sealing materials of the reactor at higher temperatures.

Same apparatus is used for the study of $SO_2$ removal by barrier discharge. In addition, three rectangular reactors and one square reactor are designed and built to

investigate the effect of reactor geometry as well as barrier materials. Figure 4.3 shows their geometries. Other detailed data are listed in Table 4.2.

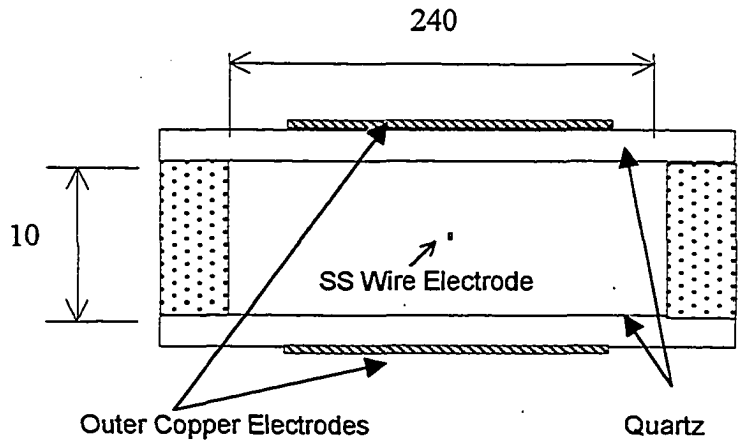


(a) Rectangular DBD Reactor – End View (dimension: mm)

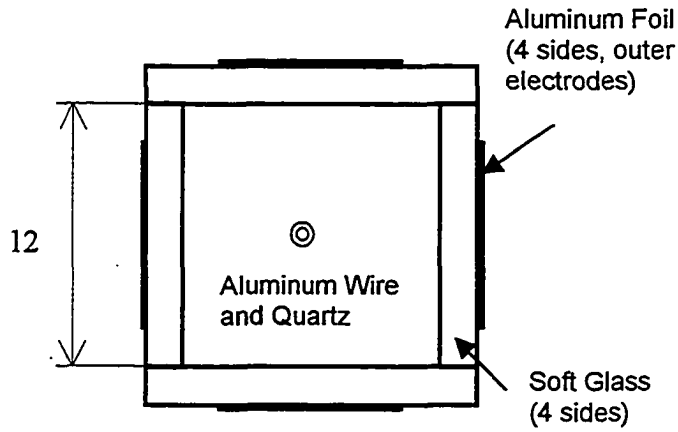


(b) Square DBD Reactor– End View (dimension: mm)

**Figure 4.3 Rectangular and Square DBD Reactors**

**Table 4.2**

**Specification of Reactors**

| Reactor Geometry | Cylindrical | Rectangular-A, B, C | Square |
|---|---|---|---|
| Electrode(high volt) | SS tube (o.d. ϕ3 ) | SS wire(ϕ0.5) | Aluminium wire(ϕ0.5) |
| Electrode(grounded) | SS tube(i.d.ϕ23 ) | Copper strips | Aluminum foil |
| Barrier covering electrode (high volt) | Quartz tube (i.d. ϕ4x1 mm ) | None | Quartz tube (i.d. ϕ1x1mm ) |
| Barrier covering Electrode(grounded) | Quartz tube (i.d. ϕ18x2 ) | Plate- A: quartz (3.2 thick) B: soft glass(3.0 thick) C: composite mica (2.4 thick) | Soft glass (15x3.0 thick) |
| Gas spacing, mm | 6 | 5 | 6 |
| Cross-section area, $mm^2$ | 226 | 24x10 | 218 |
| Length of reactor, mm | 300 | 200 | 280 |
| Volume of reactor, $cm^3$ | 69 | 48 | 61 |

Catalytic Reactor

As mentioned in the beginning of this chapter, the catalytic reactor was installed downstream of the DBD reactor. However, the piping system would allow the catalytic reactor to be fed directly with gas stream bypassing DBD reactor.

Catalytic reactor specification. The catalytic reactor consists of a Vycor tube packed with a catalyst, a thermocouple probe embedded in the center of catalyst bed, and a tubular heater. It is shown in the center section of Figure 4.1. The ID and OD of the Vycor tube are 21 and 25 mm, respectively. The reactor tube is packed with a catalyst that is held in place with ceramic wool (Cotronics Corp., containing $Al_2O_3$, CaO and $Si_3N_4$ ). The length of packed bed is 30 mm. The tubular electric heater is Type 55035 from Lindberg with maximum attainable temperature of 1100 °C.

Catalyst preparation. $\gamma$-$Al_2O_3$ as 1/16" sphere (surface area: 350 $m^2/g$, bulk density: 0.662 $g/cm^3$, Alcoa Industrial Chemicals) is used as a catalyst and support for $WO_3$ as well. Three catalysts are prepared with 1%, 3% and 12% $WO_3$ loading on $\gamma$-$Al_2O_3$ each. The precursor of $WO_3$ is ammonium metatungstate hydrate (AMT,

$(NH_4)_6W_{12}O_{39}{\cdot}xH_2O$, Aldrich). About 15 g of $\gamma$-$Al_2O_3$ is taken and put in an oven at 200 °C for about 2 hours to drive away the moisture. The alumina is cooled and weighed. On the basis of this dry weight, a corresponding amount of AMT is weighed for preparing the required $WO_3$ loading such as 1%, 3% or 12%. The required amount of AMT is dissolved in water and the solution is then added to a porcelain dish with the dry $\gamma$-$Al_2O_3$. The liquid should be well spread over all spheres by stirring gently. The dish is placed above a Bunson burner and the water is evaporated slowly to prevent AMT loss. When no liquid is observed, the dish is placed in an oven first at 100 °C for 2 hours and then at 500 °C for another 5 hours to calcinate the catalyst. The three catalysts prepared in this study have not been characterized to confirm their $WO_3$ loading amounts and dispersion due to instrumentation limitations.

## High-Voltage Power Supply and Measurement

Shown in the top section of Figure 4.1 is the system of high-voltage (HV) AC power supply. It consists of two parts – HV generation and power measurement. The detailed description can be found elsewhere (McLarnon 1996).

### HV Generation

A Powertron 500S (variable 0-120 V and variable 20-20,000 Hz) power supply is used to power a Neeltran HV transformer (KVA 0.5, Frequency 60-10 k $\phi$1, primary 120V, secondary 25,000V). A set of inductors (Stancor, two C-2687 and two C-2686 units connected in series) is connected in parallel with the HV transformer to tune the circuit to the power supply.

HV Power Measurement

The high voltage supplied to the DBD reactor is monitored and measured by a Tektronix 2211 digital storage oscilloscope sampling at 20 MHz. The HV signal is first reduced with a Tektronix P6015 HV probe (1000x) in series with a Tektronix P6109 probe (10x) before being fed to channel 1 of the oscilloscope. The current in the secondary circuit of the HV transformer is indirectly measured using a resistor of 50 Ω (CP-10 Mexico 98208, 10% Dale, 10w) and a Tektronix P6027(1x) probe. This signal is fed to channel 2 of the oscilloscope.

Power consumption in the DBD reactor is calculated using the voltage and current traces recorded and stored by the oscilloscope. By multiplying the corresponding current and voltage values at the same phase angle, a curve of point power is obtained and it is averaged to give the discharge power (Manley 1944). A computer is installed on line to read the values recorded by the oscilloscope and calculate the discharge power (McLarnon 1996).

## Gas Supply

The major components in flue gases or engine exhausts are nitrogen ($N_2$), water vapor ($H_2O$), carbon dioxide ($CO_2$) and oxygen ($O_2$). $NO_x$ are minor components present in the gas, typically of the order of hundreds ppm. Accordingly, experimental designs for $NO_x$ removal generally need to take into account the major components. On the other hand, $NO_x$ in simple gas mixtures ($N_2$, He or $N_2/O_2$) or even pure $NO_x$ have been frequently used as feed gas for bench-top studies. These simplified experiments would help identify prime

reactions and understand the complicated reaction mechanisms within DBD reactors step by step.

Gas supply section is illustrated exactly under the DBD reactor in Figure 4.1. Simulated flue or exhaust gas is prepared using cylinders of nitrogen, air, carbon dioxide, NO in nitrogen, methane, etc. Hastings model ST and 200H mass flow meters are used to measure the flow rates of dry gases from each of the cylinders. Water vapor is added to the gas stream by passing the nitrogen stream through a glass bubbler containing water. The tubing used throughout the system is either stainless steel or Teflon to minimize the adsorption on the walls of NO or any of the products from the DBD reactor. Heating tapes are used to preheat the gas stream and prevent condensation before it enters the DBD reactor if experiments are conducted at temperatures above room temperature.

## Analytical Instrumentation

The most analytical work is to measure concentrations of known gas components as well as to identify unknown gas products. The tubing system shown in Figure 4.1 allows to take sample from inlet gas stream, outlet gas stream from the DBD reactor(also inlet gas stream to the catalytic reactor for plasma-catalyst run mode), or outlet gas stream from the catalytic reactor. All gas samples are passed through a moisture trap (glass tube with cooling jacket fed with a refrigerator (-5 °C, Polyscience Division of Preston Industries, Inc) to minimize the water vapor before the gas streams are fed to any analytical equipment. The heating tapes are used to prevent condensation in the tubing between outlet of the two reactors and the moisture trap. Several commercial gas analyzers are used on-line. In

addition, gas sample can be taken in a 10cm gas cell that is exclusively used for FTIR to identify and measure $N_2O$ in particular.

NO/$NO_2$/$NO_x$ Analysis

A Thermo-Electron model 10A/R Chemiluminescent NO-$NO_2$-$NO_x$ analyzer is used to measure the NO and $NO_x$ (NO and $NO_2$ collectively referred as $NO_x$). The principle of analysis used in the device is the reaction: $NO + O_3 \rightarrow NO_2^* + O_2$. The light emitted from the excited $NO_2^*$ is measured by a photomultiplier tube and the corresponding NO concentration is determined. $NO_x$ concentration is measured by first passing the sample through a high temperature (650°C) stainless steel converter where $NO_2$ ($N_2O_4$ or $N_2O_5$ if any) is converted to NO, which is subsequently measured. The difference between NO and $NO_x$ readings is taken to be the concentration of $NO_2$.

Nitrous Oxide ($N_2O$) Analysis

In the present study, Nicolet 520 FTIR Spectrometer is used to analyze the products of the gas streams from the plasma reactor and catalytic reactor. This instrument is not installed on line. A gas cell is used to transport samples. The path length of the gas cell is 10 cm. The detection limit for $N_2O$ is found to be 3 ppm for this gas cell using a calibration standard gaseous mixture of $N_2O$-$N_2$.

Data in the literature (Wallin 1997) show that $N_2O$ peak is well-formed around the 2270 - 2159 $cm^{-1}$ region using a FTIR spectrometer and good for a quantitative analysis. The peak height of a gas is given in terms of absorbance and it is in linear relationship with the gas concentration.

$O_2$-$CO_2$-CO Analysis

A Nova model 375 portable combustion analyzer is used to measure the $O_2$, $CO_2$ and CO concentrations in the gas stream. The $O_2$ and CO analyses are performed using electrochemical cells while the $CO_2$ analysis is realized using an infrared cell.

Hydrogen, Methane, Ethylene and Acetylene Analysis

A Hewlett-Packard 5890 Series II gas chromatograph with a SUPELCO column packed with 60/80 Carboxen-1000 is used to analyze $CH_4$, $C_2H_4$ and $C_2H_2$ in the gas stream when a reducing agent such as $CH_4$ or $C_2H_4$ is added to the simulated gas mixture. A thermal conductivity detector equipped in the GC is used with helium as carrier and reference gas. Hydrogen could be one of products from DBD reactor. The measurement of a small amount of hydrogen with TCD needs nitrogen as reference and carrier gas because the thermal conductivity coefficients of both hydrogen and helium are of the same magnitude. This arrangement has the advantage of avoiding large signal of balance nitrogen gas in the sample.

Humidity Analysis

A Traceable Hygrometer (VWR) with probe is used to measure the humidity of the gas stream. The meter is of accuracy within $\pm$ 2% for a relative humidity (RH) range of 40-80%. It also reads temperature of the gas stream. By referring to the saturated water vapor content at the measured temperature, the water vapor concentration present in the gas stream is calculated with the RH reading.

$SO_2$ Analysis

A Rosemount model 880 non-dispersive infrared analyzer is used to measure $SO_2$ concentration in gas stream when a $SO_2$-$N_2$ mixture is passed through the DBD reactor.

# CHAPTER V

# RESULTS AND DISCUSSION

This chapter is divided into four sections. The first section deals with the reactions of $NO_x$ in a dielectric barrier discharge (DBD) reactor. The second pertains to the selective catalytic reduction (SCR) of $NO_x$ in a catalytic reactor. Hybrid plasma-catalyst system for $NO_x$ removal is studied in the third section. The fourth section is focused on DBD reactor design parameters.

## Section I Dielectric Barrier Discharge for $NO_x$ Removal

A systematic fundamental investigation of DBD plasma for the removal of $NO_x$ is undertaken and the results are presented in this section. Experiments are conducted with respect to electrical parameters and chemical compounds.

Electrical Parameters:

- Electric voltage
- Electric frequency
- Energy density
- Temperature

Chemical Compounds:

- Pollutant concentration
- Total flow rate (residence time)
- Oxygen concentration

- $CO_2$ concentration
- Water vapor concentration
- Reducing compounds: CO, $CH_4$ and $C_2H_4$

Conversion of pollutants is measured in terms of inlet and outlet concentrations as follows:

$$\text{Pollutant Conversion (\%)} = \frac{C_{inlet} - C_{outlet}}{C_{inlet}} \times 100 \qquad (5.1)$$

where: $C_{inlet}$ = Concentration of Inlet Pollutant (ppmv)
$C_{outlet}$ = Concentration of Outlet Pollutant (ppmv)

NO conversion is referred as percentage of inlet NO converted to $NO_2$, $N_2$, $HNO_3$ and/or $N_2O$. Since $NO_x$ represents both NO and $NO_2$, $NO_x$ conversion can be used to estimate inlet NO converted to $N_2$ if no $HNO_3$ and $N_2O$ are formed in the process.

The discharge energy is calculated either as specific energy (kJ/mole-$NO_x$ removed, kJ/mole-$NO_x$ inlet or eV/molecule-$NO_x$ removed) or energy density ( J/L). The specific energy is defined as the energy supplied to the gas per mole of the removed $NO_x$, per mole of inlet $NO_x$ or per molecule of the $NO_x$ removed. The energy density is referred as the energy supplied to a unit volume of gas stream. Specific energy is only associated with the total amount of $NO_x$ while energy density takes into account the whole gas stream. Energy density is used in this study because its concept is simple and direct.

The electrical variables, in a barrier discharge, affect the operation of the system in two major ways. First, the effective use of these parameters can enhance the efficiency of the discharge process to achieve an optimal conversion as measured by the pollutant

conversion, voltage and energy requirements. Secondly, the reaction path sequence and consequently the product slate can be controlled. All of the experimental results are obtained using a simulated mixture of a pollutant and other gas(es).

Effects of Operating Conditions

Electric frequency selection. In a barrier discharge system with an ac power supply, the reactions are a function of the electric energy deposited into the gas passing through rather than voltage or frequency. An increase in voltage or frequency will result in an increase in energy input. Total energy consumption is the sum of discharge power and other circuit consumption (transformer, inductors, etc.).

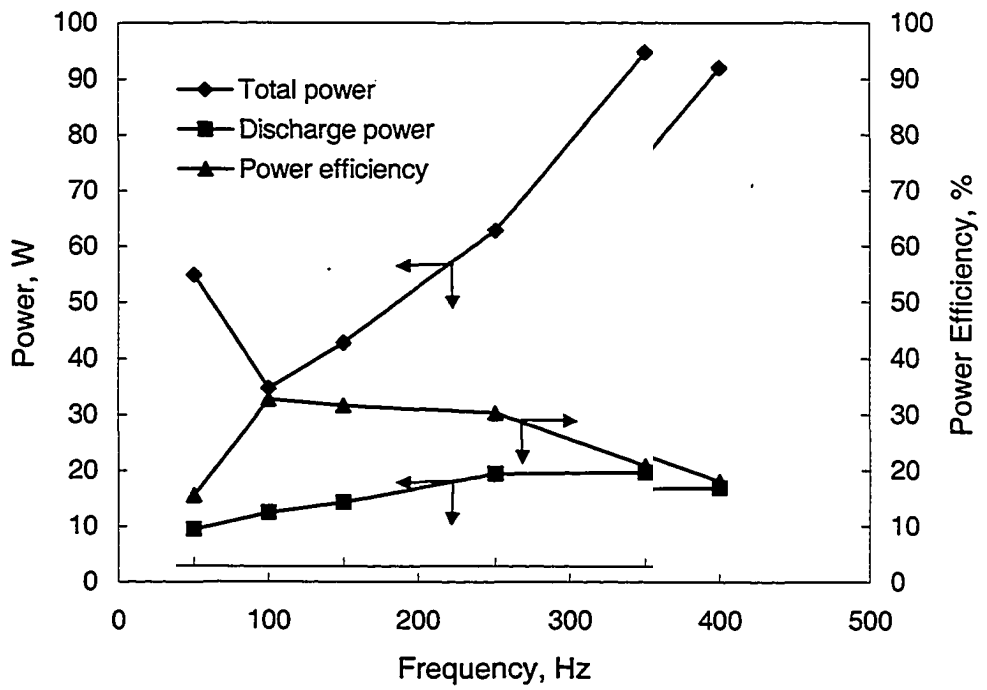


**Figure 5.1 Power Input/Efficiency vs. Frequency.** Primary voltage 80 V (peak voltage 27.6 kV), test gas 1900 SCCM nitrogen at room temperature.

The present study investigates the effects of frequency on total energy consumption and discharge power. Power efficiency is referred to the ratio of discharge power to total power. Since $N_2$ serves as balance gas and it accounts for 90 - 99.9% of mixtures used in the present study, for simplicity, a pure $N_2$ gas is fed to the DBD reactor. It is found that the power efficiency reached the maximum at a frequency of 150 Hz for this barrier discharge system (Figure 5.1). Therefore, most of the experiments are conducted at a frequency of 150 Hz. It should note that other components such as $O_2$ and $H_2O$ in particular could have strong effects on DBD plasma process. Therefore, a more appropriate frequency could exist.

Effect of temperature on $NO/NO_x$ conversions. The temperature variation of an inlet gas stream depends on its source and operating conditions. The temperature of exhaust from an engine or flue gas from a combustion process is generally much higher than room temperature. Depending upon the materials of construction of the DBD reactor, gas temperature change can range from 25 to 65 °C. A mixture of 250 ppm NO in balance $N_2$ is used for this study. Figure 5.2 shows that $NO/NO_x$ conversions at 65 °C are higher than those at 25 °C. The increase in conversion can be as high as 15 percent points at an energy density of 150 J/L.

A change in temperature would have an effect on $NO/NO_x$ conversions because it causes changes in reaction rates, gas volume (i.e., residence time change), barrier material properties associated with DBD, etc. Within the range of temperature change (25-65 °C), gas volume increases by about 13% but the dielectric constant of quartz remains unchanged (Hippel and Robert 1954). According to reaction kinetics, higher gas

temperatures generally increase reaction rate. The following two main reactions can be used to explain the increase in conversion (Gentile and Kusher 1996):

$$NO + N \Longrightarrow N_2 + O \qquad k_1 = 3.1X10^{-11}(T/300)^{1/2}\ cm^3s^{-1} \tag{5.2}$$

$$N + N + M \Longrightarrow N_2 + M \quad k_2 = 3.9X10^{-33}(T/300)^{-3/2}\ cm^6s^{-1} \tag{5.3}$$

An increase in temperature will favor reaction (5.2), resulting in a higher reaction rate of conversion of NO into $N_2$. $k_2$ will decrease as temperature increases, thereby limiting active nitrogen atom combination as per reaction (5.3) and leaving more N available for reaction (5.2). Therefore, higher gas temperature will help $NO/NO_x$ conversions.

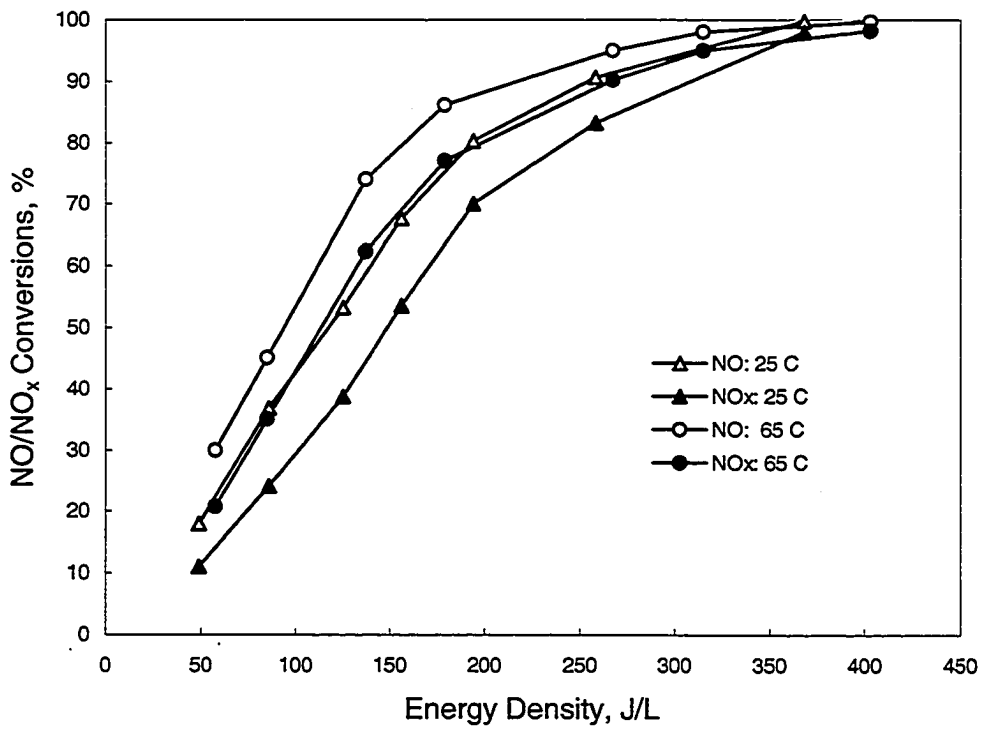


**Figure 5.2 Effect of Temperature on Dry $NO/NO_x$ Conversions.** Frequency 150 Hz, total flow rate 1000 SCCM: 250 ppm NO and $N_2$ balance.

Effect of total flow rate (residence time). Figure 5.3 shows that NO conversion is almost the same for an increase in the total flow rates from 1000 to 2000 SCCM (i.e.,

residence time from 8 to 4 seconds) at a given energy density of less than 250 J/L. However, $NO_x$ conversion is improved from 54% to 64% as the flow rate increases from 1000 to 2000 SCCM at the energy density of 150 J/L. Under present operating condition, higher flow rate, i.e., lower residence time is beneficial to $NO_x$ conversion.

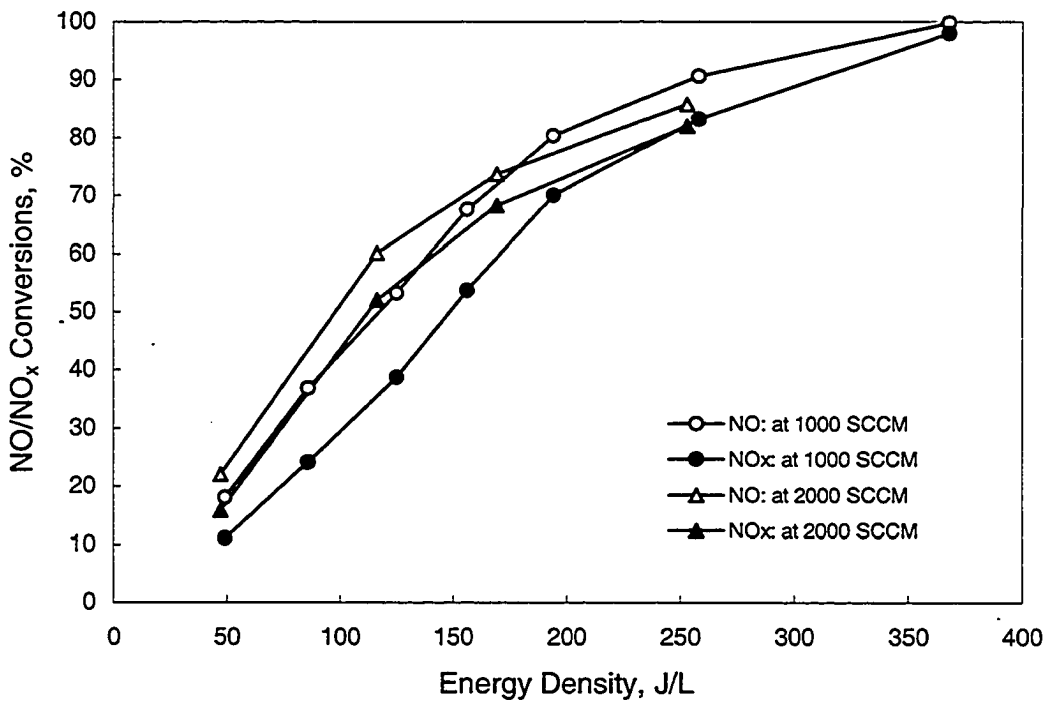


**Figure 5.3 Effect of Total Flow Rate on $NO/NO_x$ Conversions.** Inlet NO concentration 250 ppm, $N_2$ balance, 150 Hz, room temperature.

This observation is in agreement with McLarnon's (1996) experimental result that the residence time in the reactor did not affect $NO_x$ conversion. However, the methods for obtaining varied residence time were different. In the present study, total flow rate is varied to change residence time. The change in residence time in McLarnon (1996) was realized by changing the length of the inner electrode, thereby changing the volume of discharge region. It might significantly change the capacitance of the reactor and affect the discharge efficiency.

Effect of inlet NO concentration. Concentrations of 250 and 510 ppm NO in $N_2$ are used to investigate the effect of inlet NO concentration on $NO/NO_x$ conversions. Figure 5.4 shows that lower inlet concentration of NO leads to higher conversion under the same energy density. At an energy density of 250 J/L, 90% and 60% NO conversions are achieved for inlet concentrations of 250 and 510 ppm, respectively. Lower NO concentrations effectively give a larger excess of radicals and electrons. Therefore, there is a greater likelihood for reactions converting NO to $N_2$. It is also observed that the conversion for 250 ppm inlet NO at an energy density of $E$ is equal to the conversion for 510 ppm inlet NO at $2E$. In other word, twice the NO concentration requires double energy input for a given $NO/NO_x$ conversions.

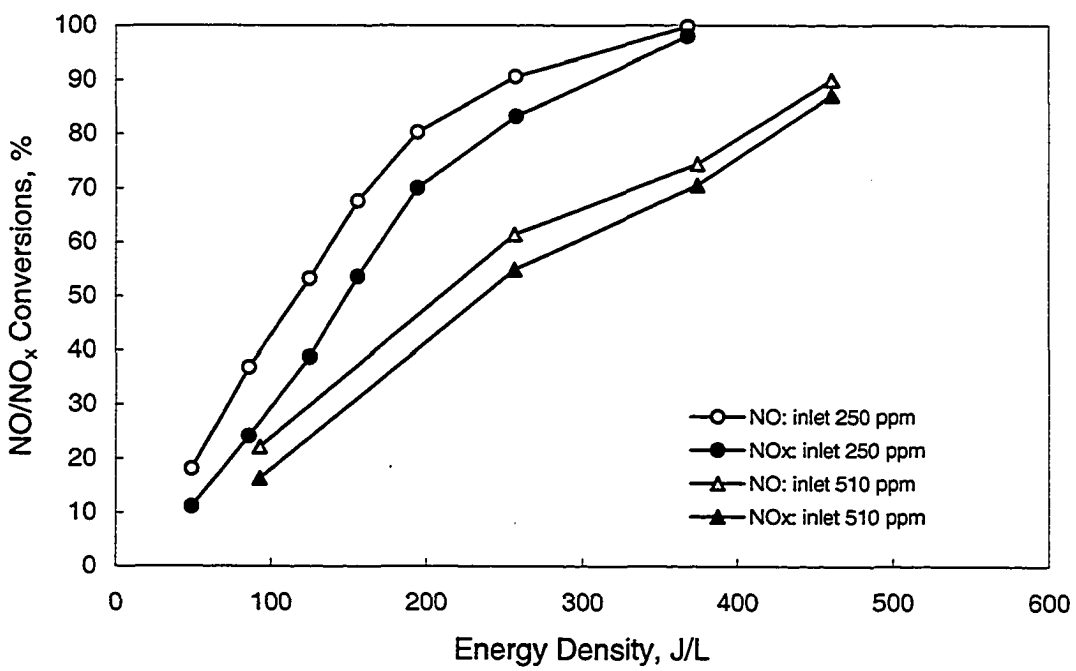


**Figure 5.4 Effect of inlet NO Concentration on $NO/NO_x$ Conversions.** Total flow rate 1000 SCCM, NO and $N_2$. 150 Hz, room temperature.

Effect of both total flow rate and inlet NO concentration. Comparing Figure 5.5 with Figures 5.3 and 5.4, it is found that the two factors, inlet NO concentration and total flow rate have independent effects on $NO/NO_x$ conversions. The $NO/NO_x$ conversions are 40 and 50%, respectively for the feed of 510 ppm NO and 2000 SCCM at 200 J/L. This results are comparable with those for the feed of 510 ppm NO and 1000 SCCM. Therefore, the effect of inlet NO concentration on $NO/NO_x$ conversions is dominant.

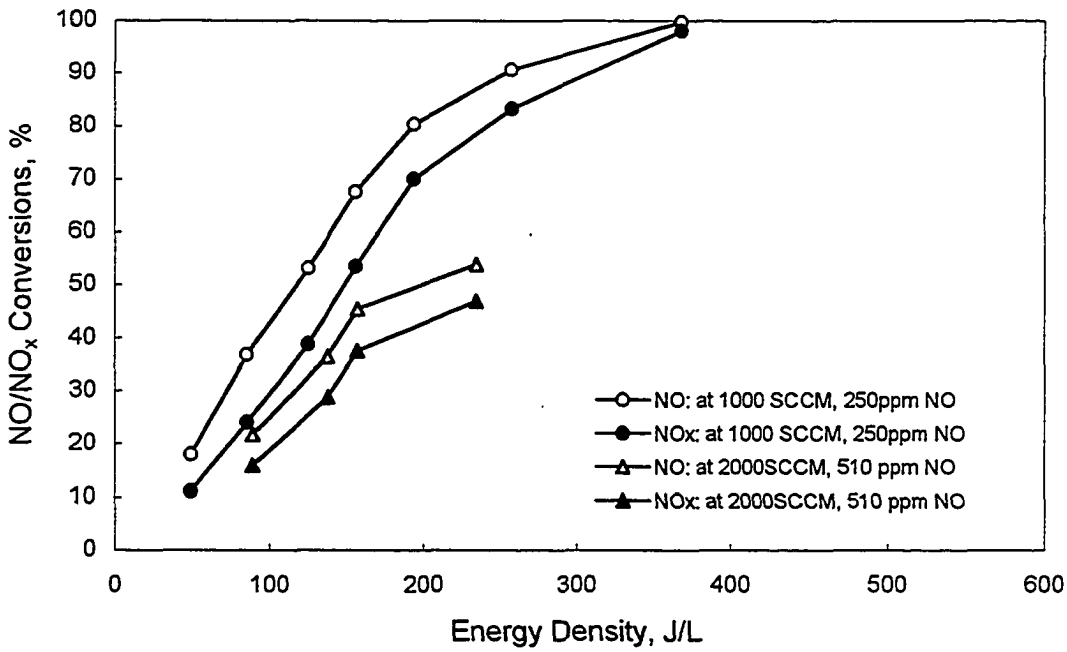


**Figure 5.5 Effect of both Residence Time and Inlet NO Concentration on $NO/NO_x$ Conversions.** 150 Hz, room temperature.

$NO/NO_x$ conversions in moist Mixture with He as balance gas. A literature review reveals that some workers (Luo and others 1998) investigated NO removal by employing He as carrier gas instead of $N_2$ (present with most flue gas or engine exhaust). Two factors should receive special consideration while interpreting experimental results:

1) the difference of energy absorption between He and $N_2$
2) N radicals participate in the main reaction for NO-$N_2$ gas mixture:

$$N + NO \rightarrow N_2 + O \qquad (5.4)$$

Experiments are conducted with inlet NO concentrations of 50 and 360 ppm in the presence of moisture with He as balance gas. Results presented in Figure 5.6 show that outlet $NO/NO_x$ concentrations approach zero as energy density is increased. It is proposed that the reactions (5.5) and (5.6) are highly dominant, accounting for the 100% conversion.

$$H_2O + e \rightarrow H + OH + e \quad (5.5)$$

$$OH + NO \rightarrow HNO_2 \quad (5.6)$$

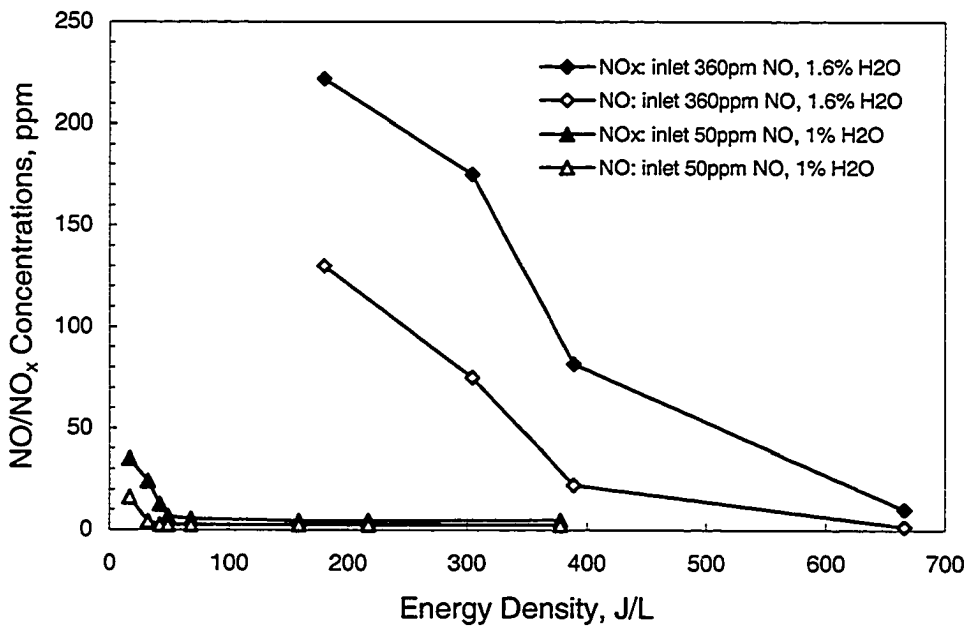


**Figure 5.6 Outlet $NO/NO_x$ Concentrations in the Presence of Water with He as Balance Gas.** Total flow rate 1000 SCCM, 150 Hz, room temperature.

$NO/NO_x$ conversions in the presence of moisture with $N_2$ balance. Experiments are conducted with inlet NO concentrations of 0, 50 and 250 ppm when moisture is present with $N_2$ as balance gas. Results presented in Figure 5.7 show that outlet $NO/NO_x$ concentrations for 50 ppm and 250 ppm inlet NO remain above 50 ppm even at a high energy density of greater than 500 J/L. Under the same experimental conditions without

NO in the feed stream, $NO/NO_x$ are detected from the outlet of the DBD reactor, 50 ppm $NO_x$ at energy density of 500 J/L. This suggests that $NO_x$ is formed in the DBD reactor. The following reaction is proposed to take place at high energy density (greater than 100 J/L):

$$N + OH \rightarrow NO + H \qquad (5.7)$$

Reaction (5.7) accounts for $NO_x$ formation. It can be concluded that in the presence of moisture and $N_2$ only, the concentrations of outlet $NO/NO_x$ from the DBD reactor probably cannot be reduced much below 50 ppm.

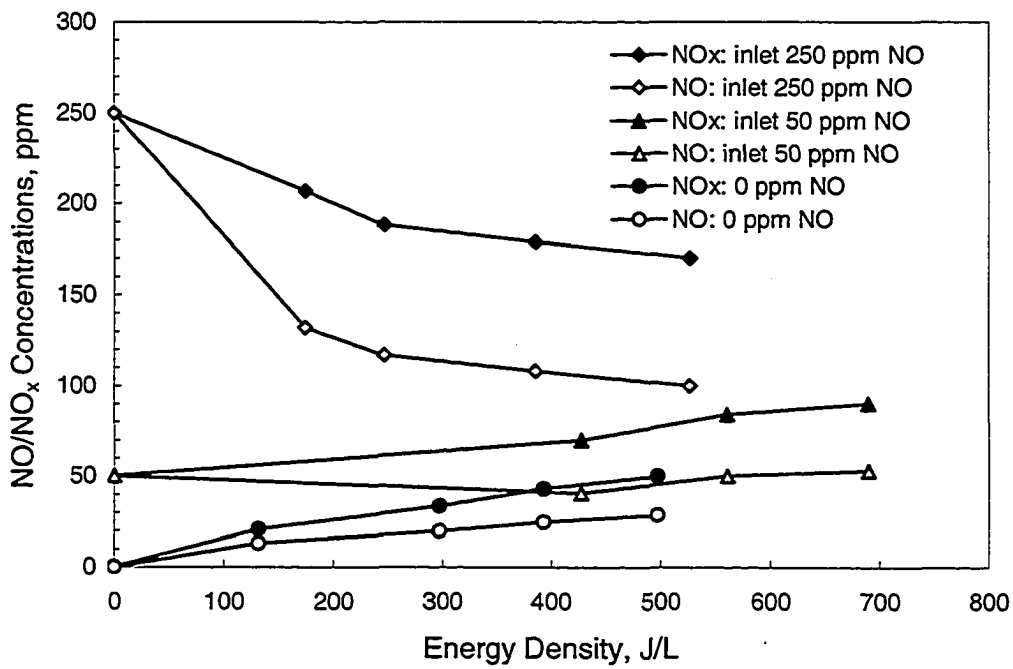


**Figure 5.7 Outlet $NO/NO_x$ Concentrations in the Presence of 1% Water with $N_2$ as Balance Gas.** Vapor Total flow rate 1000 SCCM, 150 Hz, room temperature.

$NO/NO_x$ Conversions under Dry and Wet Conditions

Effect of oxygen concentration on $NO/NO_x$ conversions. Considerable amount of oxygen is present in power plant flue gases or engine exhausts, especially in exhausts

from lean-burn systems. Oxygen is a very active component and its effect on $NO/NO_x$ conversions in a DBD reactor needs to be studied in detail. Several oxygen concentrations ranging from 0 to 10% are used to investigate the effect. Figures 5.8 and 5.9 show the effects of oxygen concentration on NO and $NO_x$ conversions as a function of energy density, respectively. In general, the $NO/NO_x$ conversions decrease significantly in the presence of oxygen. The effect of $O_2$ on $NO/NO_x$ conversions is significant under dry conditions. When $O_2$ concentration increases from 0 to 6%, $NO/NO_x$ conversions decrease significantly from 99% to 50% and from 98% to 6%, respectively at the energy density of 370 J/L. As $O_2$ concentration increases from 6% to 10%, NO conversion goes up while $NO_x$ conversion keeps decreasing slowly toward zero. A detailed kinetic explanation is provided later.

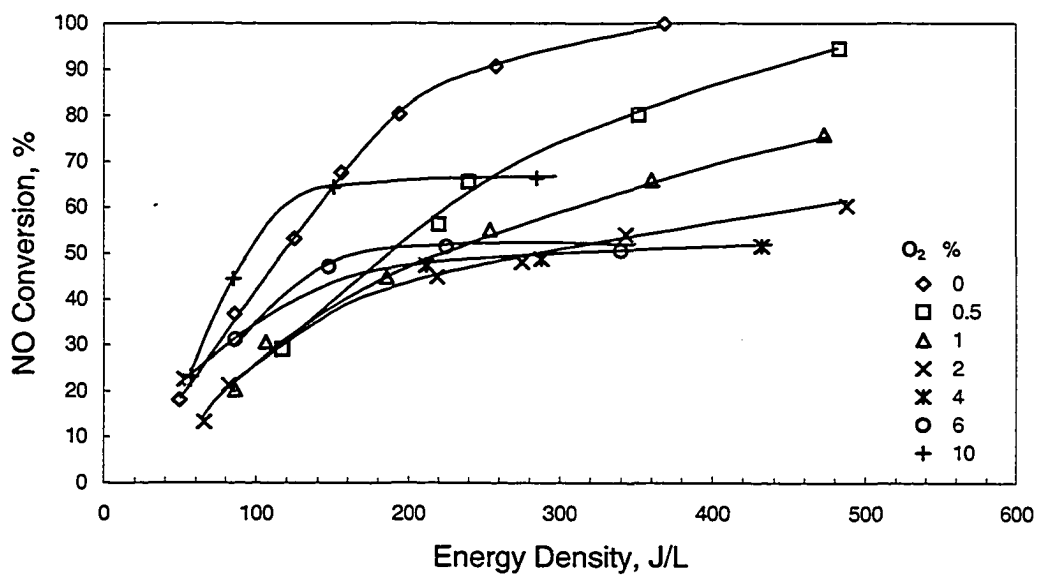


**Figure 5.8 Effect of Oxygen Concentration on NO Conversion as a Function of Energy Density.** Total flowrate 1000 SCCM, 250 ppm NO with $N_2$ balance, 150 Hz, room temperature.

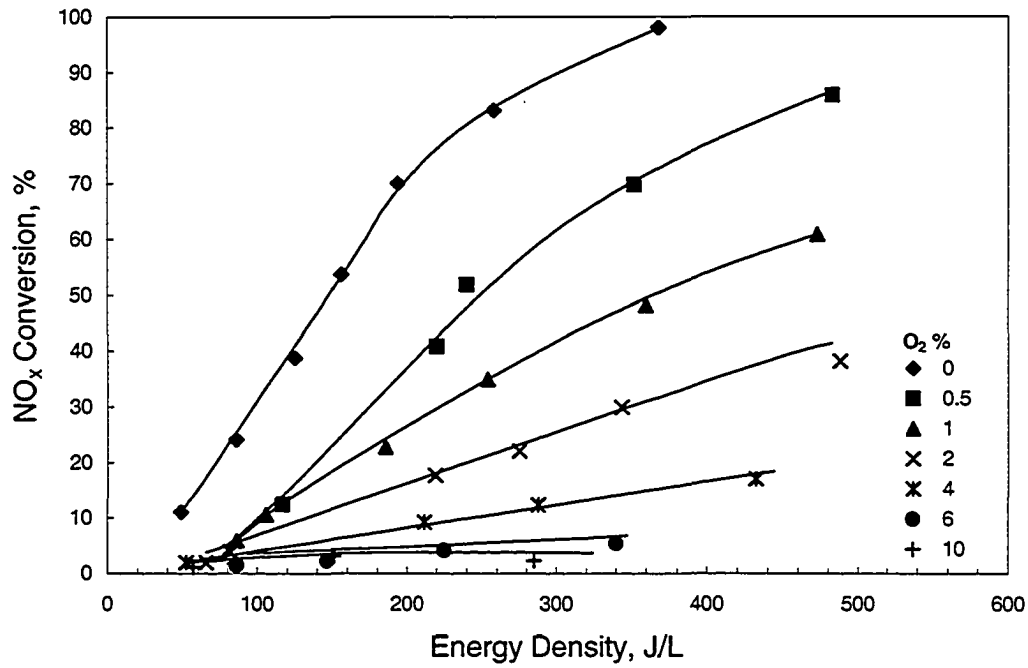


**Figure 5.9 Effect of Oxygen Concentration on $NO_x$ Conversion as a Function of Energy Density.** Total flowrate 1000 SCCM, 250 ppm NO with $N_2$ balance, 150 Hz, room temperature.

Chemistry. At energy densities of 80, 150 and 320 J/L, data taken from Figures 5.8 and 5.9 are plotted as Figure 5.10. The result presented in Figure 5.10 shows the effect of oxygen concentration in a mixture of $NO/O_2/N_2$ on $NO/NO_x$ conversions. At low $O_2$ concentrations(<1%), a small increase in $O_2$ content results in a significant drop in $NO/NO_x$ conversions at 150 J/L. An increase in energy density to 320 J/L greatly enhances $NO/NO_x$ conversions. At higher $O_2$ concentration (>1%), NO conversion increases as $O_2$ concentration is increased while $NO_x$ conversion decreases close to zero. An increase in $O_2$ concentration from 1% to 10% leads to a significant increase in $NO_2$ formation. There are several reactions proposed by McLarnon and Penetrante (1998) to occur in the plasma as follows:

$$e + N_2 \rightarrow e + N + N \qquad (5.8)$$

$$N + NO \rightarrow N_2 + O \quad (5.9)$$

$$e + O_2 \rightarrow e + O(^3P) + O(^3P) \quad (5.10)$$

$$e + O_2 \rightarrow e + O(^3P) + O(^1D) \quad (5.11)$$

$$O(^1D) + M \rightarrow O(^3P) + M \quad (5.12)$$

$$O(^3P) + NO + M \rightarrow NO_2 + M \quad (5.13)$$

$$O(^3P) + O_2 + M \rightarrow O_3 + M \quad (5.14)$$

$$O_3 + NO \rightarrow NO_2 + O_2 \quad (5.15)$$

where, $O(^3P)$ and $O(^1D)$ are ground-state and metastable excited-state oxygen atoms, respectively and M is either $N_2$ or $O_2$.

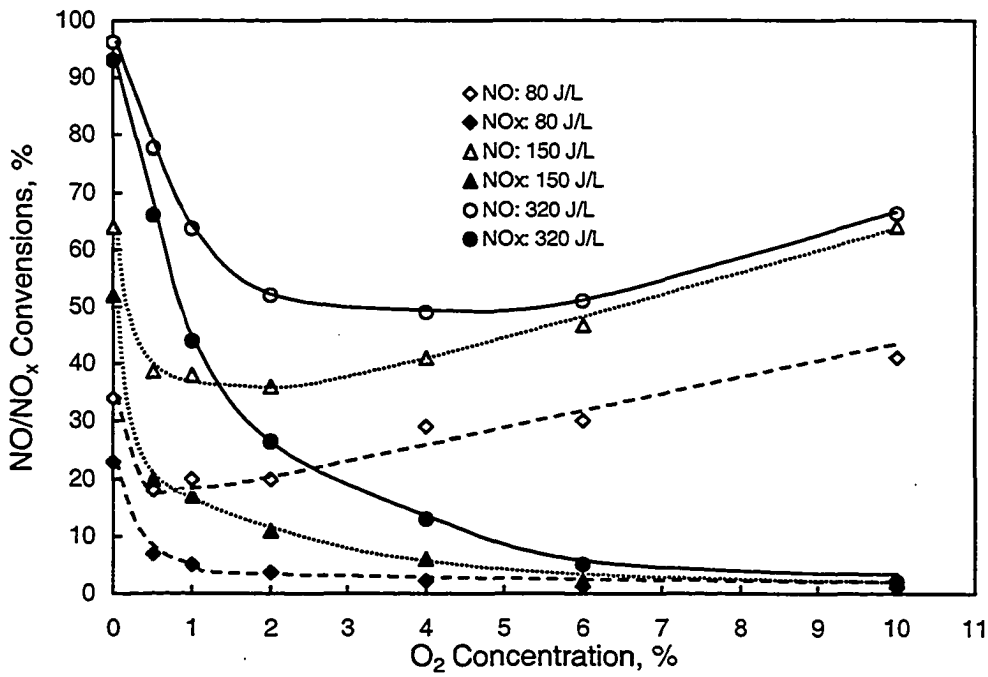


**Figure 5.10 Effect of Oxygen Concentration on $NO/NO_x$ Conversions.** Total flow rate 1000 SCCM, 250 ppm NO with $N_2$ balance, 150 Hz, room temperature.

Variations in NO conversions at different energy densities are due to the competition between reactions (5.9) and (5.13) or (5.15). At $O_2$ concentration less than

1%, the dominant reaction (5.9) mainly contributes to NO conversion into $N_2$ although the presence of $O_2$ competes for consuming electrons via reactions (5.10) and (5.11). At $O_2$ concentration greater than 1%, however, reaction (5.13) or (5.15) becomes dominant and more oxygen molecules compete for electrons, resulting in increasing amount of $NO_2$ formation while NO conversion via reaction (5.9) into $N_2$ decreases. Both reaction (5.13) at low energy density (<100 J/L) and reaction (5.15) at high energy density (>100 J/L) demonstrate dominance. When $O_2$ concentration is high, an increase in energy density from 150 to 320 J/L does not help NO conversion because reaction (5.15) needs three oxygen atoms to convert one NO molecule while reaction (5.13) only needs one oxygen atom. This counterbalances the effect of reactions (5.10) and (5.11) at high energy density.

Effect of water vapor. Effect of water vapor on $NO/NO_x$ conversions is investigated with varied water compositions in the 250 ppm NO in $N_2$ mixture. The power frequency is 150 Hz. The DBD reactor is operated at 65 °C to prevent condensation of water vapor. Both NO and $NO_x$ conversions significantly decrease with the addition of 1% $H_2O$. As the $H_2O$ concentration is increased from 1 to 5%, however, both NO and $NO_x$ conversions change little. $NO/NO_x$ conversions decrease significantly from 99% to 54% and from 98% to 25%, respectively at the energy density of 400 J/L. An increase in energy density does not promote $NO/NO_x$ conversions significantly.

In the absence of $O_2$ and $H_2O$, the dominant reaction is the reduction of NO to $N_2$ as shown in reaction (5.9) and Figure 5.11. However, electron-impact dissociation of $H_2O$ competes for electrons and accounts for the conversion drop as follows:

$$e + H_2O \rightarrow e + H + OH \qquad (5.16)$$

$$OH + NO + M \rightarrow HNO_2 + M \quad (5.17)$$

Fewer electrons are available for reaction (5.8) and thus fewer nitrogen atoms are available for reaction (5.9), leading to possibly lower NO and $NO_x$ conversions. However, reactions (5.16) and (5.17) enhance NO conversion which counterbalances the effect of reaction (5.9), resulting in little overall change in $NO/NO_x$ conversions. An increase in energy density helps N and OH formation but does not promote NO and $NO_x$ conversions significantly as shown in Figure 5.11.

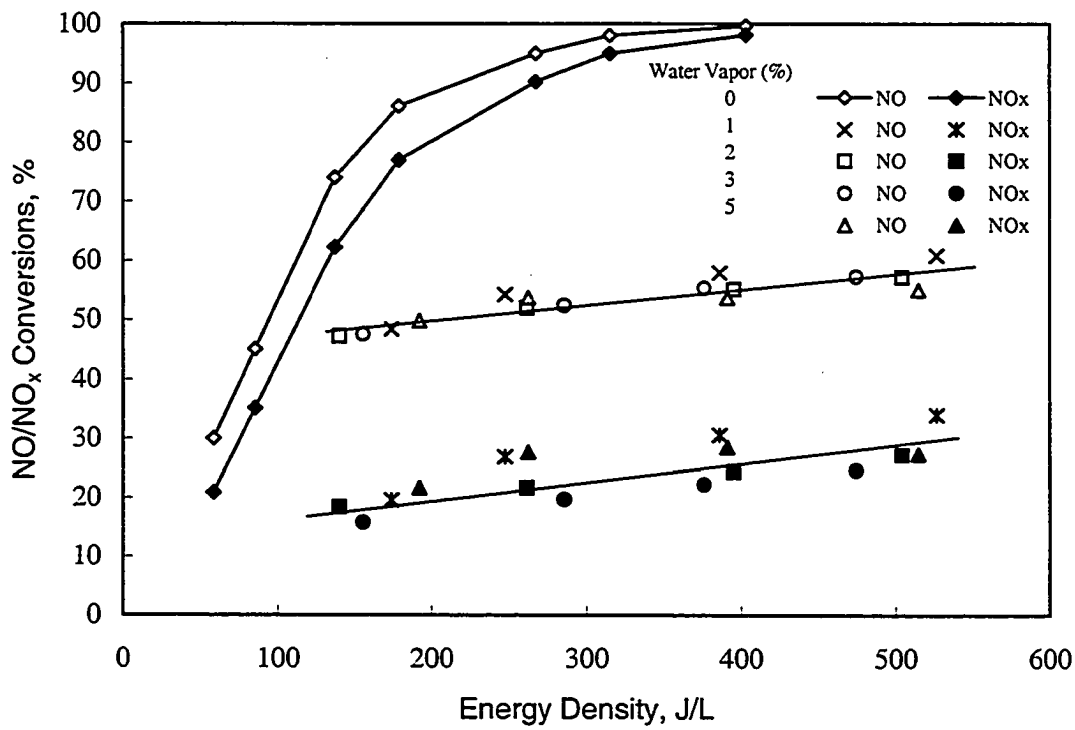


**Figure 5.11 Effect of Water Vapor Concentration on $NO/NO_x$ Conversions.** Frequency 150 Hz, total flow rate 1000 SCCM, 250 ppm NO with $N_2$ balance, temperature 65 °C.

Effect of coexisting water vapor and oxygen. Experiments are conducted in the presence of 1% water vapor and 8.3% $O_2$ in the inlet $NO/N_2$ gas stream. Significant increases in $NO/NO_x$ conversions are observed even at a much lower energy density of 200 J/L in the presence of $O_2$ and $H_2O$ than in the presence of either $O_2$ or $H_2O$ alone

(Figure 5.12). $NO/NO_x$ conversions of 90% and 40% are achieved, compared to 50% and 4% for $O_2$ alone or 50% and 20% for $H_2O$ alone. A strong acid is observed in the condensate of the moisture trap. The following reactions may provide an explanation:

$$O(^1D) + H_2O \rightarrow 2\,OH \qquad (5.18)$$

$$NO_2 + OH + M \rightarrow HNO_3 + M \qquad (5.19)$$

Reaction (5.18) contributes OH radicals in the presence of $O_2$. Reactions (5.17) and (5.19) account for much of the higher NO conversion because the presence of $O_2$ promotes $NO_2$ formation. $NO_x$ conversion increases in the presence of 1% water mainly because of reaction (5.19) rather than reaction (5.9). It can be predicted that considerable increase in NOx conversion can be achieved as water concentration is increased from 1% to the level in the flue gases.

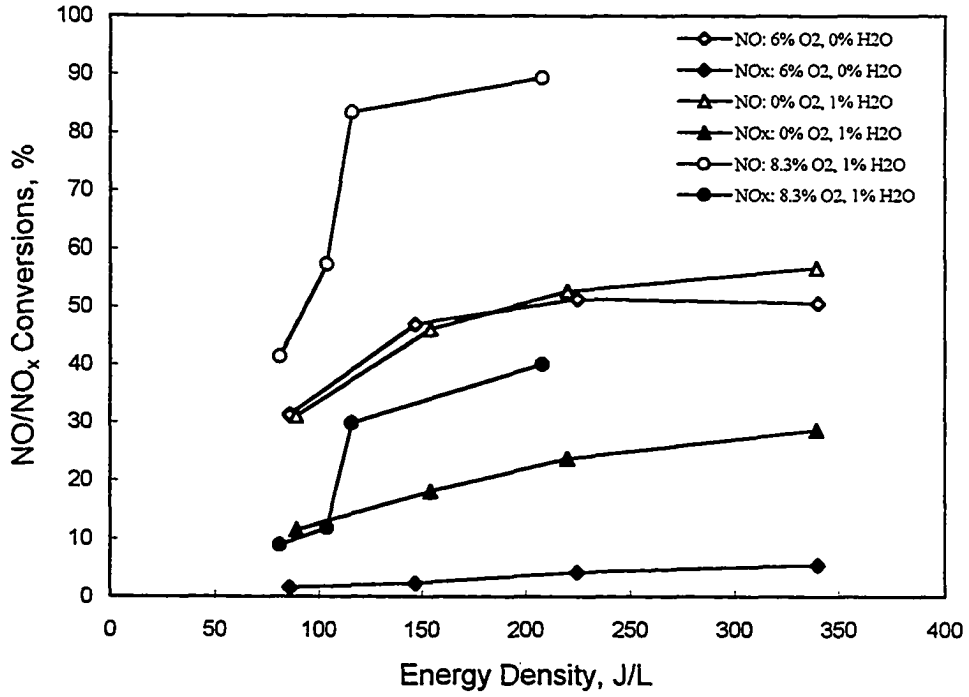


**Figure 5.12 Effect of 1% Water Vapor and 8.3% $O_2$ on $NO/NO_x$ Conversions.** Frequency 150 Hz, total flow rate 1000 SCCM, 250 ppm NO with $N_2$ balance, temperature 65 °C.

Effect of $CO_2$, CO, $CH_4$ and $C_2H_4$ on $NO/NO_x$ Conversions

Effect of carbon dioxide. $CO_2$ is added to the mixture of $NO/O_2/N_2$ to investigate its effect on $NO/NO_x$ conversions. Addition of $CO_2$ decreases NO and $NO_x$ conversions slightly as shown in Figure 5.13. $NO/NO_x$ conversions decrease from 51 to 44% and from 20 to 9%, respectively as $CO_2$ concentration increases from 0 to 7.6%. A large CO formation of 400 ppm is observed due to the electron-impact dissociation of $CO_2$ in a mixture of $NO/O_2/N_2/CO_2$ in a plasma system:

$$e + CO_2 \rightarrow e + O + CO \qquad (5.20)$$

Reaction (5.20) competes for electrons leading to fewer electrons available for radicals formation such as N and O to convert NO into $N_2$ or $NO_2$.

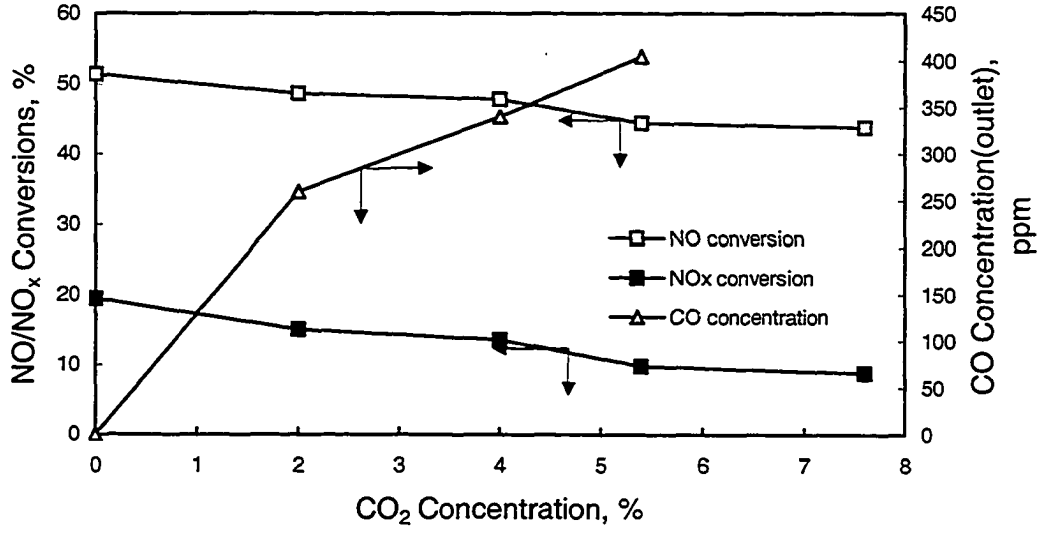


**Figure 5.13 Effect of $CO_2$ Concentration on $NO/NO_x$ Conversions.** Total flow rate 1000 SCCM, 250 ppm NO, 3% $O_2$ and $N_2$ balance. Plasma 320 J/L at room temperature.

Effect of carbon monoxide. Chemical compounds such as CO, $CH_4$ and $C_2H_4$ play an important role in the catalytic reduction of $NO_x$. Experiments are conducted to study their effects in the presence of non-thermal plasma.

Figure 5.14 shows that there is only a small increase in NO conversion when energy density is increased from 150 to about 400 J/L. However, there is a significant increase in CO formation. Reaction (5.20) suggests that CO is formed in the plasma process from $CO_2$ present in the gas mixture. The addition of small amount of CO probably has no significant effect on $NO/NO_x$ conversions since a large amount of CO is formed from $CO_2$ via reaction (5.20).

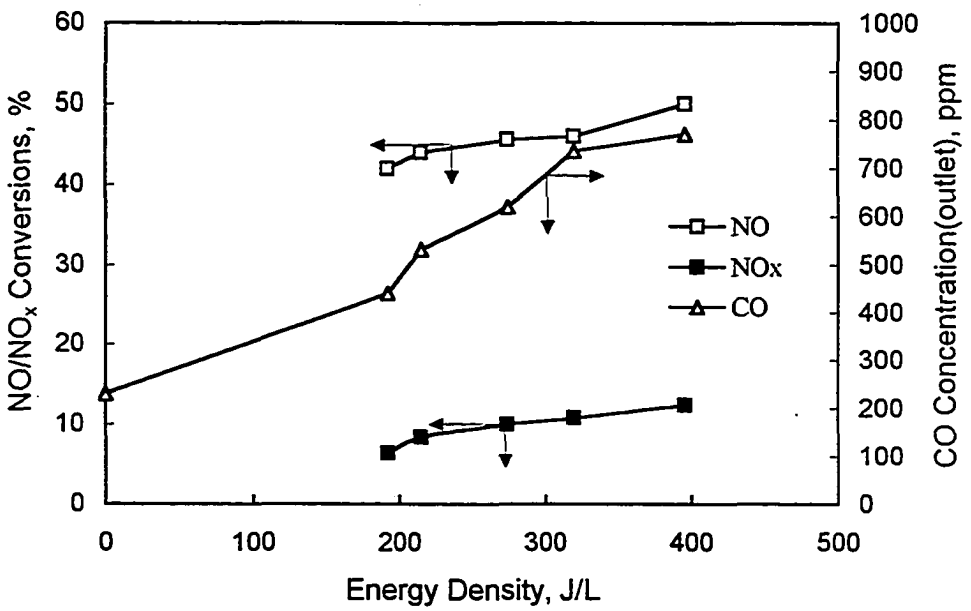


**Figure 5.14 $NO/NO_x$ Conversions and CO Concentration vs. Energy Density.** Total flow rate 1000 SCCM. Inlet: 250 ppm NO, 230 ppm CO, 3% $O_2$, 7.6% $CO_2$, $N_2$ balance.

Effect of methane. Methane is added to the mixture of $NO/O_2/CO_2/N_2$ to investigate the effect of saturated hydrocarbons on $NO/NO_x$ conversions. Figure 5.15 shows that NO conversion slowly increases from 44 to 66% as methane concentration is increased from 0 to 3000 ppm while $NO_x$ conversion decreases a little. The following reactions are proposed to occur in the presence of non-thermal plasma:

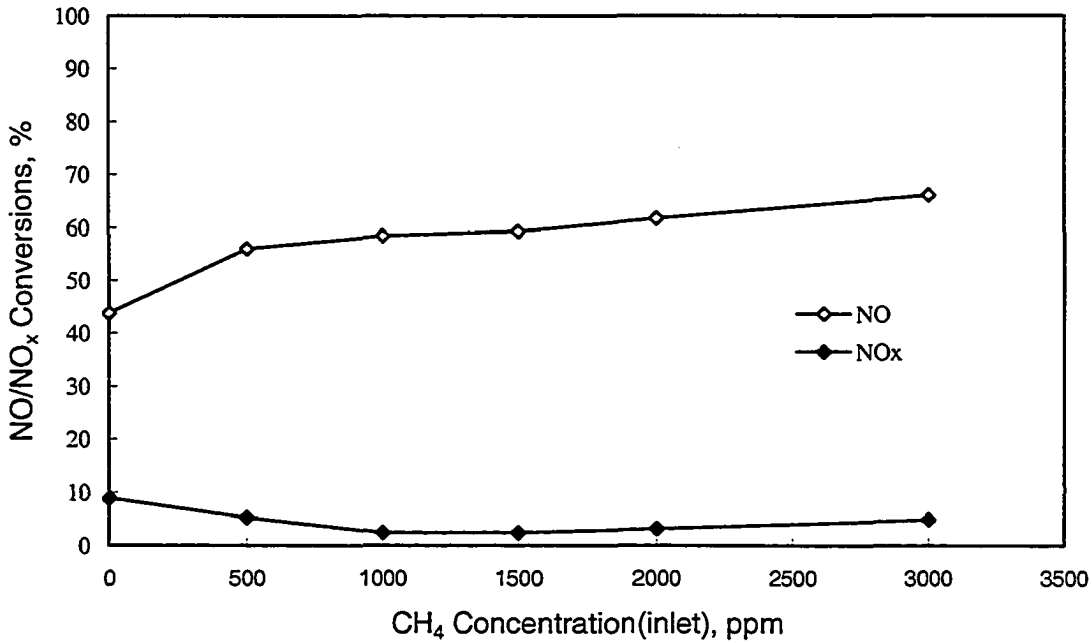


**Figure 5.15 Effect of $CH_4$ Concentration on $NO/NO_x$ Conversions.** Total flow rate 1000 SCCM. 250 ppm NO, 3% $O_2$, 7.6% $CO_2$, $N_2$ balance. Plasma: 320 J/L at room temperature.

$$CH_4 + e \rightarrow CH_3 + H + e \quad (5.21)$$

$$CH_4 + O \rightarrow CH_3 + OH \quad (5.22)$$

$$CH_4 + O(^1D) \rightarrow CH_3OH \quad (5.23)$$

$$HO_2 + NO \rightarrow NO_2 + OH \quad (5.24)$$

where, $HO_2$ is formed mainly via the following reactions (Penetrante and others 1998):

$$H + O_2 \rightarrow HO_2 \quad (5.25)$$

$$CH_3OH + O_2 \rightarrow CH_3O + HO_2 \quad (5.26)$$

$$CH_3O + O_2 \rightarrow CH_2O + HO_2 \quad (5.27)$$

Saturated hydrocarbon methane can undergo electron-impact dissociation reaction (5.21) at a slow rate. Therefore, reactions (5.21) and (5.22) are limited and consequently $HO_2$ available for reaction (5.24) is limited, resulting in a small increase in NO conversion to

$NO_2$ from 56 to 66% as methane concentration is increased from 500 to 3000 ppm. $NO_x$ conversion is almost maintained unchanged since no $NO_2$ is further reduced into $N_2$.

Effect of ethylene. Ethylene is added to the reactor to test the effect of unsaturated hydrocarbons on $NO/NO_x$ conversions. Figure 5.16 shows that $C_2H_4$ significantly enhances NO conversion to $NO_2$. The following two reactions are proposed to occur in the plasma process:

$$C_2H_4 + O \rightarrow CH_2CO + H + H \quad (5.28)$$

$$C_2H_4 + O + O \rightarrow HCO + HCO + H + H \quad (5.29)$$

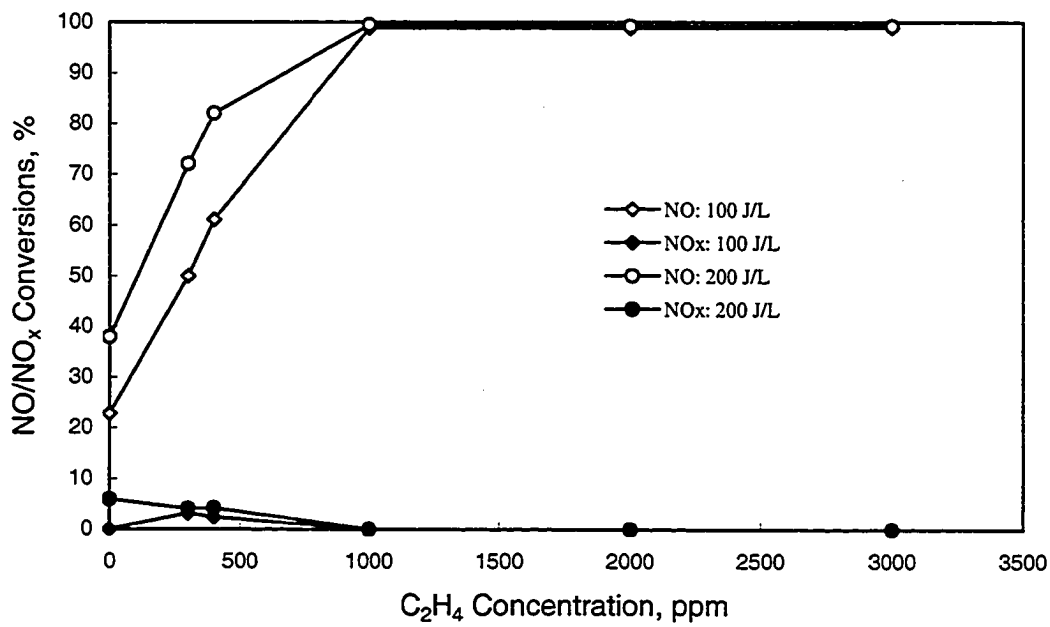


**Figure 5.16 Effect of $C_2H_4$ Concentration on $NO/NO_x$ Conversions.** Total flow rate 1000 SCCM. 250 ppm NO, 3% $O_2$, 7.6% $CO_2$, $N_2$ balance. Temperature 60 °C, frequency 150 Hz.

Unsaturated hydrocarbon $C_2H_4$ consumes most of the O atoms via reactions (5.28) and (5.29). As $C_2H_4$ concentration is increased, more $HO_2$ is produced via reactions (5.25) and (5.30) (Penetrante 1998):

$$HCO + O_2 \rightarrow CO + HO_2 \quad (5.30)$$

The reaction (5.24) becomes dominant, leading to almost 100% NO conversion to $NO_2$.

Effect of Packing in Plasma Reactor

The effects of reactor packing on $NO/NO_x$ conversion and discharge stability is investigated with an inlet NO concentration of 250 ppm in various gas mixtures. Glass wool is packed in the space between the two concentric barriers. The density of the packing is 0.3 $g/cm^3$.

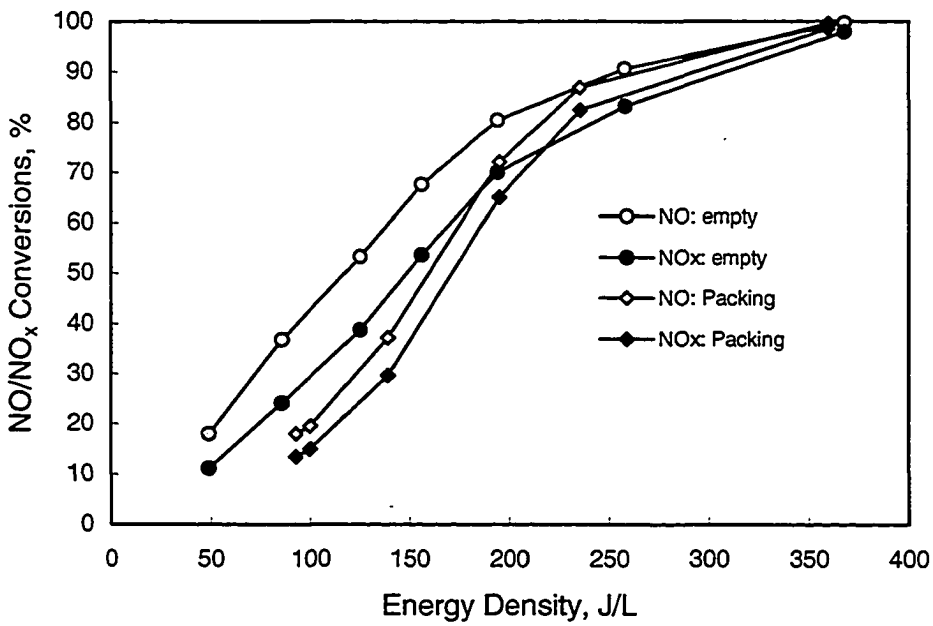


**Figure 5.17 Effect of Packing on $NO/NO_x$ Conversions for $NO/N_2$ Gas Mixture**

Effect of packing on $NO/NO_x$ conversions. Figure 5.17 shows that, at energy density less than 225 J/L, $NO/NO_x$ conversions for packing are less than for no-packing experimental runs. At energy density greater than 225 J/L, however, $NO/NO_x$ conversions for packing are almost the same as for no-packing. Electrical and hydrodynamic factors probably account for the difference at low energy density (<225

J/L). The glass wool packing with higher dielectric constant increases the capacitance of the reactor, probably causing a decrease in discharge efficiency. Packing also considerably shortens the gas residence time in the reactor, resulting in lower $NO/NO_x$ conversions. At high energy density (>225 J/L), however, these factors appear to have little effect on $NO/NO_x$ conversions.

Effect of packing on discharge stability. In a separate set of experiments, it is found that a glass-wool packing helps in stabilization of discharge especially when $C_2H_4$ is added to the inlet gas mixture.

Reaction Kinetics and Modeling of NO Conversion under DBD Conditions

The chemistry of NO oxidation under non-thermal plasma is very different from that of oxidation in a combustion process or under atmospheric conditions. The gaseous reactions in plasma can be very complex involving energetic electrons, ions, metastable neutral compounds, etc. resulting in tens of reactions.

Kinetic rate equation for dry NO oxidation. The main reactions for dry NO oxidation described earlier in this study can be simplified as follows:

$$O_2 + e \rightarrow O(^3P) + O(^1D) + e \quad (5.31)$$

$$O + O_2 \rightarrow O_3 \quad (5.32)$$

$$NO + O \rightarrow NO_2 \quad (5.33)$$

$$NO + O_3 \rightarrow NO_2 + O_2 \quad (5.34)$$

$$\text{Overall reaction: } NO + \tfrac{1}{2}O_2 \rightarrow NO_2 \quad (5.35)$$

The rate equation for reaction (5.35) can be expressed as follows

$$-d[NO]/dt = k_p [NO]^{\alpha}[O_2]^{\beta} \quad (5.36)$$

where [NO] and [$O_2$] represent concentrations of NO and $O_2$, respectively in the plasma reactor and $k_p$ is specific reaction rate. In addition to the effect of concentrations, the impact of all other variables such as electrical, chemical and hydrodynamic on reaction rate is accounted for by the specific reaction rate, $k_p$. Under non-thermal plasma conditions in which reactions are mostly conducted at ambient temperature, the effect of temperature on reaction is negligible compared with discharge energy input. It is expected that higher discharge energy input will result in higher reaction rate. Therefore, an Arrhenius-type correlation can be proposed as follows:

$$k_p = A_p\, e^{-Ea/E_d} \tag{5.37}$$

where $A_p$ is frequency factor, $E_a$ is effective activation energy (J/mol of NO) and $E_d$ is energy density (discharge power divided by gas flow rate, J/mol of gas mixture) under plasma conditions.

Reaction orders $\alpha$ and $\beta$ for equation (5.36) have been estimated to be about ½ through regression analysis of experimental data by varying inlet NO and $O_2$ concentrations at a constant energy density ( Appendix C). The rate equation becomes:

$$-\,d[NO]/dt = k_p\,[NO]^{1/2}\,[O_2]^{1/2} \tag{5.38}$$

Frequency factor $A_p$ and effective activation energy $E_a$ for equation (5.38) have been estimated to be 0.0143 and 1,865 J/mol, respectively by regression analysis (Appendix C). Therefore, equation (5.38) can be written as:

$$k_p = 0.0143\, e^{-1865/E_d} \tag{5.39}$$

The value of $E_a$ for NO-$O_2$ reaction in a conventional reactor is not available. However, the activation energy for a conventional NO-$O_3$ (ozone) reaction is reported to be 10,290 J/mol (Bailar and others 1984). The much lower $E_a$ of 1,865 J/mol in the plasma specific

reaction rate equation (5.39) indicates that the plasma reaction can be conducted at much lower activation energy. Shown in Figure 5.18 is the comparison of experimental and kinetic model results.

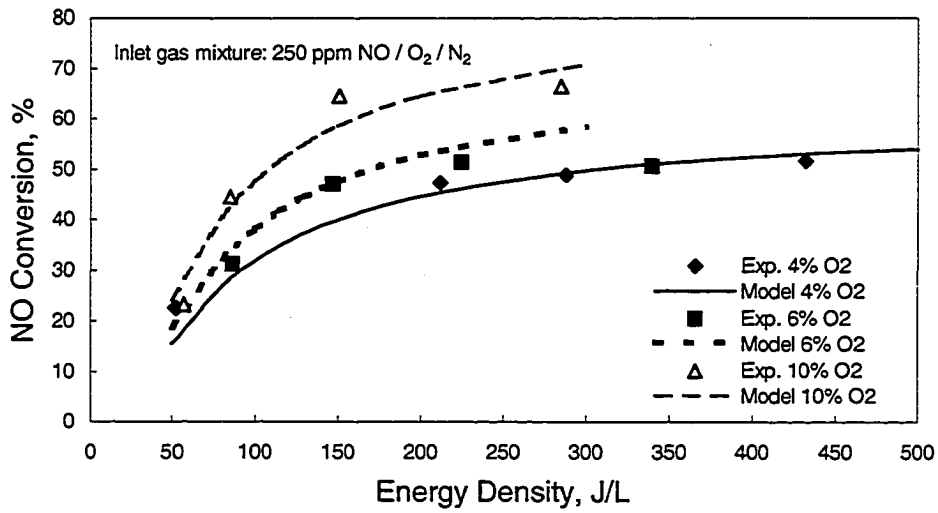


**Figure 5.18 Comparison of Experimental and Kinetic Model Results of Dry NO Conversion**

Correlation of NO conversion in the presence of moisture. As mentioned earlier the presence of $H_2O$ vapors in plasma reactions has a major effect. Efforts have been made to obtain an empirical equation for wet conditions. For this case, following equation has been proposed:

$$[X]/[X]_0 = \exp\{-(E_d - E_i)/\gamma\} \quad (5.40)$$

where $[X]_0$ and $[X]$ are inlet and outlet $NO_x$ concentrations, respectively and $\gamma$ is scale factor. This equation incorporates the term $E_i$, the minimum energy density required for initiating plasma reactions (Figure 5.19), a significant modification to the equation proposed by Rosocha *et al.*(1993). The equation (5.40) has also been extended to the experimental data from an earlier study (McLarnon 1996). Regression analysis of

experimental data yields the values of $\gamma$ and $E_i$ as shown in Table 5.1. For details please refer to Appendix C. Figure 5.19 shows the comparison of experimental and model results.

**Table 5.1**

**$\gamma$ and $E_i$ under Different Conditions**

| **Experiment** | **Present study** | **Earlier study** (McLarnon 1996) |
|---|---|---|
| **Feed** | Simulated mixture:<br>NO- 250ppm<br>$O_2$- 8.3%<br>$H_2O$-1%<br>$N_2$ balance | Natural gas combustion exhaust:<br>$NO_x$- 288ppm<br>$O_2$- 2.3%<br>$H_2O$-16.6%<br>$CO_2$-8.7%<br>$N_2$ balance |
| **Reactor** | 18mm IDx300 mm long<br>Dual barriers | 25.4mm ID x 610 mm long<br>Central barrier only |
| **$\gamma$ (J/L)** | 61 | 133 |
| **$E_i$ (J/L)** | 45 | 14 |

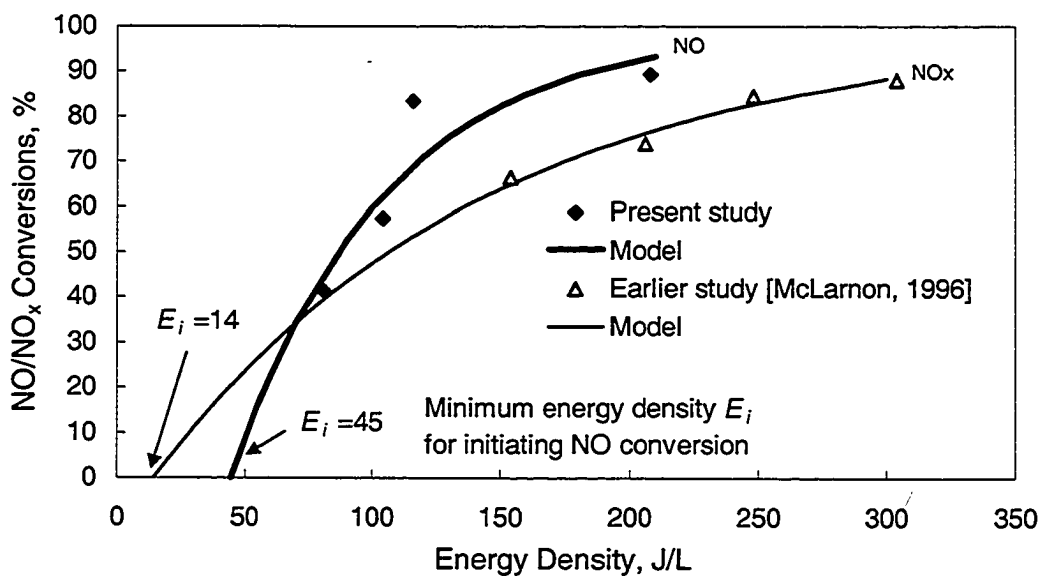


**Figure 5.19 Comparison of Experimental and Model Results of Wet NO Conversion**

This model work would provide an effective guidance in laboratory experiments and the commercialization of the DBD technique.

Section Conclusions

In this section, a non-thermal plasma technique in the form of dielectric barrier discharge (DBD) has systematically been investigated for the removal of $NO_x$. The major work has been focused on NO plasma reactions and kinetic modeling. The following main conclusions can be drawn:

1. Over 95% $NO/NO_x$ conversions have been achieved in $NO/N_2$ mixture. They decrease to 50% and 6%, respectively in the presence of 6% $O_2$ and to 60% and 30%, respectively with 1-5% $H_2O$. The simultaneous presence of $O_2$ and $H_2O$ shows up to 90% and 40% for $NO/NO_x$ conversions.
2. The kinetic equation for dry NO oxidation with $O_2$ in DBD is established as $-d[NO]/dt = k_p[NO]^{1/2}[O_2]^{1/2}$ with $k_p = 0.0143 \exp(-1865/E_d)$. The wet NO oxidation is modeled as NO removal rate $=1-\exp(-(E_d - 45)/61)$.
3. Addition of HCs significantly promotes NO oxidization into $NO_2$. NO conversions are increased from 43% to 66 and almost 100%, respectively for 3000ppm $CH_4$ and 1000 ppm $C_2H_4$ additions.
4. Most pathways for NO conversion show that formation of O and OH radicals plays an important role.
5. Power consumption is key parameter in reactor performance and must be minimized for commercial operation.

## Section II Selective Catalytic Reduction of $NO_x$

As discussed in preceding sections, non-thermal plasma in the DBD form is able to chemically reduce $NO_x$ into $N_2$ under controlled conditions. However, the reactions in the DBD reactor significantly change as other components such as $O_2$ or $H_2O$ are included in the feed gas. In the presence of $O_2$ and/or $H_2O$, NO oxidation into $NO_2$ becomes dominant, partly forming $HNO_3$. Therefore, plasma alone can not complete the task of $NO_x$ removal. Literature review reveals that considerable effort has been made to remove $NO_x$ via catalytic reactions. The development of De-$NO_x$ catalysts has been carried out with focus on conversion, temperature range, life (resistance to poisons like steam, sulfur, etc.) and manufacturing cost (replacing noble metals with inexpensive metals).

Recently, coupling the plasma process with catalytic reactions for a better $NO_x$ removal has received more and more attention primarily because of the $NO_x$ removal from diesel truck exhausts. To gain a better understanding and knowledge of the hybrid system, it is important to first investigate catalytic effect alone on $NO_x$ removal. Presented in this section is experimental data on $NO_x$ removal with a catalytic process. The next section is focused on the hybrid plasma-catalyst system for $NO_x$ removal.

### Parameters and Operating Conditions

In this study, reactor variables such as catalyst and temperature are selected as major parameters for experimental investigation. Other factors of interest include components normally present in a pollution stream such as $O_2$, $H_2O$ etc. and the reducing agents such as CO, $CH_4$ and $C_2H_4$ as added to plasma reactor as discussed earlier.

- Catalysts

  Five catalysts are used to study their capability of converting $NO_x$ into $N_2$. They are $\gamma$-$Al_2O_3$ (Alcoa Industrial Chemicals), 1%, 3% and 12% $WO_3$/ $Al_2O_3$ catalysts (laboratory-made) and Co-Mo/0402T (Harshaw, 2.1% Si, 1.9% Co, 8.6% Mo, 37.4% Al, 1/8"). $\gamma$-$Al_2O_3$ has found wide applications in chemical process industries. It is used as a catalyst as well as a support for a catalyst. $WO_3$ loading on $Al_2O_3$ is thought to be helpful in increasing the activity of catalyst for NO/$NO_x$ reduction (Kudla and others 1996 ).

- Temperature

  A low temperature with wide range is considered the best for catalytic reduction of $NO_x$ especially coming from exhaust gas at varied conditions from mobile diesel engines. The present study uses a temperature range of 450 - 650 °C.

- Oxygen concentration

  Oxygen concentration of 3% and 6% are used in the gas mixture, individually to investigate concentration effect on NO/$NO_x$ conversions.

- Water vapor concentration

  Water vapor concentrations of 1% and 2% in the inlet gas mixture are used to study the effect of water vapor on NO/$NO_x$ conversions.

- Reducing compounds: carbon monoxide, methane and ethylene

  Addition of a reducing compound such as $H_2$, CO, $NH_3$ or hydrocarbons could significantly promote NO/$NO_x$ catalytic reduction. CO is selected in this study because it is generally present in gasoline engine and diesel engine exhausts. $CH_4$ is also selected as a hydrocarbon for its plentiful and cheap supply. In addition,

$C_2H_4$ is used to compare with $CH_4$. The concentration effect of each compound on $NO/NO_x$ conversions is investigated.

A simulated gas mixture is prepared with a composition-certified cylinder of $NO/CO/O_2/CO_2/N_2$ and a pure $N_2$ cylinder. The simulated gas feed is 250 ppm NO, 230 ppm CO, 3% $O_2$, 7.6% $CO_2$ and $N_2$ balance unless otherwise noted.

Effects of Catalysts on $NO/NO_x$ Conversions

Control experiment. An experiment is conducted to determine whether $NO/NO_x$ get converted in the absence of a catalyst. The reactor tube is packed with ceramic wool of 10.38 $cm^3$ (Cotronics Corp., $Al_2O_3$, CaO and $Si_3N_4$ ), a material used for holding a catalyst in place in later experiments. The temperature is maintained at 550 °C. Gas feed consists of 250 ppm NO, 230 ppm CO, 3% $O_2$, 7.6% $CO_2$ and $N_2$ balance. The flow rate is 1000 SCCM and the space velocity is 5,780/h. It is found that $NO/NO_x$ conversions are negligible. When 3270 ppm $CH_4$ is added to the gas mixture, however, $NO/NO_x$ conversions are 14% and 5%, respectively.

$CH_4$ probably reacts with $O_2$ and produces $CO_2$ as well as CO at 550 °C in the form of incomplete combustion. CO may contribute to the $NO_x$ reduction. This mechanism will be discussed later while investigating methane effect on $NO_x$ reduction using a catalyst.

Catalyst effect on $NO/NO_x$ conversions. The catalyst used for these experiments is 3% $WO_3/ Al_2O_3$. Gas feed composition of the simulated gas is 250 ppm NO, 230 ppm CO, 3% $O_2$, 7.6% $CO_2$ and $N_2$ balance. The temperature in the reactor is maintained in the range of 450 to 575 °C. Figure 5.20 shows that maximum $NO/NO_x$ conversions are

60% and 15% at 500 °C, respectively. Obviously, the catalyst helps to increase NO oxidation to $NO_2$. The dominant reaction can be:

$$NO + 1/2\ O_2 \rightarrow NO_2 \qquad (5.41)$$

The catalyst probably enhances the chemical reduction of NO by CO as follows:

$$2\ NO + 2\ CO \rightarrow N_2 + 2\ CO_2 \qquad (5.42)$$

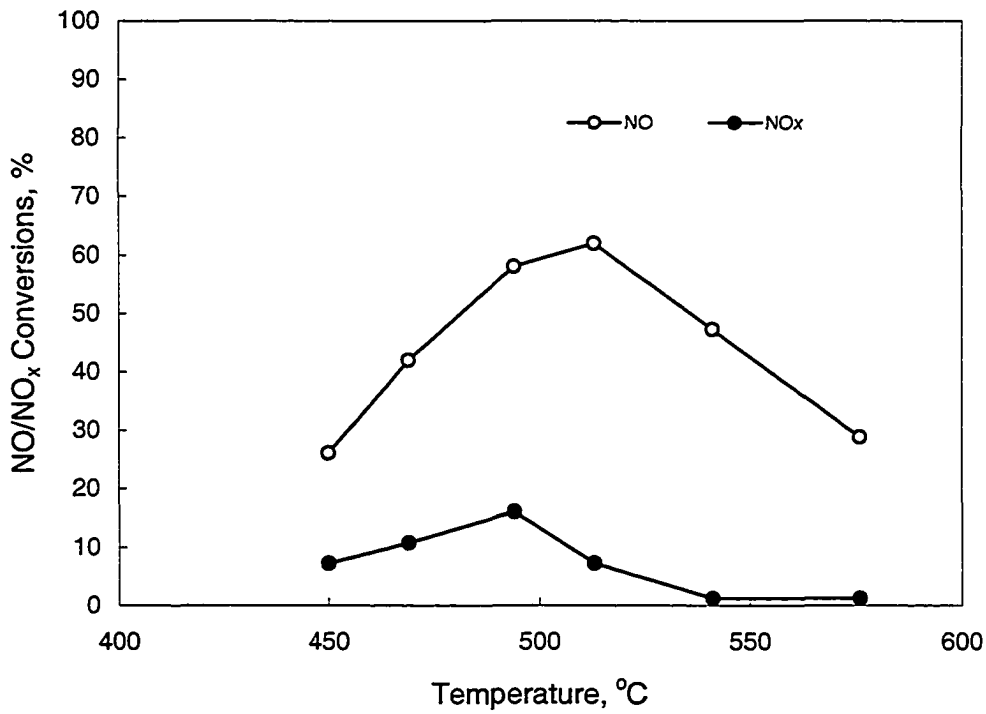


**Figure 5.20 Effect of Catalyst on $NO/NO_x$ Conversions as a Function of Temperature.** Total flowrate 1000 SCCM, 250 ppm NO, 230 ppm CO, 3 % $O_2$, 7.6 % $CO_2$, and $N_2$ balance. 3% $WO_3$ loading on $Al_2O_3$. Space velocity 5,780 /h.

Another type of catalyst Co-Mo/0402T (Harshaw, 2.1% Si, 1.9% Co, 8.6% Mo, 37.4% Al, 1/8") is also tested for $NO/NO_x$ conversions. The gas feed composition is 250 ppm NO, 230 ppm CO, 3% $O_2$, 7.6% $CO_2$, 3270 ppm $CH_4$ and $N_2$ balance. Total flow rate is 1000 SCCM. When the feed is passed through the catalyst maintained at 600 °C, $NO/NO_x$ conversions obtained are 36.5% and 1.7%, respectively. However, when a new

feed (250 ppm NO, 3270 ppm $CH_4$ and balance $N_2$) without CO and $O_2$ is used, no $NO/NO_x$ conversions are observed at temperature up to 600 °C. These two experiments show that Co-Mo/0402T catalyst is not effective for NO reduction.

Effect of $WO_3$ loading on $NO/NO_x$ conversions. Catalysts with 0%, 1%, 3% and 12% $WO_3$ loading are used to investigate $WO_3$ loading effect on $NO/NO_x$ conversions. The composition of simulated gas is 250 ppm NO, 230 ppm CO, 3 % $O_2$, 7.6 % $CO_2$, 3270 ppm $CH_4$, 6.2% Ar and $N_2$ balance. Total flow rate is 1000 SCCM and space velocity is 5,780 /h.

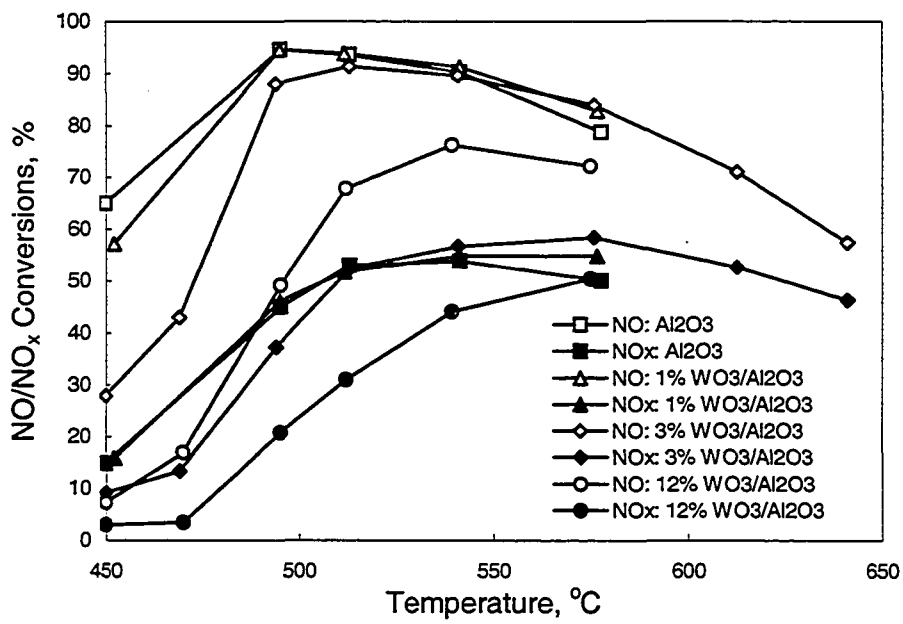


**Figure 5.21 Effect of $WO_3$ Loading on $NO/NO_x$ Conversions as a Function of Temperature.** Total 1070 SCCM, 233 ppm NO, 214 ppm CO, 2.7% $O_2$, 7.1% $CO_2$, 3270 ppm $CH_4$, 6.2% Ar, $N_2$ balance. Space velocity 5,780 /h.

Presented in Figure 5.21 are $NO/NO_x$ conversions as a function of temperature at different $WO_3$ loadings. NO conversion reaches a maximum of 94% for both $\gamma$-$Al_2O_3$ and 1% $WO_3$/ $Al_2O_3$ while $NO_x$ conversion is about 53% for both $\gamma$-$Al_2O_3$ and 1% $WO_3$/

$Al_2O_3$. The maximum $NO_x$ conversion is found to be 59% with 3% $WO_3$/ $Al_2O_3$ catalyst. However, a higher $WO_3$ loading of 12% lowers NO conversion down to 76% and $NO_x$ conversion down to 50% at 575 °C. Therefore, the catalysts with 0%, 1% and 3% $WO_3$ loading are selected for subsequent experimental work.

High $WO_3$ loading on $Al_2O_3$ of 12% inhibits NO/$NO_x$ conversions probably because the excess of $WO_3$ occupies part of the surface of $Al_2O_3$ that would otherwise be available for NO/$NO_x$ reactions.

Selective Catalytic Reduction of $NO_x$ by CO

CO in the exhaust gas from automobile engines has been well studied with automotive three-way catalysts that consist mainly of platinum and rhodium as a catalyst (Kyriacopoulou and others 1994). However, development of better catalysts is still attractive for selective catalytic reduction (SCR) of NO by CO. The effect of inlet CO concentration on NO/$NO_x$ conversions is investigated over 1% $WO_3/Al_2O_3$ catalyst in the present study. Total flow rate is 1000 SCCM with inlet gas mixture of 250 ppm NO, 3% $O_2$, 2.5-7.6% $CO_2$ and $N_2$ balance. Inlet CO concentrations are maintained at 77, 154 and 230 ppm. The space velocity is 5,780 /h. Temperature is held at 450 °C. Figure 5.22 shows that NO conversion increases significantly to 45% as inlet CO concentration increases to 230 ppm. $NO_x$ conversion increases from zero to the maximum of 15% at inlet CO concentration of 154 ppm. Outlet CO concentration is 69 ppm corresponding to an inlet CO concentration of 230 ppm, resulting in 72.4% CO conversion. It is anticipated that $NO_x$ conversion will increase if inlet CO concentration is increased above 230 ppm.

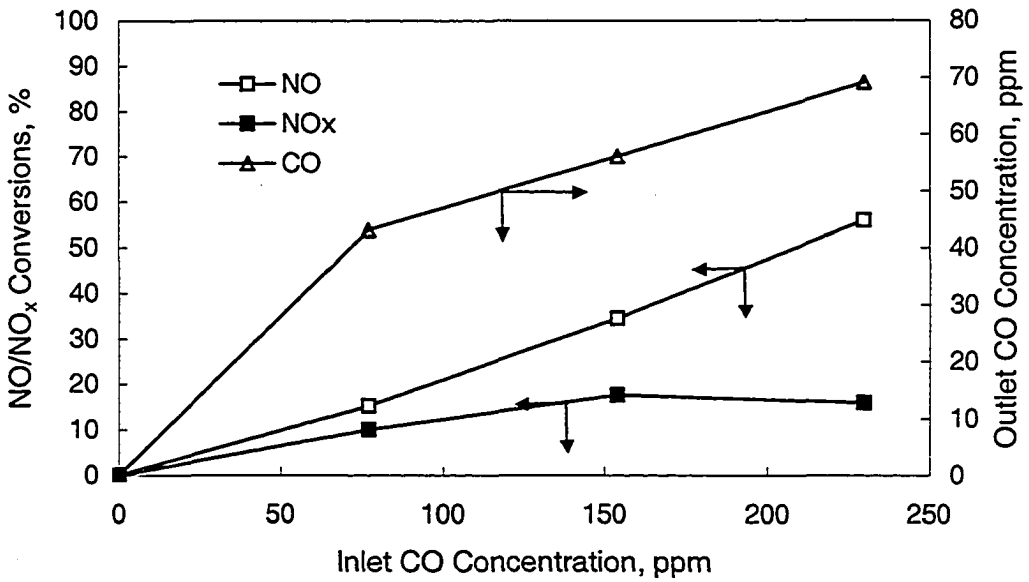


**Figure 5.22 Effect of Inlet CO Concentration on $NO/NO_x$ Conversions.** Total flow rate 1000 SCCM, simulated inlet gas: 250 ppm NO, 3% $O_2$, 2.5-7.6% $CO_2$, $N_2$ balance. Catalysis: 1% $WO_3/Al_2O_3$, 450 °C, space velocity 5,780 /h.

The presence of CO promotes the reaction NO +1/2 $O_2$ → $NO_2$ leading to a high NO conversion. The mechanism for CO catalytic reaction over 1%$WO_3/Al_2O_3$ catalyst is proposed as follows:

$$2\{CO\} + 2\{NO\} \rightarrow \{CNO\text{-}NCO\} + 4\{O\} \quad (5.43)$$

Where, { } indicates active species adsorbed on catalyst surfaces. Schmal *et al.* (1999) reported that the above reaction over Pd-x$Mo/Al_2O_3$ formed isocyanate (CNO-NCO). CNO-NCO was thought to be an intermediate in the selective catalytic reduction (SCR) of NO by $C_3H_6$ over $Pt/Al_2O_3$ (Captain and Amiridis 1999). The following reactions are proposed for the present study:

$$NO + \{O\} \rightarrow NO_2 \quad (5.44)$$

$$\{CNO\text{-}NCO\} \rightarrow N_2 + 2\,CO \quad (5.45)$$

$$CO + O_2 \rightarrow CO_2 \quad (5.46)$$

Reaction (5.43) is the key step to form the intermediate and active O atom. Subsequently, as CO concentration increases, reactions (5.44) and (5.45) account for the increases in NO and $NO_x$ conversions, respectively. When inlet CO concentration is maintained at 230 ppm, about 160 ppm CO is converted finally via reaction (5.46). $NO_x$ conversion of 15% indicates that about 19 ppm {CNO-NCO} and 4x19 ppm {O} are formed. All {O} of 76 ppm is consumed by reaction (5.44), producing $NO_2$ of 76 ppm. This is in good agreement with the experimental data of 75 ppm.

Selective Catalytic Reduction of $NO_x$ by $CH_4$

Effect of methane addition on $NO_x$ catalytic reactions over 3% $WO_3$ / $Al_2O_3$. An experiment is conducted to investigate the effect of methane addition. The composition is 250 ppm NO, 230 ppm CO, 3 % $O_2$, 7.6 % $CO_2$, 3270 ppm $CH_4$, 6.2% Ar and $N_2$

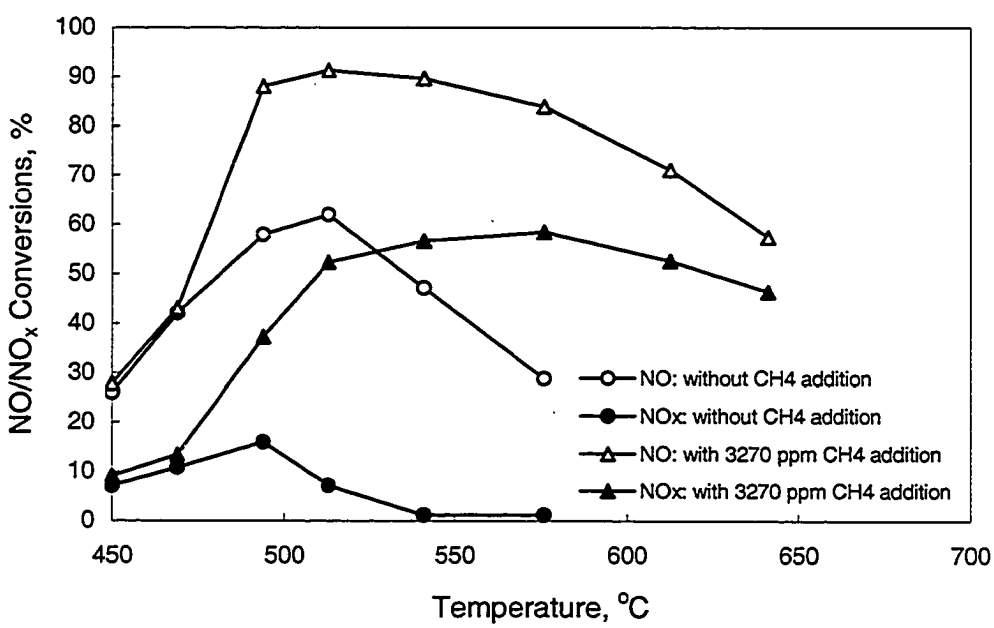


**Figure 5.23 Effect of $CH_4$ on $NO/NO_x$ Conversions as a Function of Temperature.** Total flowrate 1000 SCCM, 250 ppm NO, 230 ppm CO, 3% $O_2$, 7.6% $CO_2$, 6.2% Ar and $N_2$ balance. 3% $WO_3$ / $Al_2O_3$. Space velocity 5,780 /h.

balance. Total flow rate is 1000 SCCM in both cases and space velocity is 5,780 /h. Figure 5.23 shows that addition of methane significantly increases maximum $NO/NO_x$ conversions from 60% to 90% and from 15% to 58%, respectively.

Effect of methane concentration on $NO/NO_x$ conversions and CO formation. Being chemically active, propylene is often used as a reducing agent by many researchers in conducting studies of selective catalytic reduction (SCR) of NO (Denton and others 2000; Kudla and others 1996). Methane, however, is attractive because of its low cost and easy availability. Especially for a natural gas combustion system, the exhaust probably contains unburned methane that could be used in a downstream catalytic process.

The effect of methane is studied by varying the concentration of the hydrocarbon. The composition of feed gas is 250 ppm NO, 230 ppm CO, 3% $O_2$, 7.6% $CO_2$, 6.2% Ar and $N_2$ balance with varied concentrations of methane from 0 to 3270 ppm. Total flow rate is 1000 SCCM. 3% $WO_3/Al_2O_3$ is used and temperature is maintained at 513 °C. Presented in Figure 5.24 is the effect of methane concentration on $NO/NO_x$ conversion and CO formation. NO conversion increases quickly to 88% while $NO_x$ conversion reaches 20% at methane concentration of 690 ppm only. When methane concentration is further increased from 690 ppm to 3270 ppm, NO conversion only increases by 2 percent while $NO_x$ conversion increases linearly from 20% to 52%. It is found that a large amount of CO is formed, finally reaching 730 ppm when inlet methane concentration is 3270 ppm.

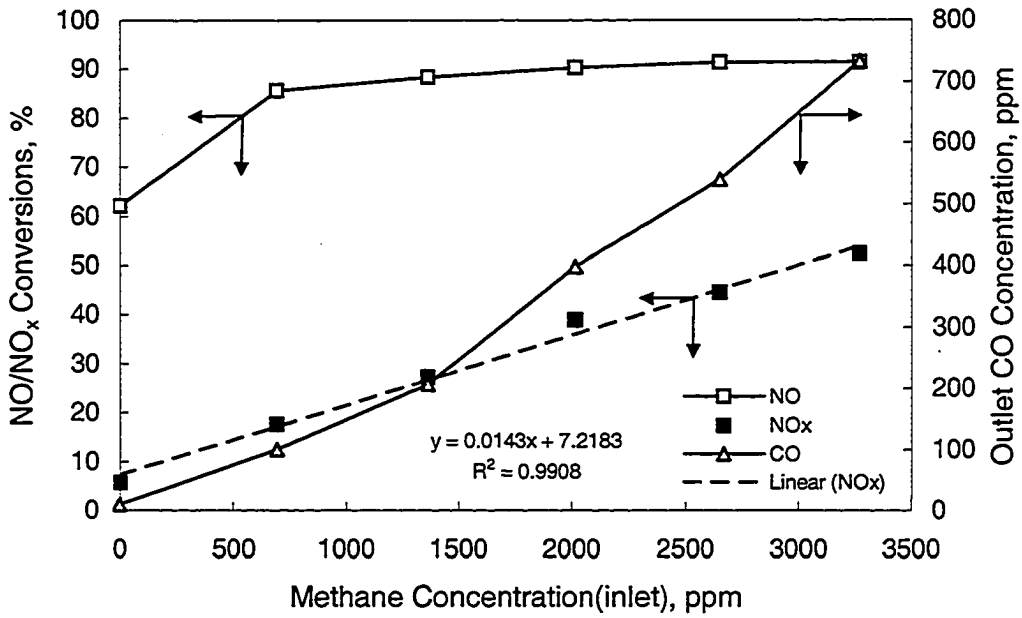


**Figure 5.24 Effect of $CH_4$ Concentration on $NO/NO_x$ Conversions and CO Formation.** Total flow rate 1000-1070 SCCM, 250-233 ppm NO, 230-214 ppm CO, 3-2.7% $O_2$, 7.6-7.1% $CO_2$, 0-6.2% Ar and $N_2$ balance. Catalysis: 3% $WO_3$/ $Al_2O_3$, 513 °C.

An increase in outlet CO concentration from 50 to 730 ppm suggests that incomplete $CH_4$ conversion takes place in the catalytic reactor. Liese *et al.* (2001) proposed a mechanism for SCR of NO by $CH_4$ with $CeO_2$-Zerolite catalysts. It may be used to explain SCR of NO by $CH_4$ in the present study with 3% $WO_3/Al_2O_3$ catalyst as follows:

$$NO + \tfrac{1}{2} O_2 <==> NO_{2,ads} \quad (5.47)$$

$$CH_4 + \{O_s\} \rightarrow CH_3^* + OH_s^* \quad (5.48)$$

$$NO_{2,ads} + CH_3^* \rightarrow CH_3 NO_2 \quad (5.49)$$

$$2\ CH_3 NO_2 + O_2 \rightarrow N_2 + CO + CO_2 + 3\ H_2O \quad (5.50)$$

$$2\ CH_3 NO_2 + 5/2\ O_2 \rightarrow NO + NO_2 + CO + CO_2 + 3\ H_2O \quad (5.51)$$

CO contributes to $NO_x$ conversion via the isocyanate (CNO-NCO) pathway (reactions 5.43, 5.44, 5.45) discussed earlier, although its effect is limited compared to $CH_4$ effect.

The relationship between $NO_x$ conversion and inlet $CH_4$ concentration is regressed from experimental data (Figure 5.24):

$$X = 0.0143\, C_i + 7.2 \tag{5.52}$$

Where, $X$ is $NO_x$ conversion (%) and $C_i$ is inlet $CH_4$ concentration (ppm). This equation can be used to estimate $NO_x$ conversion or inlet $CH_4$ concentration required for a given $NO_x$ conversion. It is expected that the linearity could not be held in the high conversion range. The curve would turn flat as $C_i$ is further increased. However, the equation is helpful in finding the minimum concentration of $CH_4$ for a required conversion $NO_x$. For example, if 80% conversion of $NO_x$ is required, equation (5.52) would give $C_i$ of 5090 ppm, which is the minimum concentration of $CH_4$ required.

Selective Catalytic Reduction of $NO_x$ by $C_2H_4$

Effect of ethylene concentration on $NO/NO_x$ conversions. Ethylene is added to the inlet stream to study its effect on $NO/NO_x$ conversions. Ethylene ($C_2H_4$) is used rather than propylene ($C_3H_6$) as it is closer to $CH_4$ with respect to the numbers of C and H atoms. Very little information is available in the literature for its use a reducing chemical agent in the SCR reactions.

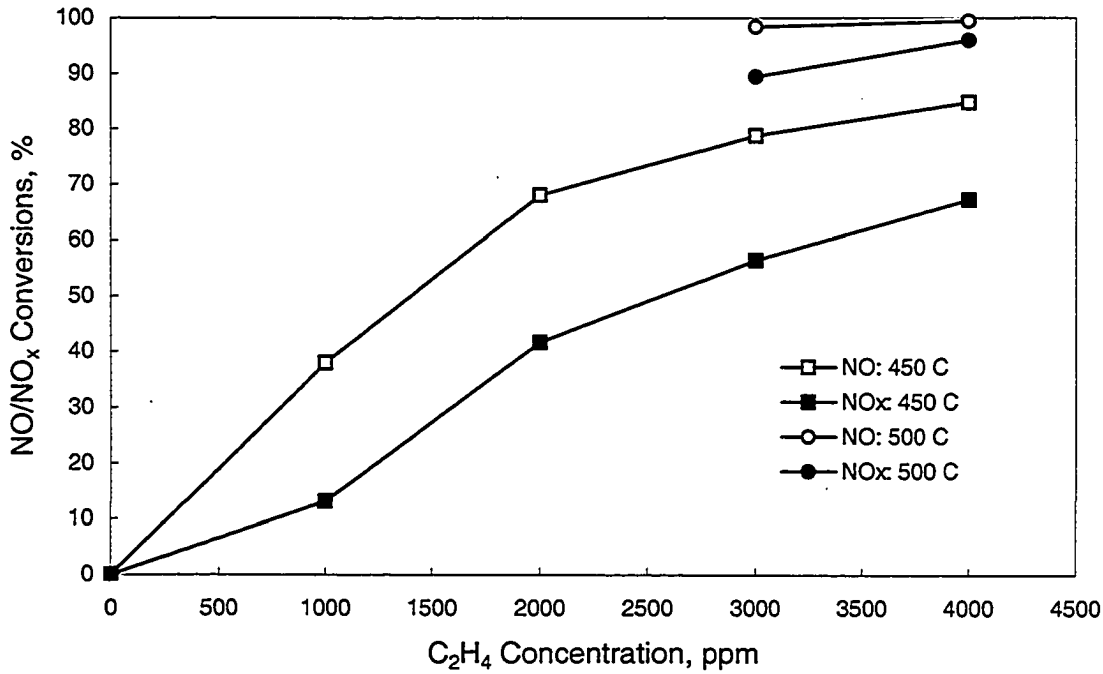


**Figure 5.25 $NO/NO_x$ Conversions vs. Concentration of $C_2H_4$ Added.** Total flow rate 1000 SCCM: 250 ppm NO, 3% $O_2$, $N_2$ balance. Catalysis: 1%$WO_3/Al_2O_3$, 450 and 500 °C, space velocity 5,780/h.

The effect of $C_2H_4$ on $NO/NO_x$ conversions is investigated by varying the concentration of $C_2H_4$ between 0 and 4000 ppm in the feed gas. Total flow rate is 1000 SCCM with 250 ppm NO, 3 % $O_2$ and $N_2$ balance. 1% $WO_3/Al_2O_3$ catalyst is used. Experiments are conducted at 450 and 500 °C. The results are presented in Figure 5.25. Outlet CO concentration can not be measured with the Nova model 375 portable combustion analyzer due to a strong signal of $C_2H_4$. The $NO/NO_x$ conversions are 80 and 55%, respectively at 3000 ppm $C_2H_4$ in the inlet gas and 450 °C reactor temperature. The $NO_x$ conversion is found to increase to 90% as temperature is increased to 500 °C. The $NO_x$ conversion of 90% with $C_2H_4$ is greater than that of 50% with $CH_4$ under the same

experimental conditions. It can be concluded that $C_2H_4$ is an effective agent for chemically reducing NO into $N_2$.

Captain and Amiridis (1999; 2000) reported that formation of isocyanate (CNO-NCO) species are the major pathway for NO reduction over $Pt/Al_2O_3$. Similarly, isocyanate as an intermediate may also provide a pathway for $NO_x$ reduction with CO (equations 5.43-45). The second possible pathway could be that adsorbed $C_2H_4$ combines with $NO_2$, following a similar pathway (equations 5.47-51) as for methane discussed earlier. The third pathway can be the formation of hydrogen from $C_2H_4$ by its dissociation over catalysts. Hydrogen then contributes to NO reduction:

$$C_2H_4 + O_2 \rightarrow 2\,CO + 2\,H_2 \qquad (5.53)$$

$$NO + H_2 \rightarrow \tfrac{1}{2}\,N_2 + H_2O \qquad (5.54)$$

The three pathways probably work together for an effective $NO_x$ reduction with $C_2H_4$.

Effect of water vapor on $NO/NO_x$ conversions. As mentioned earlier in plasma section, water vapor is one of the basic components of flue gases and diesel-engine exhausts. It has a considerable effect on catalytic process of NO from reaction pathways to catalyst life. In the present experiments, 1% and 2% water vapors are incorporated in the simulated feed gas. Total flow rate is 1000 SCCM with 250 ppm NO, 3% $O_2$, 7.6% $CO_2$, 3000 ppm $C_2H_4$ and $N_2$ balance. Catalyst used is $1\%WO_3/Al_2O_3$. Presented in Figure 5.26 is the effect of water vapor on $NO/NO_x$ conversions as a function of temperature.

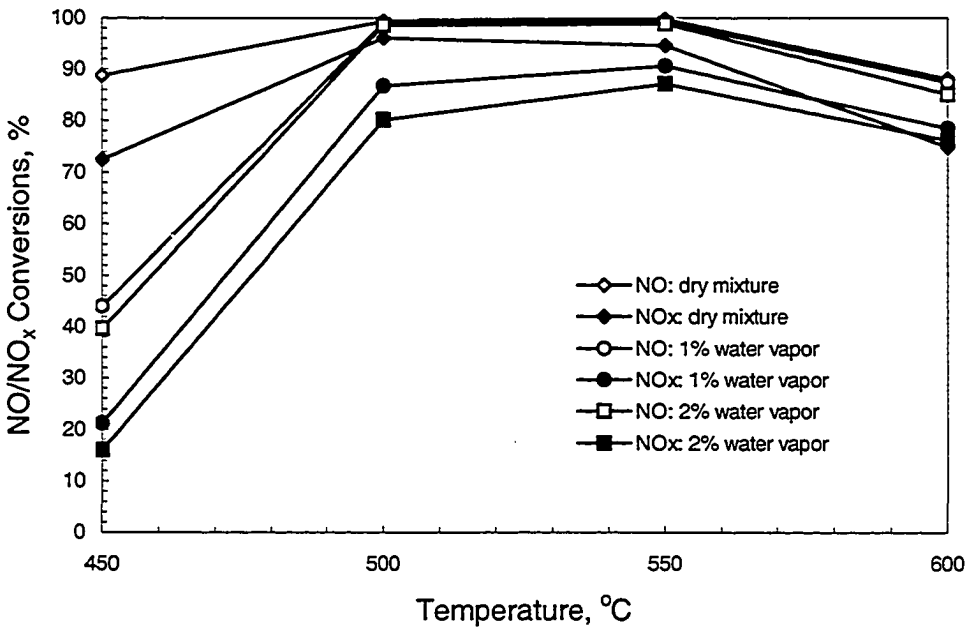


**Figure 5.26 Effect of $H_2O$ on $NO/NO_x$ Conversions as a Function of Temperature.** Total flow rate 1000 SCCM: 250 ppm NO, 3% $O_2$, 7.6% $CO_2$, 3000 ppm $C_2H_4$, $N_2$ balance. Catalysis: 1%$WO_3/Al_2O_3$, space velocity 5,780/h.

It is seen that for 1-2% water vapor at low temperature of 450 °C, $NO/NO_x$ conversions decrease from 89% for dry mixture to 40-44% and from 70% to 16-20%, respectively. As temperature increases to 550 °C, the NO conversion is nearly 100% and the $NO_x$ conversion increases to 88-91%. When temperature increases to 600 °C, however, the $NO/NO_x$ conversions reduce to about 90% and about 80%, respectively for the same water vapor content.

Effect of oxygen concentration. Oxygen effect on $NO/NO_x$ conversion is investigated in the presence of 3000 ppm $C_2H_4$ and 2% water vapor content in the feed gas. Total flow rate is 1000 SCCM. The feed composition is 250 ppm NO, 7.6% $CO_2$, 3000 ppm $C_2H_4$, 2% $H_2O$ and balance $N_2$. Catalyst used is bald $\gamma$-$Al_2O_3$. Experiments are conducted at 3% and 6% $O_2$ concentrations. The results are presented in Figure 5.27.

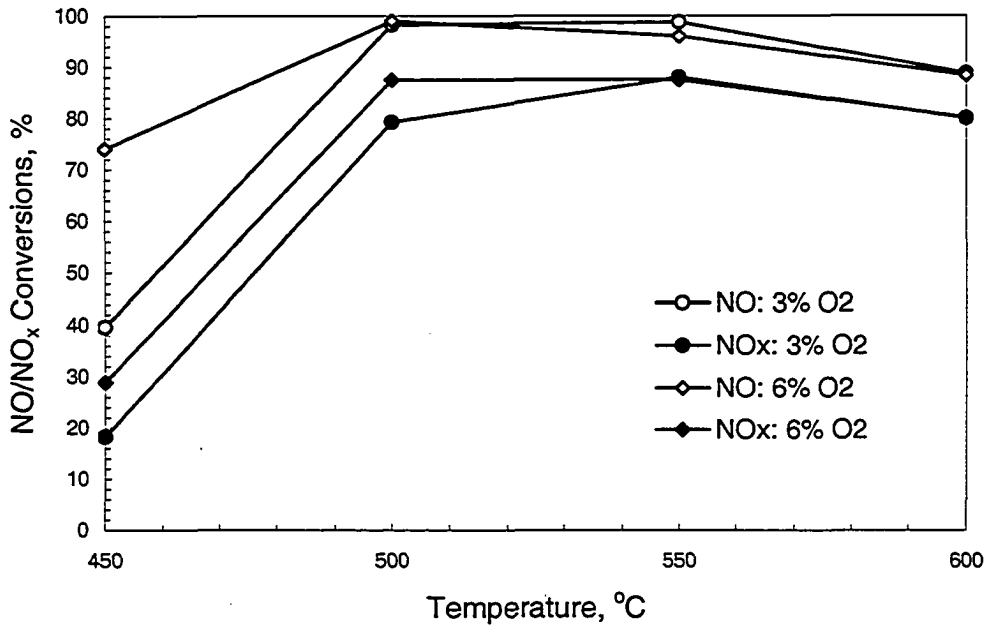


**Figure 5.27 Effect of $O_2$ on $NO/NO_x$ Conversions as a Function of Temperature.** Total flowrate 1000 SCCM: 250 ppm NO, 3 and 6% $O_2$, 7.6% $CO_2$, 3000 ppm $C_2H_4$, 2% water vapor, $N_2$ balance. Catalysis: bald $Al_2O_3$, space velocity 5,780/h.

It is found that the difference between the NO conversions for 3% and 6% $O_2$ decreases from 34 to 0% while the difference between the $NO_x$ conversions is about 10% as temperature increases from 450 to 500°C. In higher temperature range of 500-600 °C, the NO conversions for both $O_2$ levels are held the same (90-98%) while the $NO_x$ conversions for both $O_2$ levels reach the same of 85% at 550 °C. It can be concluded that the effect of $O_2$ concentration on $NO/NO_x$ conversions become less significant as temperature increases.

$NO/NO_x$ conversions in the presence of $C_2H_4$ with 1% $WO_3/Al_2O_3$ and bald $\gamma$-$Al_2O_3$. Separate experiments are conducted with 1% $WO_3/Al_2O_3$ and bald $\gamma$-$Al_2O_3$ to investigate the effect of $WO_3$ loading in the presence of $C_2H_4$. The composition of simulated gas feed is 250 ppm NO, 3% $O_2$, 7.6% $CO_2$, 3000 ppm $C_2H_4$, 1% water vapor

and $N_2$ balance. Total flow rate is 1000 SCCM. Presented in Figure 5.28 are the experimental results. There is no difference in $NO/NO_x$ conversions when 1% $WO_3/Al_2O_3$ and bald $\gamma$-$Al_2O_3$ are used in the presence of $C_2H_4$ at temperature range of 450 – 600 °C. This indicates that 1% $WO_3$ loading on $Al_2O_3$ does not increase $NO/NO_x$ conversions in the presence of $C_2H_4$.

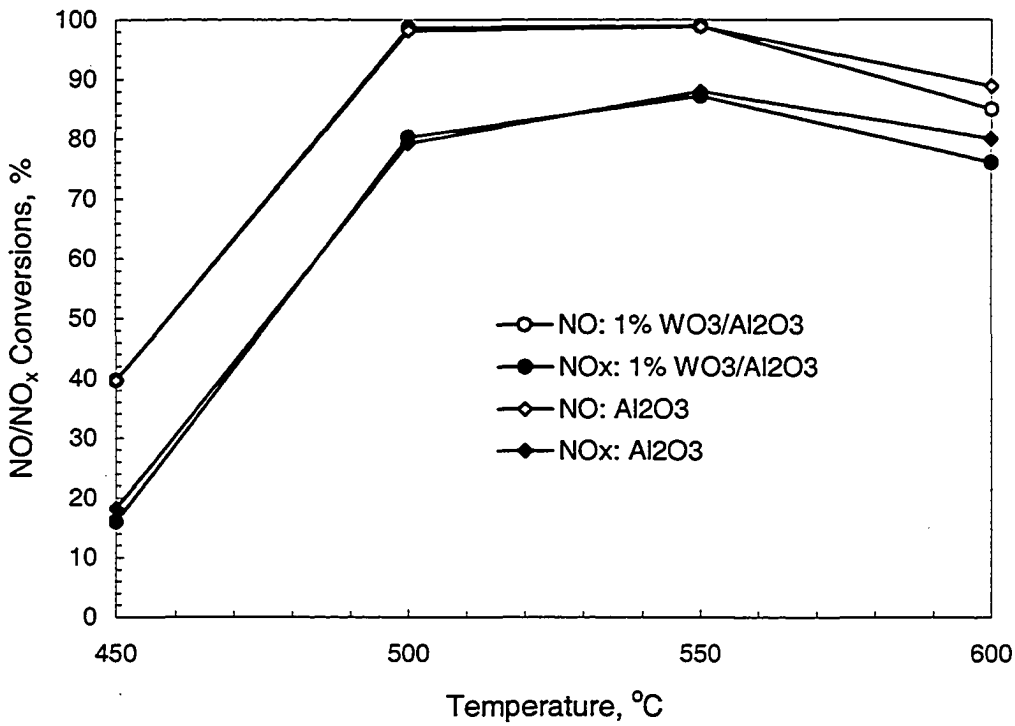


**Figure 5.28 Effect of $WO_3$ Loading on $NO/NO_x$ Conversions as a Function of Temperature.** Total flow rate 1000 SCCM: 250 ppm NO, 3% $O_2$, 7.6% $CO_2$, 3000 ppm $C_2H_4$, 1% water vapor, $N_2$ balance. Catalysis: 1%$WO_3/Al_2O_3$ and bald $\gamma$-$Al_2O_3$, space velocity 5,780/h.

Section Conclusions

In this section, an investigation of selective catalytic reduction (SCR) of $NO_x$ has been conducted for the purpose of comparison with P-C system and finding cheaper SCR catalysts, which may be suitable for hybrid plasma-catalyst system (details provided in

next Section). No work has been reported on SCR of $NO_x$ by $C_2H_4$. The following conclusions can be drawn:

1. $\gamma$-$Al_2O_3$ is a good material to serve as SCR catalyst. Loading of $WO_3$ on $\gamma$-$Al_2O_3$ does not significantly enhance catalyst activity. 1-3% loading increases $NO_x$ conversion by merely 5%. A high loading of 12% $WO_3$ instead inhibits $NO_x$ conversion.
2. An increase in CO in the gas feed promotes $NO/NO_x$ conversions in the SCR system.
3. Addition of $CH_4$ significantly increases $NO/NO_x$ conversions, from 60% to 90% and from 15% to 58%, respectively. The best temperature range for NO conversion in the presence of $CH_4$ is found to be 500-600 °C. An incomplete conversion of $CH_4$ in the SCR process results in up to 730 ppm CO formation.
4. The presence of $C_2H_4$ has a significant effect on $NO/NO_x$ conversions. At 500 °C, $NO_x$ conversion of 90% is realized when 3000 ppm $C_2H_4$ is added to the inlet mixture of 250ppm NO/3% $O_2/N_2$. The $NO_x$ conversion drops to 55% as temperature is decreased from 500 to 450°C.

## Section III Hybrid Plasma-Catalyst System for $NO_x$ Removal

As discussed in the preceding sections, the plasma reactor could effectively oxidize NO into $NO_2$ with $CH_4$ or $C_2H_4$ added. The catalytic reactor with $\gamma$-$Al_2O_3$ as a main catalyst has the potential to reduce $NO_x$ into $N_2$ with the aid of $CH_4$ or $C_2H_4$ addition.

The objective of this part of study is to investigate the synergetic effect on $NO_x$ reduction in a plasma-catalyst (P-C) system that combines non-thermal plasma in the form of dielectric barrier discharge (DBD) with a catalytic reactor. The parameters of interest are configuration of P-C system, catalyst temperature, space velocity, reducing agent concentrations (CO, $CH_4$ and $C_2H_4$), $NO_2$ concentration and $NO/NO_x$ conversions. It is important to note that NO conversion is referred to percentage of NO converted to $NO_2$, $N_2$, $HNO_3$ and/or $N_2O$ while $NO_x$ conversion is percentage of $NO_x$ converted to $N_2$, $HNO_3$ and/or $N_2O$, if any. In addition, a series of experiments are conducted to investigate the potential of $N_2O$ formation in the P-C system.

Configuration of a Plasma-Catalyst System

The physical combination of non-thermal plasma and catalytic reactors can be achieved with two types of configurations. One is referred to two-stage system consisting of a plasma reactor and catalytic reactor connected in series. The other is called one-stage system with the plasma reactor space packed with a catalyst. Each configuration has its own advantages and disadvantages. In a two-stage system, plasma reactor can be maintained at room temperature while catalytic reactor can run at much higher temperatures. It is also easy to fabricate and maintain as well as has more flexibility of operation as it deals with two separate reactors. The disadvantage for two-stage system is more space requirement. For one-stage system, a significant advantage is space saving. The disadvantages include temperature limit and difficulties in fabrication and maintenance. The literature information is not very clear on whether there is any scientific benefit in keeping plasma and catalyst in one-stage configuration. It is reported

that the same De-$NO_x$ results are achieved for the two configurations (Penetrante and others 1998). Balmer *et al.* (1998) reports that the energy efficiency in the two-stage configuration is about ten times higher than in the one-stage configuration. A high energy efficiency in a two-stage system could be attributed to different conditions maintained in plasma and catalytic reactors. The catalyst packing in one-stage system could affect the capacitance of the plasma space as well as shorten gas stream residence time. The dielectric properties of the catalyst would also have a strong effect on the discharge quality.

In the present study, the DBD reactor could only run at low temperature range (room temperature to 65 °C) because the insulation and sealing materials (Teflon end caps, rubber rings) of the reactor could not be subjected to high temperatures. Taking into account the several advantages of two-stage configuration over of one-stage, a two-stage system is used for the present study (Figure 4.1).

CO Effect on $NO_x$ Reduction with Plasma-Catalyst System

The experimental study in Section II shows that CO could be used for enhancing $NO_x$ catalytic reduction. As presented in Section I of this chapter, CO can be formed via electron-impact dissociation of $CO_2$ in the DBD reactor. The CO concentration is about 736 ppm in the outlet gas stream from the DBD reactor at energy density of 320 J/L when inlet mixture of 250 ppm NO, 230 ppm CO, 3% $O_2$, 7.6% $CO_2$ and $N_2$ balance is passed through the reactor at room temperature (Section I, Figure 5.14). Experiments are conducted with the same feed gas as used for plasma alone to investigate the CO effect on $NO_x$ reduction in the P-C system. The plasma reactor is run at an energy density of

320 J/L and room temperature. The concentration of CO from the plasma reactor to the catalytic reactor is about 700 ppm. The catalyst used is 1% $WO_3/Al_2O_3$ (Section II of this chapter shows that the effect of either $\gamma$-$Al_2O_3$ or 1%$WO_3/Al_2O_3$ is the same on $NO/NO_x$ conversions). The catalytic reactor temperature ranges from 350 to 575 °C. Sampling points are outlets of plasma reactor and catalytic reactor. The same feed gas is bypassed the plasma reactor and fed directly to the catalytic reactor to obtain the effect on $NO/NO_x$ conversions by catalysis alone for comparison.

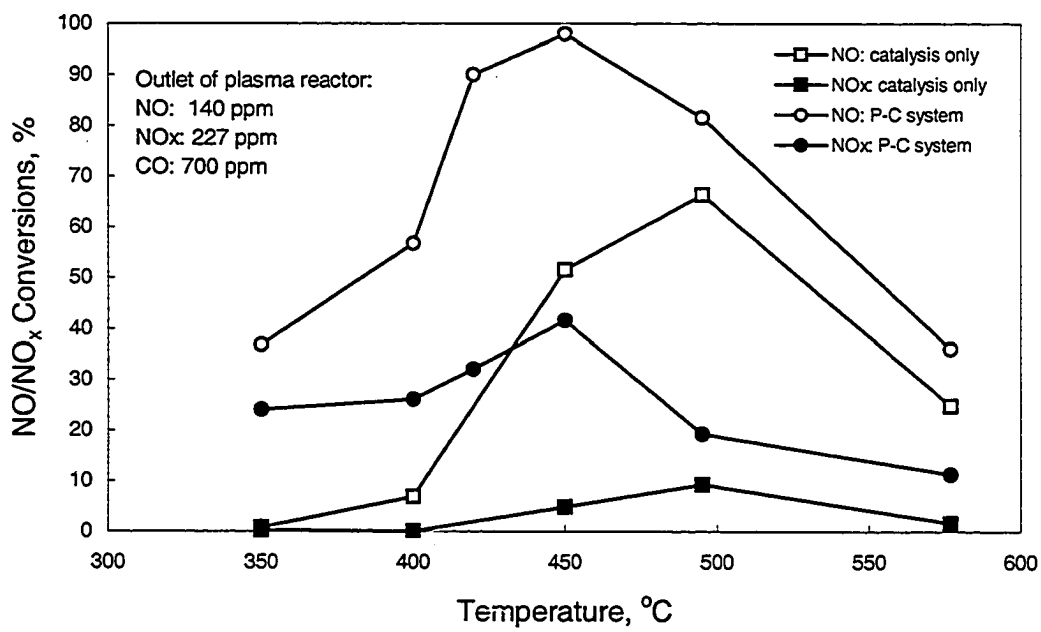


**Figure 5.29 Effects of Catalysis Alone and Plasma-Catalysis on $NO/NO_x$ Conversions as a Function of Temperature.** Total flow rate 1000 SCCM, 250 ppm NO, 230 ppm CO, 3% $O_2$, 7.6% $CO_2$, $N_2$ balance. Plasma: 320 J/L, room temperature. Catalysis: 1% $WO_3/Al_2O_3$, space velocity 5,780 /h.

Presented in Figure 5.29 are the $NO/NO_x$ conversions as a function of temperature. The catalytic reactor alone provides a maximum of $NO/NO_x$ conversions of 66% and 9%, respectively for the above stated experimental parameters at 495 °C. When the plasma and catalytic reactors are combined, the P-C system provides a maximum of

$NO/NO_x$ conversions of 98 % and 42%, respectively at 450 °C. The plasma helps to increase the $NO/NO_x$ conversions even at a slight lower temperature. Table 5.2 presents the $NO/NO_x$ conversions for three systems for comparison.

**Table 5.2**

**Comparison of Maximum Conversions of $NO/NO_x$**

| Conversion | Plasma Alone | Catalysis Alone | P-C System |
|---|---|---|---|
| % NO | 44 | 66 | 98 |
| % $NO_x$ | 9 | 9 | 42 |

**Table 5.3**

**Composition Comparison between Original and Plasma-Conditioned Feed Streams**

| Feed Stream | NO | $NO_2$ | $O_2$ | $CO_2$ | CO | $N_2$ |
|---|---|---|---|---|---|---|
| Original | 250 ppm | 0 ppm | 3% | 7.6% | 230 ppm | balance |
| Conditioned | 140 ppm | 87 ppm | 3% | 7.6% | 700 ppm | balance |

The $NO_x$ conversion of 42% by the P-C system is not a simple addition of the individual conversions by plasma and catalysis (9% each). There is a great synergy achieved with this P-C system. $NO_x$ reduction in the P-C system can be considered due to conditioning of gas stream by plasma which significantly changes the gas mixture components and compositions (Table 5.3). A considerable increase in CO concentration from 230 to 736 ppm after plasma conditioning probably accounts for the remarkable increase in $NO_x$ conversion to $N_2$. The De-$NO_x$ pathway can be considered the same as proposed in earlier Section II, i.e., CO and NO form isocyanate as an intermediate. Table

5.3 shows that $NO_2$ concentration increases from 0 to 87 ppm after conditioning. It may also contribute to the increase in $NO_x$ conversion by the catalytic reactor if $NO_2$ is an intermediate, indicating another pathway to $NO_x$ reduction.

$CH_4$ Effect on $NO_x$ Reduction with Plasma-Catalyst System

In order to identify $CH_4$ effect, experiments are conducted in the absence of $CO_2$ since plasma would dissociate $CO_2$ into CO that would enhance $NO_x$ conversion. The feed gas mixture is 1000 SCCM of 250 ppm NO, 3% $O_2$ and $N_2$ balance. The same P-C system is used except the plasma reactor is packed with glass wool for a better discharge stability and a lower energy density. The plasma reactor is operated at the energy density of 260 J/L and room temperature. The catalyst used is $\gamma$-$Al_2O_3$ at 500 °C. The experiments are conducted at $CH_4$ additions of 0, 1000, 2000 and 3000 ppm. For comparison, the same gas feed is bypassed around the plasma reactor and is directly fed to the catalytic reactor to obtain the effect by catalytic reactor alone on $NO/NO_x$ conversions.

Figure 5.30 shows the $NO/NO_x$ conversions as a function of concentrations of $CH_4$ added to the inlet feed stream to the P-C system. Comparing the $NO_x$ conversions between P-C system and catalysis alone, the improvement in $NO_x$ conversion is found to be constant at 15 % in the $CH_4$ concentration range of 1000-3000 ppm. Presented in Table 5.4 is the comparison of conversions for $CH_4$ addition of 3000 ppm. The $NO/NO_x$ conversions for the P-C system are 94% and 55%, respectively, compared with 65% and 8% for the plasma alone, 85% and 40% for catalysis alone.

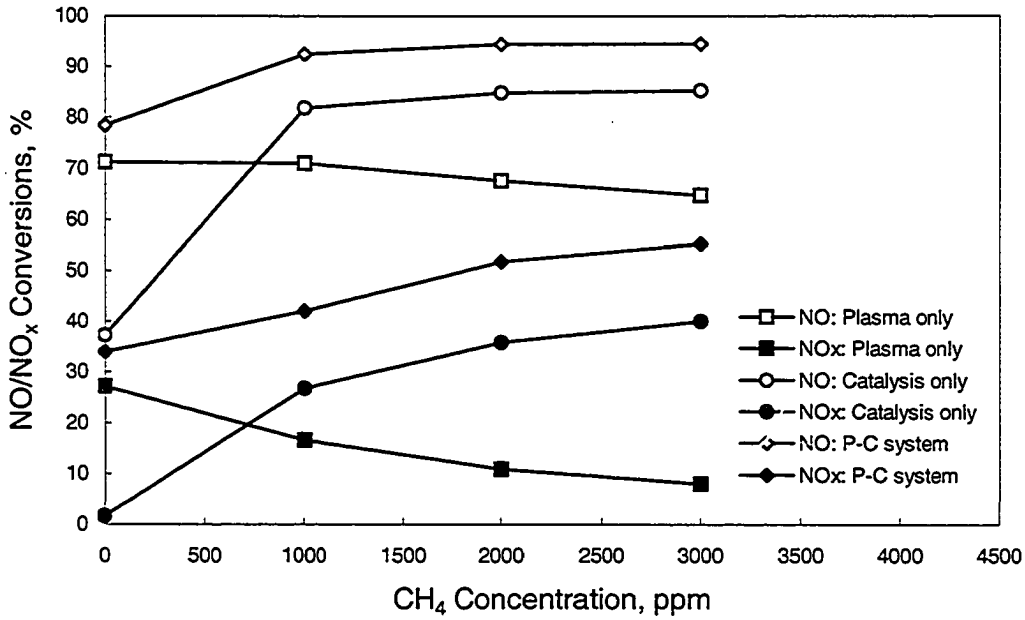


**Figure 5.30 $NO/NO_x$ Conversions vs. Concentrations of $CH_4$ Added.** Total flow rate 1000 SCCM: 250 ppm NO, 3% $O_2$ and $N_2$ balance. Plasma: 150 Hz, 260 J/L, glass wool packing. Catalysis: $\gamma$-$Al_2O_3$, 500 °C, space velocity 5,780 /h.

**Table 5.4**

**Comparison of $NO/NO_x$ Conversions with 3000 ppm $CH_4$ Addition**

| Conversion | Plasma Alone | Catalysis Alone | P-C System |
|---|---|---|---|
| NO, % | 65 | 85 | 94 |
| $NO_x$, % | 8 | 40 | 55 |

Table 5.5 compares the compositions of original and conditioned feeds. Plasma conditioning of the feed stream accounts for the higher $NO_x$ conversion by the P-C system compared to the catalytic reactor alone as shown in Table 5.4. In the case of conditioned feed, there are CO and other $CH_4$-oxidized products due to partial oxidation of $CH_4$ by the plasma process. A high $NO_2$ concentration of 141 ppm (Table 5.5) is found in the conditioned feed. These compounds may play an important role in the selective

catalytic reduction of $NO_x$. One of the De-$NO_x$ pathways can be considered the same as proposed in earlier Section II, i.e., CO and NO form isocyanate, an intermediate. $CH_4$ and $CH_4$-oxidized products probably combine with $NO_2$, forming $CH_3NO_2$, an intermediate indicating another pathway to $NO_x$ reduction as reaction (5.50) shown in Section II:

$$2\ CH_3\ NO_2 + O_2 \rightarrow N_2 + CO + CO_2 + 3\ H_2O$$

**Table 5.5**

**Composition Comparison between Original and Plasma-Conditioned Feed Streams for 3000 ppm $CH_4$ Addition**

| Feed Stream | NO | $NO_2$ | $O_2$ | $CH_4$ | $N_2$ |
|---|---|---|---|---|---|
| Original | 250 ppm | 0 ppm | 3% | 3000 ppm | balance |
| Conditioned | 89 ppm | 141 ppm | 3% | 2850 ppm * | balance |

* 5% of original $CH_4$ is oxidized into CO and HC-oxidized products.

$C_2H_4$ Effect on $NO_x$ Reduction with Plasma-Catalyst System

In order to investigate $C_2H_4$ effect on $NO/NO_x$ conversions, experiments are conducted in the absence of $CO_2$ since plasma would dissociate $CO_2$ into CO that would affect $NO_x$ conversion. The feed gas mixture is 1000 SCCM of 250 ppm NO, 3% $O_2$ and $N_2$ balance. The same P-C system is used except the plasma reactor is packed with glass wool as in previous case for a better discharge stability and a lower energy density. The plasma reactor is operated at an energy density of 260 J/L and room temperature. The catalyst used is $\gamma$-$Al_2O_3$ at 500 °C. The experiments are conducted with $C_2H_4$ additions of 0, 1000, 2000 and 3000 ppm to the inlet stream. For comparison, the same gas feed is bypassed around the plasma reactor and is directly fed to the catalytic reactor to obtain

the effect by catalyst alone on $NO/NO_x$ conversions. Figure 5.31 shows the $NO/NO_x$ conversions as a function of concentration of $C_2H_4$ added to the various systems.

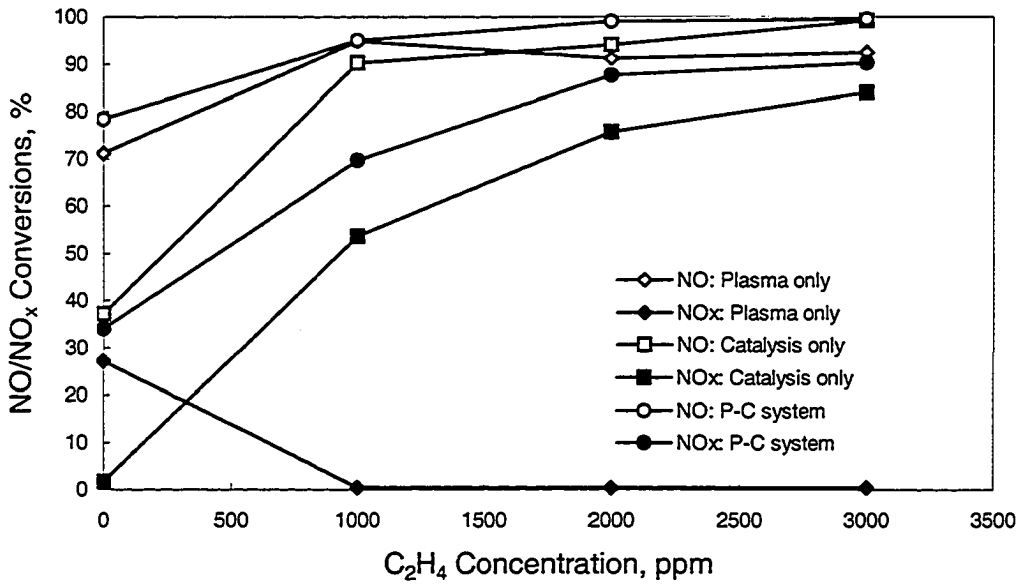


**Figure 5.31 $NO/NO_x$ Concentrations vs. Concentrations of $C_2H_4$ Added.** Total flow rate 1000 SCCM: 250 ppm NO, 3% $O_2$ and $N_2$ balance. Catalysis: $\gamma$-$Al_2O_3$, 500 °C. Plasma: 150 Hz, 260 J/L, glass wool packing, space velocity 5,780 /h.

**Table 5.6**

**Comparison of Conversions for 3000 ppm $C_2H_4$ Addition**

| Conversion | Plasma Alone | Catalysis Alone | P-C System |
|---|---|---|---|
| NO, % | 92 | 99 | 99 |
| $NO_x$, % | 0.4 | 84 | 90 |

Presented in Table 5.6 is the comparison of $NO/NO_x$ conversions with $C_2H_4$ addition of 3000 ppm in the inlet feed streams. The $NO/NO_x$ conversions for the P-C system are 99% and 90%, respectively, compared with 92% and 0.4% for the plasma

alone, 99% and 84% for catalysis alone. Comparing the $NO_x$ conversions achieved between P-C system and catalysis alone, the improvement in $NO_x$ conversion is found to be about 6 percent for $C_2H_4$ addition of 3000 ppm.

**Table 5.7**

**Improvement of $NO_x$ Conversions by P-C System**

| $C_2H_4$ Addition, ppm | 0 | 1000 | 2000 | 3000 |
|---|---|---|---|---|
| Catalysis alone (a), $NO_x$ % | 2 | 54 | 76 | 84 |
| P-C System (b), $NO_x$ % | 34 | 70 | 88 | 90 |
| Improvement (b-a), $NO_x$ % | 32 | 16 | 12 | 6 |

For both P-C system and catalysis alone, $NO_x$ conversion to $N_2$ is of importance. Therefore, only $NO_x$ conversions for different $C_2H_4$ concentrations are listed in Table 5.7 for comparison. The highest improvement of 32% for the P-C system without $C_2H_4$ addition is of little importance since the total $NO_x$ conversion is only 34%. When 1000 ppm $C_2H_4$ is added, the $NO_x$ conversion is 70% for the P-C system, 16% higher than 54% for the catalysis alone. The improvement decreases from 16% to 6% as $C_2H_4$ concentration increases from 1000 to 3000 ppm. Only 2 percentage advantage of $NO_x$ conversion is achieved by the P-C system when $C_2H_4$ concentration is increased from 2000 to 3000 ppm.

Table 5.8 compares the compositions between original and plasma-conditioned feeds. Plasma conditioning of the feed stream accounts for the higher $NO_x$ conversion by the P-C system compared to the conversion by the catalytic reactor alone. In the conditioned feed, there are CO and other $C_2H_4$-oxidized products due to partial

oxidization of $C_2H_4$ by the plasma process. These compounds play an important role in the selective catalytic reduction of $NO_x$. One of the De-NOx pathways can be considered the same as proposed in earlier Section II, i.e., CO and NO form isocyanate, an intermediate. A very high $NO_2$ concentration of 230 ppm is found in the conditioned feed. It may contribute to the increase in $NO_x$ conversion by the catalytic reactor if $NO_2$ is also an intermediate and assists in $NO_x$ reduction.

**Table 5.8**

**Composition Comparison between Original and Plasma-Conditioned Feed Streams for 3000 ppm $C_2H_4$ Addition**

| Feed Stream | NO | $NO_2$ | $O_2$ | $C_2H_4$ | $N_2$ |
|---|---|---|---|---|---|
| Original | 250 ppm | 0 ppm | 3% | 3000 ppm | balance |
| Conditioned | 19 ppm | 230 ppm | 3% | 2640 ppm * | balance |

* 12% of original $C_2H_4$ is oxidized into CO and other HC-oxidized products.

$NO_2$ Effect on Catalytic Reduction in the Presence of $C_2H_4$

In the preceding experiments in the P-C system, there is a great amount of $NO_2$ formed by the plasma conditioning along with CO and $C_2H_4$-oxidized products in the first stage. In order to identify the effect of $NO_2$ formation on the catalytic reduction of $NO_x$, separate experiments are conducted with $NO_2$ gas mixture as feed to the catalytic reactor only. This experiment design also eliminates the effect of CO and $C_2H_4$-oxidized products on $NO_x$ catalytic reduction since the feed composition is 175 ppm $NO_2$, 3% $O_2$ and $N_2$ balance. Total flow rate is 1000 SCCM and space velocity is 5,780 /h. The catalyst used is $\gamma$-$Al_2O_3$. For comparison, 175 ppm NO is also used for the same experimental conditions. Experiments are conducted under two conditions: change in the

concentration of $C_2H_4$ at a constant temperature of 500 °C and change in temperature at a constant concentration of 3000 ppm $C_2H_4$.

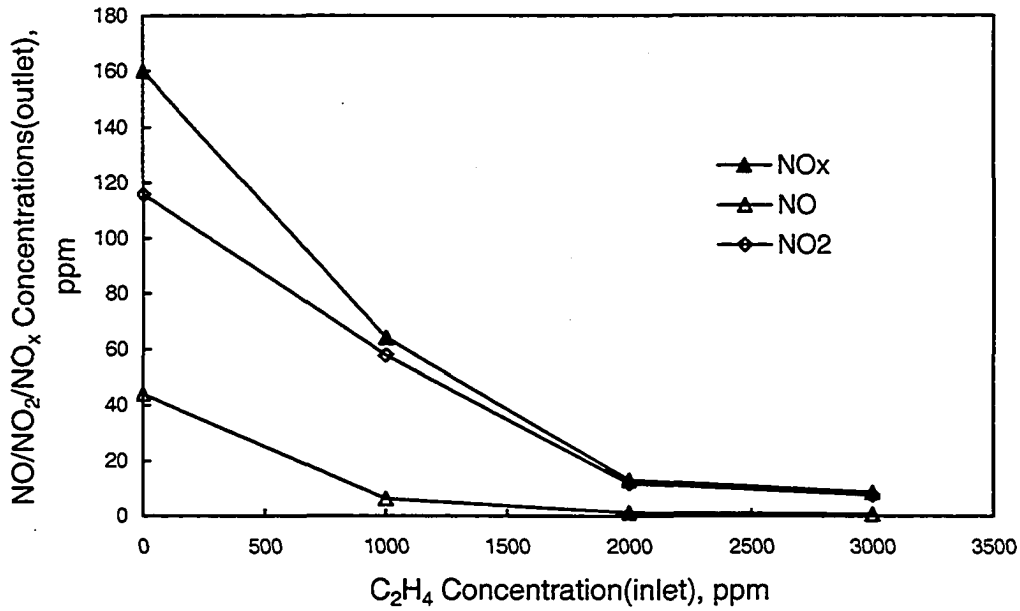


**Figure 5.32 Effect of $C_2H_4$ Concentration on Catalytic Reduction of $NO_2$.** Total flow rate 1000 SCCM. Feed: 175 ppm $NO_2$, 3% $O_2$ and $N_2$ balance. Catalysis: $\gamma$-$Al_2O_3$, 500 °C, space velocity 5,780/h.

Figure 5.32 shows the outlet $NO/NO_2/NO_x$ concentrations from the catalytic reactor for the $C_2H_4$ concentrations of 0-3000 ppm in the $NO_2$ gas feed. In the absence of $C_2H_4$, about 8.6 % $NO_x$ conversion is achieved in the catalytic reactor with a formation of 44 ppm NO. This can be explained by the following reversible reaction:

$$NO_2 <==> NO + ½\ O_2 \qquad (5.55)$$

The $NO_x$ conversion of 8.6 % may be the result of either or both of the reactions:

$$2\ NO_{ads} \rightarrow N_2 + O_2 \qquad (5.56)$$

$$2\ NO_{2,ads} \rightarrow N_2 + 2\ O_2 \qquad (5.57)$$

In the presence of $C_2H_4$, the outlet NO concentration decreases to 6.2, 1.2 and 0.8 ppm for $C_2H_4$ concentrations of 1000, 2000 and 3000 ppm, respectively.

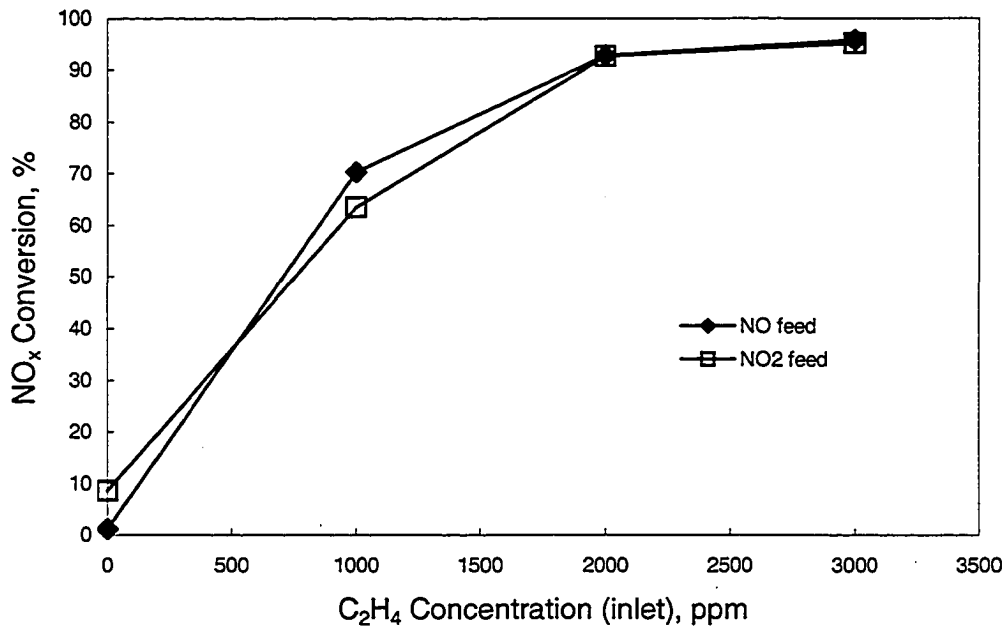


**Figure 5.33 Effect of $C_2H_4$ Concentration on $NO_x$ Conversions for Different Feeds.** 175 ppm NO feed with 3% $O_2$ and $N_2$ balance; 175 ppm $NO_2$ feed with 3% $O_2$ and $N_2$ balance. Catalysis: $\gamma$-$Al_2O_3$, 500 °C, space velocity 5,780/h.

Presented in Figure 5.33 are the $NO_x$ conversions as a function of $C_2H_4$ concentration for both NO and $NO_2$ feeds at 500 °C. For the catalytic reactor alone, the $NO_x$ conversions for both feeds are found to be the same at a given $C_2H_4$ concentration. A direct $NO_2$ feed does not give a higher $NO_x$ conversion than NO at 500 °C. It appears that NO oxidization into $NO_2$ is not the control reaction step for SCR of NO with $C_2H_4$ over catalyst $\gamma$-$Al_2O_3$.

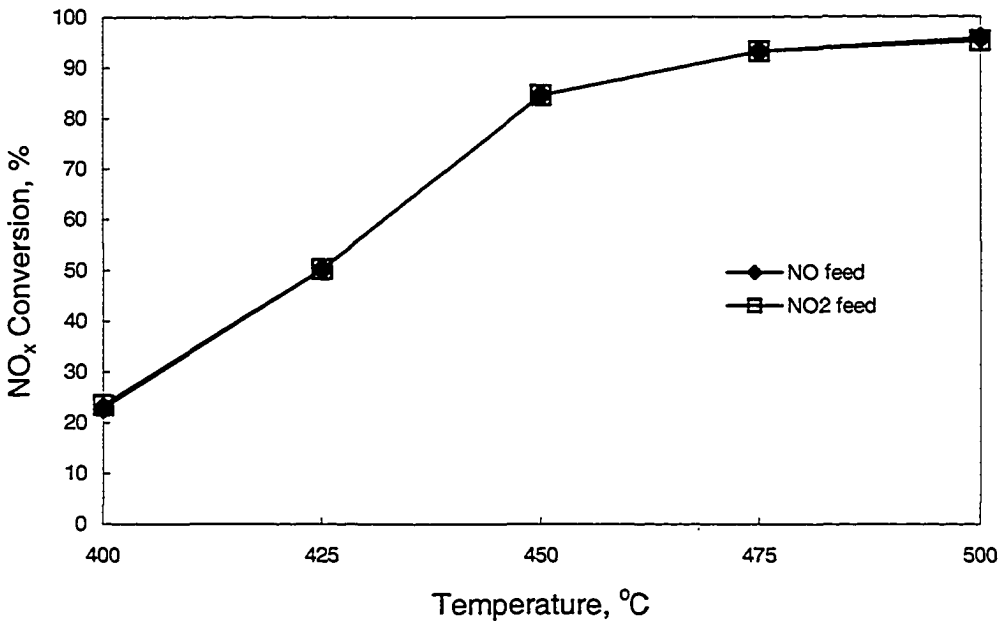


**Figure 5.34 Temperature Effect on $NO_x$ Conversions for Different Feeds with 3000 ppm $C_2H_4$ Added.** 175 ppm NO feed with 3% $O_2$ and $N_2$ balance; 175 ppm $NO_2$ feed with 3% $O_2$ and $N_2$ balance. Catalysis: $\gamma$-$Al_2O_3$, 400-500 °C, space velocity 5,780/h.

Figure 5.34 shows the temperature effect on $NO_x$ conversions for both NO and $NO_2$ feeds with 3000 ppm $C_2H_4$ added. The $NO_x$ conversions for both NO and $NO_2$ feed are the same at any temperature in the range of 400-500 °C. This further suggests that the control step of SCR of NO with $C_2H_4$ is not NO oxidization into $NO_2$. $NO_2$ may not be considered an intermediate for $NO_x$ reduction to $N_2$ under the given experimental conditions.

Investigation of $N_2O$ Formation

Nitrous oxide ($N_2O$) is one of the six greenhouse gases listed in the Kyoto Protocol. Therefore, attention should be paid when a process is used to remove nitrogen oxides for the possible formation of $N_2O$. Literature review reveals that $N_2O$ may be formed during plasma process. The reaction

$$NO_2 + N \rightarrow N_2O + O \quad (5.58)$$

may take place forming $N_2O$ (Matzing 1991). The formation of $N_2O$ in a positive-pulsed corona discharge reactor was reported and its amount was measured under several experimental conditions (Mok and others 2000). In the presence of $O_2$ and $H_2O$, Mot *et al.* reported up to 10 ppm of $N_2O$.

A series of separate experiments are conducted in this study to investigate the possible $N_2O$ formation in the DBD reactor, SCR reactor and P-C system. The total inlet flow rate is 1000 SCCM. Various gas feeds shown in Table 5.9 are passed through reactors. The operating conditions of the DBD reactor are room temperature with a glass-wool packing. The SCR reactor is operated with $\gamma$-$Al_2O_3$ as catalyst at 500 °C. The space velocity is 5,780 $h^{-1}$. Table 5.9 gives the summary of $NO/NO_x$ conversions and $N_2O$ formation.

Non-thermal plasma DBD reactor. 19 ppm of $N_2O$ is formed when 250 ppm NO in $N_2$ is passed through the DBD plasma reactor. In the presence of 3% oxygen, a concentration of 25 ppm $N_2O$ is recorded. The increase of 6 ppm may be attributed to the presence of oxygen that oxidizes NO into $NO_2$ leading to the formation of $N_2O$ through reaction (5.58). However, no $N_2O$ is detected when 2% water vapor is added to the gas feed. The effect of adding reducing agents such as $CH_4$ on $N_2O$ formation is investigated using the same reactor. In dry condition, addition of 3000ppm $CH_4$ does not reduce $N_2O$ formation. Addition of both 3000 ppm $CH_4$ and 2% water vapors reduces $N_2O$ formation from 20 to 5 ppm.

**Table 5.9 Summary of $N_2O$ Formations under Different Experimental Operating Conditions**

| Operating Condition / Gas Feed* | Plasma Only (room temp., glass-wool packing) | | | | Catalysis Only ($\gamma$-$Al_2O_3$, 500 °C) | | | P-C System | | |
|---|---|---|---|---|---|---|---|---|---|---|
| | Energy Density (J/L) | **$N_2O$ (ppm)** | NO** (%) | $NO_x$ (%) | **$N_2O$ (ppm)** | NO (%) | NOx (%) | **$N_2O$ (ppm)** | NO (%) | $NO_x$ (%) |
| $NO + N_2$ | 323 | **19** | 99.6 | 99.4 | | | | | | |
| $NO+ O_2+ N_2$ | 344 | **25** | 72.8 | 32 | | | | | | |
| $NO+ O_2+ N_2+ H_2O$ | 309 | **0** | 46 | 3.2 | | | | | | |
| $NO+ O_2 + N_2+ CH_4$ | 320 | **20** | 62 | 16.8 | **0** | 81.6 | 36 | **17** | 90.8 | 49.2 |
| $NO+ O_2+ CH_4+ H_2O+ N_2$ | 300 | **5** | 51.2 | 6.8 | | | | **5** | 62.8 | 23.2 |
| $NO+ O_2+ C_2H_4+ N_2$ | 200 | **n.a.** | 98 | 0 | | | | **0** | 99 | 90.4 |
| $NO+ O_2+ C_2H_4+ H_2O+ N_2$ | 288 | **n.a.** | 82.8 | 17.2 | | | | **0** | 98 | 77.2 |
| 175ppm $NO_2 + N_2$ | 221 | **25** | -18 | 70.3 | | | | | | |
| 175ppm $NO_2+ O_2+ N_2$ | 190 | **19** | -25 | 12.6 | | | | | | |

* NO =250ppm, $O_2$ = 3%, $CH_4$= 3000ppm, $C_2H_4$=3000ppm, $H_2O$=2%, $N_2$ balance. ** Negative value means formation of NO.
n.a.: not analyzed

175 ppm $NO_2$ instead of 250 ppm NO is used in gas feed to study if $NO_2$ is an intermediate in the formation of $N_2O$ as per reaction (5.58). A concentration of 25 ppm $N_2O$ in the outlet is recorded at energy density of 221 J/L, compared to 19 ppm $N_2O$ formation when 250 ppm NO is in the feed at higher energy density of 323 J/L. This shows that $NO_2$ may be an intermediate in the $N_2O$ formation. In the presence of 3% $O_2$, 175 ppm $NO_2$ feed leads to the formation of 19 ppm $N_2O$ at a much lower energy density of 190 J/L, compared to 25 ppm $N_2O$ formation when 250 ppm NO is in the feed at energy density of 344 J/L.

SCR reactor. $NO/O_2/CH_4/N_2$ gas feed is used to investigate if $N_2O$ is formed in SCR reactor with $\gamma$-$Al_2O_3$ as catalyst. In the SCR reactor at a temperature of 500 °C, $N_2O$ is not detected while $NO/NO_x$ conversions are 81.6% and 36%, respectively. In other words, the SCR reactor does not contribute $N_2O$ formation. More data points could not be obtained due to limited availability of FTIR equipment.

Hybrid P-C system. When the same feed mixture of $NO/O_2/CH_4/N_2$ is passed through the P-C system, 17 ppm $N_2O$ is found in the outlet gas from the P-C system. However, this $N_2O$ concentration is reduced to less than 5 ppm in the presence of 2% $H_2O$. Addition of 3000 ppm $C_2H_4$ to the mixture of $NO/O_2/N_2$ successfully suppresses $N_2O$ formation in the P-C system even in the absence of water vapors.

In summary, about 19-25 ppm $N_2O$ is formed when 250 ppm NO in a dry mixture of $N_2$ or $N_2$-$O_2$ is passed through the DBD reactor. However, presence of 2% water vapors in the feed mixture reduces $N_2O$ formation to less than 5 ppm in the DBD reactor. Addition of $CH_4$ as reducing agent does not help reduce this $N_2O$ formed in the DBD reactor. There is no $N_2O$ formation in the SCR reactor. No significant amount of $N_2O$

(less than 5 ppm) is detected in the outlet gas of the P-C system. Flue gas or exhaust typically contains 5-10% $H_2O$ vapors. Therefore, there is not likely to be any $N_2O$ formation problem using a P-C system for $NO_x$ removal.

Section Conclusions

In this section, experiments have been conducted with emphasis on $NO_x$ reduction to $N_2$ in a hybrid plasma-catalyst (P-C) system as very little information is available in this area. The hybrid P-C experiments show more effective $NO_x$ removal compared to the results from either DBD or SCR experiments. A mechanism that plasma preconditions the gas stream has been proposed for the synergy of the P-C system. The following main conclusions can be drawn:

1. For the gas mixture of 250ppmNO/230ppmCO/3%$O_2$/7.6%$CO_2$/$N_2$, a maximum $NO_x$ conversion of 42% is achieved in a P-C system with 1% $WO_3/Al_2O_3$ catalyst at 450 °C, compared to the $NO_x$ conversion of 9% by either plasma or catalysis alone. Plasma preconditions the gas stream producing 700 ppm CO and 87 ppm $NO_2$. It is the significant increase of 700 ppm CO that promotes the overall $NO_x$ reduction.
2. For the gas mixture of 250ppmNO/3%$O_2$ /3000ppm$CH_4$/$N_2$, the $NO_x$ conversion for the P-C system is 55%, compared with 8% for the plasma and 40% for the catalysis, individually. Comparing the $NO_x$ conversions between P-C system and catalysis system, the improvement in $NO_x$ conversion is found to remain constant at 15% when $CH_4$ concentration in the inlet gas stream is varied in the range of 1000-3000 ppm.

3. When 1000 ppm $C_2H_4$ is added to the gas mixture of 250ppmNO/3%$O_2$/$N_2$, the $NO_x$ conversion is 70% for the P-C system, 16% higher than the $NO_x$ conversion of 54% for the catalysis alone.
4. Comparison of experimental results obtained using NO and $NO_2$ feed mixtures individually show that there is no difference in $NO_x$ conversion under the same SCR operating conditions. $NO_2$ may not be an intermediate for $NO_x$ reduction to $N_2$ under those experimental conditions.
5. Passing a dry simulated gas mixture through the DBD reactor produces about 19-25 ppm $N_2O$. However, presence of 2% $H_2O$ in the mixture effectively reduces $N_2O$ formation to less than 5 ppm in the DBD. No significant amount of $N_2O$ (less than 5 ppm) is detected in the outlet stream of the P-C system in the presence of 2% $H_2O$.

## Section IV Dielectric Barrier Discharge Reactor Design Parameters

The non-thermal plasma reactor design parameters are studied in this section with respect to reactor geometry and barrier materials. Pollutant gas $SO_2$ is used as a test gas. The non-thermal experimental system described earlier is used to investigate $SO_2$ oxidation. The experiments have been extended to study the effect of cylindrical, square and rectangular reactor geometries on $SO_2$ to $SO_3$ conversion (Mathur 1999). The rectangular reactor is also used to compare effects of different materials and barrier thickness on $SO_2$ conversion. Most of the experiments are conducted with an inlet gas mixture of 770 ppm $SO_2$, 4000ppm $O_2$ and balance $N_2$ at 400Hz. The $SO_2$ concentration measurements are made with an infrared analyzer.

Effects of Voltage and Frequency on $SO_2$ Conversion

Effect of voltage on $SO_2$ conversion. Figure 5.35 shows that $SO_2$ conversion increases as applied voltage is increased. There is a significant increase in $SO_2$ conversion from 40 to 80% for a peak voltage from 21 to 25 kV. The curve shows a typical "S" shape.

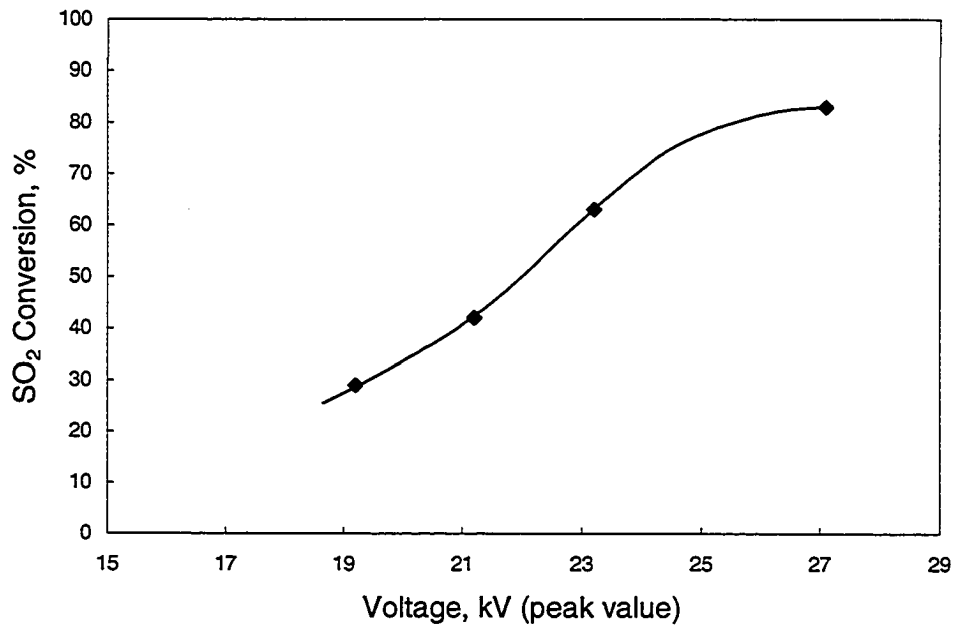


**Figure 5.35 $SO_2$ Conversion vs. Voltage(peak values).** Frequency 400 Hz, room temperature, total flow rate 510 SCCM, $SO_2$ 765 ppm, $O_2$ 4118 ppm, $O_2/SO_2$ =5.4, balance gas $N_2$.

Effect of frequency on $SO_2$ conversion. Figure 5.36 shows that $SO_2$ conversion increases linearly with frequency. Almost 100% $SO_2$ gets converted when frequency reaches 500 Hz.

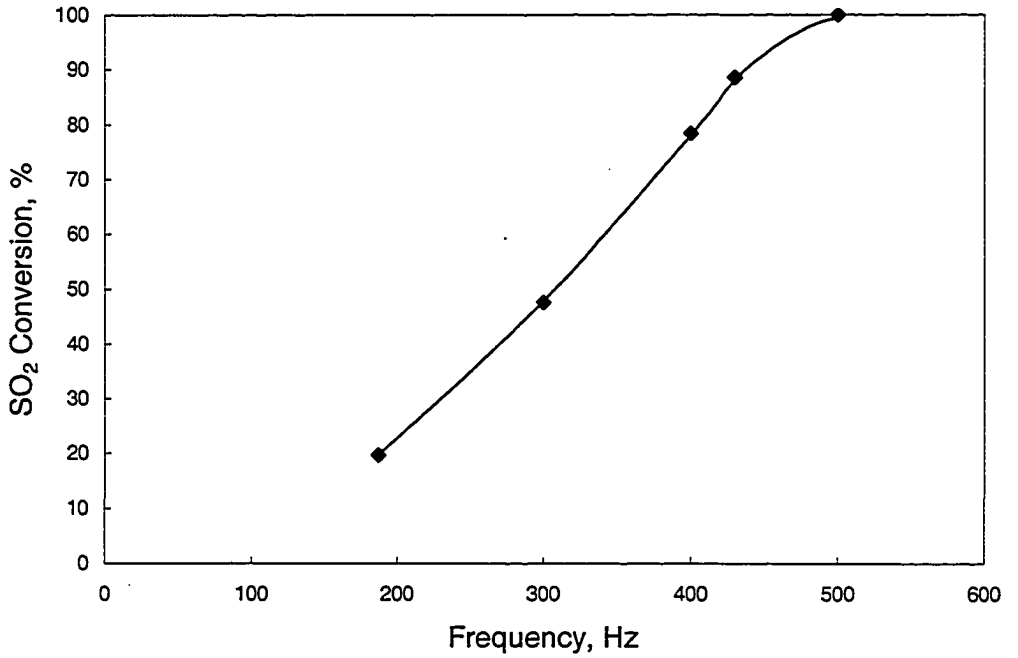


**Figure 5.36 Effect of Frequency on $SO_2$ Conversion.** Voltage 30 kV(peak value), total flow rate 510 SCCM, $SO_2$ 778 ppm, $O_2$ 4118 ppm, $O_2/SO_2$=5.3, balance gas $N_2$.

Effect of Geometry on $SO_2$ Conversion

Figure 5.37 shows that the energy requirements of cylindrical, square and rectangular reactors for the same conversion are in an increasing order under identical experimental conditions. For the same energy density of 3000 J/L, the $SO_2$ conversions are 80, 33 and 22% for cylindrical, square and rectangular reactors, respectively.

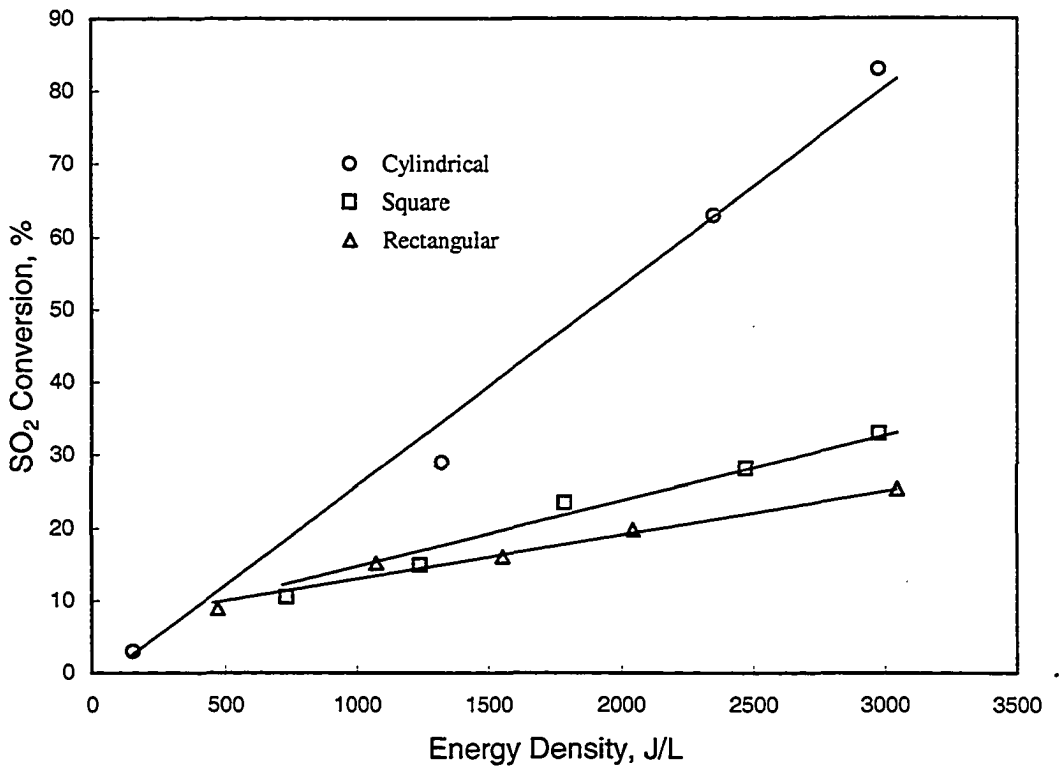


**Figure 5.37 Effect of Reactor Geometry on $SO_2$ Conversion**

Effect of Barrier Materials on $SO_2$ Conversion

The barrier materials tested are composite mica, quartz and soft glass with dielectric constants of 2.3, 3.7 and 6.4, respectively which are experimentally measured and calculated (for details see Appendix D). Figure 5.38 shows that for the same energy density, reactor with composite mica as barrier material gives the highest conversion. It appears that lower dielectric constant may be helpful in achieving higher $SO_2$ conversion. The rough surface of composite mica may cause local micro sparking areas where more concentrated and energetic electrons may enhance $SO_2$ conversion.

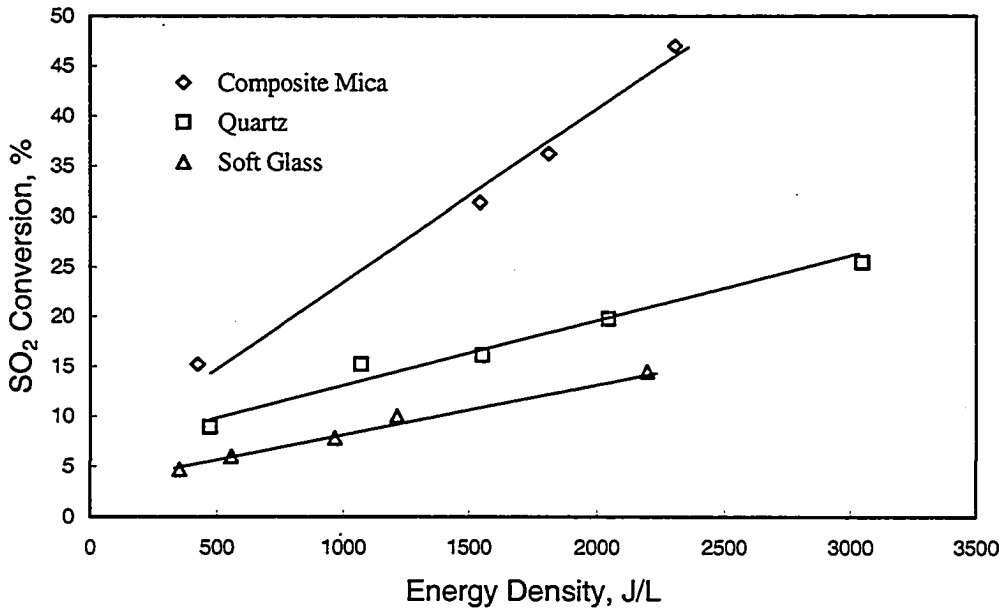


**Figure 5.38 Effect of Barrier Material on $SO_2$ Conversion**

Effect of Barrier Thickness on $SO_2$ Conversion

Composite mica is selected to investigate barrier thickness effect on $SO_2$ conversion. For the convenience of fabrication, a rectangular reactor is used. One, two and three layers of composite mica are used to obtain increases in thickness ( 0.8, 1.6, and 2.4 mm ). In each case, energy density is increased till the experiment had to be discontinued due to excessive sparking. Experimental results show that barrier thickness has little effect on $SO_2$ conversion (Figure 5.39). However, thicker barrier could stand greater discharge power leading to higher $SO_2$ conversion.

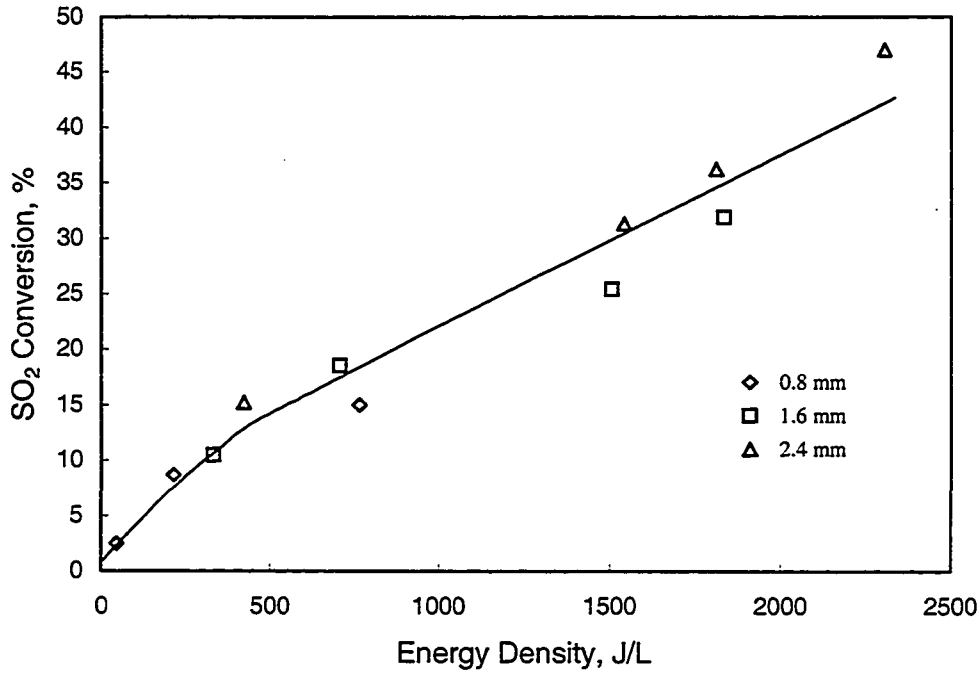


**Figure 5.39 Effect of Barrier Thickness on $SO_2$ Conversion**

Cost Estimates and Comparison

Cost projections based on bench-scale experiments are risky and uncertain. However, efforts have been made in this study to present some cost figures based on the literature information comparing a non-thermal plasma process against combined conventional processes for removing $NO_x$ and $SO_2$ from coal-fired power plant flue gases. Several terms used in this analysis are given below:

**SCR** (Selective Catalytic Reduction): It is a prevailing process for removing $NO_x$ from coal-fired flue gases. It selectively reduces $NO_x$ to $N_2$ by $NH_3$ over a catalyst (oxides of vanadium and/or tungsten). Basic reactions are

$$4\,NO + 4\,NH_3 + O_2 \rightarrow 4\,N_2 + 6\,H_2O$$

$$2\,NO_2 + 4\,NH_3 + O_2 \rightarrow 3\,N_2 + 6\,H_2O$$

**FGD** (Flue Gas Desulfurization): It is a prevailing process for scrubbing $SO_2$ from coal-fired flue gases. A typical FGD process uses limestone to capture $SO_2$ as follows:

$$CaCO_3 + SO_2 + \tfrac{1}{2}H_2O \rightarrow CaSO_3 \cdot \tfrac{1}{2}H_2O(s) + CO_2(g)$$

**DBD** (Non-thermal plasma Dielectric Barrier Discharge): This technique is under commercialization by Powerspan Corp. NO is oxidized into $NO_2$ and $HNO_3$ and part of $SO_2$ is oxidized into $SO_3$ and $H_2SO_4$ using a DBD reactor. Powerspan Corp. integrates DBD with ammonia scrubbing in one unit achieving over 90% removal of both $NO_x$ and $SO_2$.

**Capital Cost** ($/kW): The cost incurred for installing a pollutant control unit during the construction of a new power plant.

**Retrofit Cost** ($/kW): The cost incurred for retrofitting a pollutant control unit to an existing power plant. This cost includes the expenses for installing the pollutant control unit and balance of plant (BOP) modification cost. Usually, retrofit cost in power plants is significantly higher than capital cost.

**Levelized Cost** (mills/kWh): It is determined by eliminating effects of time, inflation, etc. on total cost. The present value of the total cost of constructing and operating a control unit over its economic life is distributed in equal payments per kWh. Levelized cost can be split into capital charge and O&M cost.

**O&M Cost** (mills/kWh): Operation and maintenance cost per kWh.

**Capital Charge** (mills/kWh): Capital cost per kWh.

Cost comparison for simultaneous removal of $NO_x$ and $SO_2$ between a non-thermal plasma DBD process and combined processes of SCR and FGD has been made by compiling publicly available information (DOE and SCS 1997; DOE and others 1999; McLarnon 2002). O&M cost for FGD and levelized cost for DBD have been estimated by the author of this thesis. All costs are projected for a 300-500 MWe power plant with 90% removal of both $NO_x$ and $SO_2$. Table 1 shows the comparison.

Estimation of O&M cost for FGD: The reported retrofit cost for FGD is 300 $/kW which is about three times that for SCR (105 $/kW). Therefore, the capital charge for FGD can be assumed as three times that for SCR (2.6-1.1 =1.5 mills/kWh), i.e., 4.5 mills/kWh. The O&M cost for FGD is estimated to be 7.5 mills/kWh by subtracting this capital charge from the levelized cost (12.0 mills/kWh).

Estimation of levelized cost for DBD: The reported retrofit cost for DBD is 200 $/kW which is about two times that for SCR (105 $/kW). Therefore, the capital charge for DBD can be assumed as two times for SCR(1.5 mills/kWh), i.e., 3 mills/kWh. This capital charge plus the reported O&M cost of 1.5 mills/kWh gives the levelized cost of 4.5 mills/kWh for DBD.

**Table 5.10**
**Cost Comparison between DBD and Conventional Techniques**

| Technology | Capital Cost ( $/kW ) | | Retrofit Cost ( $/kW ) | | Levelized Cost (O&M cost*) ( mills/kWh ) | |
|---|---|---|---|---|---|---|
| SCR($NO_x$) (DOE & SCS 1997) | 66 | 160 | 105 | 408 | 2.6 (1.1 ) | 14.6 ( 8.6 ) |
| FGD ($SO_2$) (DOE and others 1999) | 94 | | 300 | | 12.0 ( 7.5) | |
| DBD ($NO_x$ and $SO_2$) (McLarnon 2002) | 150 | | 200 | | 4.5 ( 1.5 ) | |

* O&M cost in parentheses.

Data in Table 1 shows that the capital cost for using DBD technique ($150/kW) is close to that of combined processes of SCR and FDG ($160/kW) during the construction of a new power plant. However, the cost for retrofitting a DBD process to an existing power plant is only $200/kW, half as much as for retrofitting a combined SCR and FGD processes ($408/kW). Based on retrofitting cost, the levelized cost for DBD process is only 4.5 mills/kWh, less than one third of that (14.6 mills/kWh) for combined processes. Based on the figures provided in the references it may be concluded that DBD process is more economical than the combined conventional processes of SCR and FGD for simultaneous removal of $NO_x$ and $SO_2$ from coal-fired utility power plants.

Section Conclusions

Literature review has shown that little work has been done in the area of evaluation of DBD reactor design parameters. This section is focused on the effects of reactor geometry and dielectric materials in terms of $SO_2$ conversion to $SO_3$ since DBD has the similar effect on $SO_2$ oxidation. The following conclusions can be drawn:

1. Over 80 % conversion of $SO_2$ can be achieved with the cylindrical DBD plasma reactor. The energy requirements of cylindrical, square and rectangular reactors for the same conversion are in an increasing order under identical experimental conditions.
2. For the same energy density, reactor with composite mica as barrier material gives a higher conversion than with quartz or soft glass. It appears that lower dielectric constant may be helpful in achieving higher $SO_2$ conversion.

3. Experimental results show that barrier thickness has little effect on $SO_2$ conversion. However, thicker barrier could stand greater discharge power leading to higher $SO_2$ conversion.
4. A DBD process is more economical than the combined conventional processes of SCR and FGD for simultaneous removal of $NO_x$ and $SO_2$ from coal-fired utility power plants.

# CHAPTER VI

# CONCLUSIONS

The present study on $NO_x$ remediation through non-thermal plasma and catalysis has led to a number of findings. Several conclusions are drawn from the four-section studies: DBD plasma system, SCR system, plasma-catalyst (P-C) system for $NO_x$ removal and DBD reactor design parameters for $SO_2$ removal. The detailed conclusions have been presented at the end of each section. The general conclusions are given as follows:

1. Non-thermal plasma DBD technology can be used to convert $NO_x$ in flue gases and diesel-engine exhausts.
2. DBD is found to be effective for the oxidation of NO into $NO_2$ in the simultaneous presence of $O_2$ and $H_2O$.
3. DBD is also found to be effective for the oxidation of $SO_2$ into $SO_3$.
4. Power consumption is key parameter in reactor performance and must be minimized for commercial operation.
5. Two models proposed in the present study introduce two concepts for plasma reactions: effective activation energy, $E_a$ and minimum energy density for initiating NO reactions, $E_i$ under plasma conditions. These two models would provide an effective guidance in laboratory experiments and commercialization of the DBD technique.

6. Addition of hydrocarbons such as $CH_4$ and $C_2H_4$ substantially promotes the oxidation of NO into $NO_2$ in the presence of $O_2$ under DBD.
7. $\gamma$-$Al_2O_3$ is an effective material to serve as a SCR catalyst. $C_2H_4$ is much more effective than $CH_4$ for selective catalytic reduction of NO.
8. Plasma-catalyst (P-C) system is found to be more effective in improving $NO_x$ reduction compared to either plasma (DBD) or catalysis alone.
9. P-C system does not add $N_2O$ to the air pollution.

The DBD process for the removal of $NO_x$ and $SO_2$ has the potential to replace the prevailing SCR and FGD techniques both technically and economically. The plasma-catalyst system has the potential to be used for the removal of $NO_x$ from diesel-engine exhausts. This work has moved the plasma technique for air pollution control to firmer scientific grounds.

# CHAPTER VII

## RECOMMENDATIONS

Several recommendations are made as follows:

1. Energy consumption needs to be reduced by developing new DBD reactors. Reactor design includes electrode geometry, distance between two electrodes, barrier materials and electrode length. Data from an earlier work on the same apparatus and a process development system are examined and it is found that a smaller gap between the two electrodes and a longer length of reactor would significantly improve the energy efficiency. This is because both smaller gap and longer reactor length increase capacitance as well as improve discharge distribution.
2. A new DBD reactor should be designed to stand high temperatures up to 500 °C, 100 °C higher than typical temperatures of 350-400 °C of exhausts from diesel engines. This will make it possible to run the plasma reactor under real gas temperatures without water condensation. Experiments should also be conducted in a P-C system with one-stage configuration. It is important to investigate how plasma interacts with a catalyst, leading to a potential effective compact unit for the removal of $NO_x$ from mobile sources.
3. More experiments need to be conducted for $SO_2$ conversion in a DBD reactor. $SO_2$ should be added to simulated gas mixture to investigate the interaction between $NO_x$ and $SO_2$ in a plasma reactor.

4. Experiments with other reducing agents such as propylene or ethane should be conducted to study their effect on $NO_x$ reduction for comparison.
5. Development of new lean-burn catalysts is necessary for the P-C system for removing $NO_x$ in diesel-engine exhausts. Characterization of such catalysts should be undertaken by means of *in situ* X-ray absorption spectroscopy (XAS) and Fourier transform infrared spectroscopy (FTIR). XAS is an atom-specific technique sensitive to the local environment of the metal ion and its oxidation state and allows determination of both oxidation state and atomic structure parameters. FTIR may be used to collect spectra of a catalyst used for SCR and identify those intermediate species adsorbed on the catalyst, providing direct chemistry of micro reaction processes.
6. Study of methane and carbon dioxide reaction over plasma can be a promising subject. Identification and quantification of products should be conducted using a GC-MS analyzer. A catalyst may be installed inside the discharge space aimed at promoting methane and carbon dioxide reactions and improving the selective production of value-added products.
7. More study needs to be conducted to enhance the knowledge of plasma chemistry and kinetic modeling work. A molecular beam mass spectrometer (MBMS) may be used on-line to identify major species and measure their concentrations inside the plasma DBD reactor. This will significantly enrich the chemistry knowledge in the DBD process leading to better kinetic modeling.
8. Non-thermal plasma has strong potential to oxidize trace elements such as mercury into HgO that can be easily removed in scrubbers. If successful, this will

be the only process which can simultaneously remove $NO_x$, $SO_2$ and Hg from coal-fired utility boiler flue gases. Trace element oxidation should be studied using non-thermal plasma technology.

9. Cost is the most important factor for a pollutant technique such as non-thermal plasma DBD aimed at finding wide commercial applications. More rigorous economic analysis need to be conducted to promote the commercialization of the DBD technique.

## LITERATURE CITED*


Almusaiteer K, Chuang S, Tan C. 2000. Reactivity of $Ph^{+}(CO)_2$ during the NO-CO and $CO-O_2$ reactions over $Rh/Al_2O_3$. J Catalysis 189: 247-52.

Amiridis M, Zhang T, Farrauto R. 1996. Selective catalytic reduction of nitric oxide by hydrocarbons. Applied Catalysis B: Environmental 10: 203-27.

Ault J, Ayen R. 1971. Catalytic reduction of nitric oxide with various hydrocarbons. AIChE J 17(2): 265-71.

Bailar J, Moeller T, Kleinberg J, Guss C, Castellion M, Metz C. 1984. Chemistry. 2nd ed. Florida, Academic Press. p 569.

Baldanza M, Mello L, Vannice A, Noronha F, Schmal M. 2000. Adsorptive and catalytic properties of alumina-supported Pd-Mo catalysts. J Catalysis 192:64-76.

Balmer M, Tonkyn R, Yoon I, Hoard J. 1998. Nitrogen measurement from $NO_x$ reduction for a plasma catalyst system in simulated diesel exhaust. Proceedings of the diesel engine emissions reduction workshop; 1998 July 6-9; Castine, ME. DOE/EE-0191. p193-9.

Bethke K, Kung H. 1997. Supported Ag catalysts for the lean reduction of NO with $C_3H_6$. J Catalysis 172: 93-102.

Breault R, McLarnon C, Mathur V. 1993. Reaction kinetics for flue gas treatment of $NO_x$. In: Penetrante B and Schultheis S editors. Non-thermal plasma techniques for pollution control, Part B: electron beam and electrical discharge processing. Proceedings of the NATO advanced research workshop on non-thermal plasma techniques for pollution control; 1992 Sept 21-25; Cambridge, England. NATO ASI Series. p 239-56.

Captain D, Amiridis M. 1999. *In situ* FTIR studies of the selective catalytic reduction of NO by $C_3H_6$ over $Pt/Al_2O_3$. J Catalysis 184: 377-89.

Captain D, Amiridis M. 2000. NO reduction by propylene over $Pt/SiO_2$: An *in situ* FTIR study. J Catalysis 194: 222-32.

Chen H, Voskoboinikov T, Sachtler W. 1999. Reaction intermediates in the selective catalytic reduction of $NO_x$ over Fe/ZSM-5. J Catalysis 186: 91-9.


* This literature citation follows CBE style.

Cho S. 1994. Properly apply selective catalytic reduction for $NO_x$ removal. Chemical Engineering Progress. January: 39-45.

Clements J, Mizuno A, Finney W, Davis R. 1989. Combined removal of $SO_2$, $NO_x$, and fly ash from simulated flue gas using pulsed streamer corona, IEEE Transactions Industry Applications 25(1): 62-9.

CPS (Constellation Power Source, Inc.), Baltimore, Maryland, H.A. Wagner plant. 2001. <http://www.powersrc.com/rightToKnow/brandon.asp>.

Denton P, Giroir-Fendler A, Praliaud H, Primet M. 2000. Role of the nature of the support (alumina or silica), of the support porosity, and of the Pt dispersion in the selective reduction of NO by $C_3H_6$ under lean-burn conditions. J Catalysis 189: 410-20.

Desai A, Kovalchuk V, Lombardo E, d'Itri J. 1999. CoZSM-5: why this catalyst selectively reduces $NO_x$ with methane. J Catalysis 184:396-405.

Dhali S, Sardja I. 1991. Dielectric-barrier discharge for processing of $SO_2/NO_x$. J Appl Phys 69(9): 6319-24.

Diaz G, Perez-Hernandez R, Benaissa A, Mariscal R, Fierro J. 1999. $CuO-SiO_2$ sol-gel catalysts: characterization and catalytic properties for NO reduction. J Catalysis 187: 1-14.

DOE, Pure Air, SCS, New York State Electric & Gas Corp. 1999. Advanced technologies for the control of sulfur dioxide emissions from coal-fired boilers. Topical report, no. 12.

DOE, SCS (Southern Company Services, Inc.). 1997. Control of nitrogen oxide emissions: selective catalytic reduction (SCR). Topical report, no. 9.

Dorai R, Hassouni K, Kushner M. 2000. Interaction between soot particles and $NO_x$ during dielectric barrier discharge plasma remediation of simulated diesel exhaust. J Applied Physics 88(10): 6060-71.

EEA(European Environmental Agency). 1999.Air Emissions Annual Topic Update 1998. Topic report, no 12. <http://reports.eea.eu.int/1299/en/1299.pdf>.

Eliasson B, Kogelschatz, U. 1991. Modeling and applications of silent discharge plasmas. IEEE Transactions Plasma Science 19 (2): 309-23.

Eliasson B, Kogelschatz U. 1991. Nonequilibrium volume plasma chemical processing. IEEE Transactions Plasma Science 19 (6): 1063-77.

Eliasson B, Liu C, Kogelschatz U. 2000. Direct conversion of methane and carbon dioxide to higher hydrocarbons using catalytic dielectric-barrier discharges with zeolites. Ind Eng Chem Res 39: 1221-7.

EPA. September 2001. National air quality 2000 status and trends. Summary report. <http://www.epa.gov/oar/aqtrnd00/>.

EPA. October 2001. Nonroad diesel emission standards. Staff technical paper. EPA420-R-01-052. <http://www.epa.gov/orcdizux/regs/nonroad/equip-hd/r01052.pdf>.

EPA. March 2000. National air pollutant emission trends 1900 – 1998. EPA454/R-00-002. <http://www.epa.gov/ttn/chief/trends/trends98/chapter3.pdf>.

Evans D, Rosocha L, Anderson G, Coogan J, Kushner M. 1993. Plasma remediation of trichloroethylene in silent discharge plasmas. J Applied Physics 74(9): 5378-86.

Fernandez-Garcia M, Martinez-Arias A, Belver C, Anderson J. Conesa J, Soria J. 2000. Behavior of palladium-copper catalysts for CO and NO elimination. J Catalysis 190:387-95.

Frank N. 1993. Economics of the electron beam process. In: Penetrante B and Schultheis S editors. Non-thermal plasma techniques for pollution control, Part B: electron beam and electrical discharge processing. Proceedings of the NATO advanced research workshop on non-thermal plasma techniques for pollution control; 1992 Sept 21-25; Cambridge, England. NATO ASI Series. p 27-32.

Frank N, Hirano S. 1993. The History of Electron beam processing for environmental pollution control and work performed in the United States. In: Penetrante B and Schultheis S editors. Non-thermal plasma techniques for pollution control, Part B: electron beam and electrical discharge processing. Proceedings of the NATO advanced research workshop on non-thermal plasma techniques for pollution control; 1992 Sept 21-25; Cambridge, England. NATO ASI Series. p 1-26.

Gates B. 1992. Catalytic Chemistry. New York: John Wiley & Sons, Inc. p 268.

Gentile A, Kushner M. 1995. Reaction chemistry and optimization of plasma remediation of NxOy from gas streams. J Appl Phys 78(3): 2074-85.

Gentile A, Kushner M. 1996. Microstreamer dynamics during plasma remediation of NO using atmospheric pressure dielectric barrier discharges. J Appl Phys 79(8):3877-85.

Gesser H, Hunter N, Probawono D.1998. The $CO_2$ reforming of natural gas in a silent discharge reactor. Plasma Chemistry Plasma Processing 18(2):241-5.

Golden C. 1997. Decomposition of refrigerants R12, R-22 and R-50 by barrier discharge [master thesis]. Durham (NH): University of New Hampshire.

Golden C, Mathur V. 1997. Barrier discharge technique for destruction of CFCs. AIChE annual meeting; 1997 Nov; Los Angela, CA.

Haneda M, Kintaichi Y, Shimada H, Hamada H. 2000. Selective reduction of NO with propene over $Ga_2O_3$-$AL_2O_3$: effect of sol-gel method on the catalytic performance. J Catalysis 192:137-148.

Hao J, Tian H, Lu Y, He K, Duan L. 2001. The anthropogenic nitrogen oxides emissions in China in the period 1990-1998. Preprints of Symposia, Division of Fuel Chemistry, ACS. 46(1):177-181.

Hardison L, Nagl G, Addison G. 1991. $NO_x$ reduction by the Econ-$NO_x$ SCR process. Environmental Progress 10(4): 314-18.

Helfritch D. 1993. $SO_2$ and $NO_x$ removal from flue gas by means of lime spray dryer followed by electron beam irradiation. In: Penetrante B and Schultheis S editors. Non-thermal plasma techniques for pollution control, Part B: electron beam and electrical discharge processing. Proceedings of the NATO advanced research workshop on non-thermal plasma techniques for pollution control; 1992 Sept 21-25; Cambridge, England. NATO ASI Series. p 33-46.

Henis J. 1976. Nitrogen oxide decomposition process. US Patent, No. 3,983,021. Sept. 28.

Hippel, V.; Robert, A. (ed). 1954. Dielectric materials and applications. MIT Press, Cambridge, MA. p 403.

Hoard J, Balmer M. 1998. Plasma-catalysis for diesel $NO_x$ remediation. Proceedings of the 1998 diesel engine emissions reduction workshop; 1998 July 6-9; Castine, ME. DOE/EE-0191. p 187-192.

Hsieh L, Lee W, Chen C, Chang M, Chang H. 1998. Converting methane by using an RF plasma reactor. Plasma Chemistry Plasma Processing 18(2): 215-39.

Joshi S. 1927. The decomposition of nitrous oxide in the silent electric discharge, part I. Trans Faraday Soc 23: 227-38.

Joshi S. 1929. The decomposition of nitrous oxide in the silent electric discharge, part II. Trans Faraday Soc 25:108-17.

Joshi S. 1929. The Decomposition of nitrous oxide in the silent electric discharge, part IV. Trans Faraday Soc 25: 137-143.

Kamata H, Takahashi K, Odenbrand C. 1999. Kinetics of the selective reduction of NO with $NH_3$ over a $V_2O_5$ $(WO_3)/TiO_2$ commercial SCR catalyst. J Catalysis 185: 106-13.

Kogelschatz U, Eliasson B, Egli W. 1997. Dielectric-barrier discharge principle and applications. Invited plenary lecture. International conference on phenomena in ionized gases (ICPIG, XXIII); 1997July 17-22; Toulouse, France.

Kogelschatz U, Eliasson B, Egli W. 1999. From ozone generators to flat television screens: history and future potential of dielectric-barrier discharges. Pure Applied Chemistry 71(10):1819-28.

Kondarides D, Chafik T, Verykios X. 2000. Catalytic reduction of NO by CO over rhodium catalysts. J Catalysis 191:147-64.

Koshkarian K, Chanda A, Palekar V, Ramavajjala M. 1998. Evaluation of gas phase pulsed plasma emissions system for diesel exhaust aftertreatment. Proceedings of the diesel engine emissions reduction workshop; 1998 July 6-9; Castine, ME. DOE/EE-0191. p199-213.

Kraus M, Eliasson B, Kogelschatz U, Wokaun A. 2001. $CO_2$ reforming of methane by the combination of dielectric-barrier discharges and catalysis. Physical Chemistry Chemical Physics 3: 294-300.

Kudla R, Subramanian S, Chattha M, Hoost T. 1996. Effect of tungsten oxide addition on the catalytic activity of $\gamma$-$Al_2O_3$ for $NO_x$ reduction from fuel-lean gas mixtures. Ind Eng Chem Res 35: 4394-7.

Kung M, Park P, Kim D, Kung H. 1999. Lean $NO_x$ catalysis over Sn/$\gamma$-$Al_2O_3$ catalysts. J Catalysis 181: 1-5.

Kyriacopoulou V, Psyllos A, Philippopoulos C. 1994. Diffusional effects and intrinsic kinetics for NO reduction by CO over Pt-Rh/$\gamma$-$Al_2O_3$ monolithic catalysts. Ind Eng Chem Res 33:1669-73.

Larkin D, Lobban L, Mallinson R. 2001. Production of organic oxygenates in the partial oxidation of methane in a silent electric discharge reactor. Ind Eng Chem Res 40:1594-601.

Li Z, Flytzani-Stephanopoulos M. 1999. On the promotion of Ag-ZSM-5 by cerium for the SCR of NO by methane. J Catalysis 182:313-27.

Liese T, Loffler E, Grunert W. 2001. Selective catalytic Reaction of NO by methane over $CeO_2$-zerolite catalysts – active sites and reaction steps. J Catalysis 197:123-130.

Lobree L, Aylor A, Reimer J, Bell A. 1999. NO reduction by $CH_4$ in the presence of $O_2$ over Pd-H-ZSM-5. J Catalysis 181: 189-204.

Long R, Yang R. 1999. Catalytic performance of Fe-ZSM-5 catalysts for selective catalytic reduction of nitric oxide by ammonia. J Catalysis 188: 332-9.

Long R, Yang R. 1999. Selective catalytic reduction of nitrogen oxides by ammonia over $Fe^{3+}$ -exchanged $TiO_2$-pillared clay catalysts. J Catalysis 186: 254-68.

Long R, Yang R. 2000. FTIR and kinetic studies of the mechanism of $Fe^{3+}$ -exchanged $TiO_2$-pillared clay catalyst for selective catalytic reduction of NO with ammonia. J Catalysis 190:22-31.

Luo J, Suib S, Marquez M, Hayashi Y, Matsumoto H. 1998. Decomposition of $NO_x$ with low-temperature plasmas at atmospheric pressure: neat and in the presence of oxidants, reductants, water, and carbon dioxide. J Phys Chem A 102:7954-63.

Macleod N, Isaac J, Lambert R. 2000. Sodium promotion of the NO+$C_3H_6$ reaction over Rh/$\gamma$-$Al_2O_3$ catalysts. J Catalysis 193:115-22.

Maezawa A, Izutsu M. 1993. Application of e-beam treatment to flue gas cleanup in Japan. In: Penetrante B and Schultheis S editors. Non-thermal plasma techniques for pollution control, Part B: electron beam and electrical discharge processing. Proceedings of the NATO advanced research workshop on non-thermal plasma techniques for pollution control; 1992 Sept 21-25; Cambridge, England. NATO ASI Series. p 47-54.

Manley T. 1944. The electric characteristics of the ozonator discharge. Trans Electrochem Soc 84: 83-96.

Mathur V, Chen Z, Carlton J. 1999 Aug. Electrically induced chemical reactions in a barrier discharge reactor. Technical report, Zero Emissions Technolog, Inc. (Powerspan Corp.). 50 p.

Mathur V, Breault R, McLarnon C, Medros F. 1992. $NO_x$ reduction by sulfur tolerant coronal-catalytic apparatus and method. US Patent, No. 5,147,516, September 15.

Matzing H. 1991. Chemical kinetics of flue gas cleaning by irradiation with electrons. In: Prigorgine I, Rice S, editors. Advances in Chemical Physics, volume LXXX. New York: John Wiley & Sons. P 315-59.

McLarnon C. 1989. Electro-catalytic reduction of nitrogen oxides [ master's Thesis]. Durham (NH): University of New Hampshire.

McLarnon C. 1996. Nitrogen oxide decomposition by barrier discharge [dissertation]. Durham (NH): University of New Hampshire.

McLarnon C. 2002. Update on the ECO™ process for multi-pollutant control of coal-fired utility boilers. Electric power 2002 conference; 2002 Mar 21.

McLarnon C, Jones M. 2000. Electro-catalytic oxidation process for multi-pollutant control at FirstEnergy's R.E. Burger Generating Station. Electric power 2000 conference; 2000; Cincinnati, OH.

McLarnon C, Mathur V. 1991. Corona-catalytic reduction of nitrogen oxides. AIChE national meeting (Environmental Division); 1991 Apr 7-11; Houston, TX.

McLarnon C, Mathur V. 2000. Nitrogen oxide decomposition by barrier discharge. Ind Eng Chem Res 39: 2779-87.

McLarnon C, Penetrante B. 1998. Effect of gas composition on the $NO_x$ conversion chemistry in a plasma. SAE technical paper series 982433; 1998 Oct.; San Francisco, CA.

McLarnon C, Someshwar A, Mathur V. 1990. Electro-catalytic reduction of nitrogen oxides. AIChE national meeting; 1990 Aug 19-23; San Diego, CA.

Meunier F, Breen J, Zuzaniuk V, Olsson M, Ross J. 1999. Mechanistic aspects of the selective reduction of NO by propene over alumina and silver-alumina catalysts. J Catalysis 187: 497-505.

Millar G, Canning A, Rose G, Wood B, Trewartha L, Machinnon D. 1999. Identification of copper species present in Cu-ZSM-5 catalysts for $NO_x$ reduction. J Catalysis 183: 169-81.

Mok Y, Ham S, Nam I. 1998. Evaluation of energy utilization efficiencies for $SO_2$ and NO removal by pulsed corona discharge process. Plasma Chemistry Plasma Processing 18(4): 535-50.

Mok Y, Kim J, Nam I, Ham S. 2000. Removal of NO and formation of byproducts in a positive-pulsed corona discharge reactor. Ind Eng Chem Res 39: 3938-44.

Nikravech M, Massereau V, Motret O, Pouvesle J, Charpelle J. 1994. Treatment of gaseous wastes in a very high voltage dielectric barrier discharge. Bulletin American Physical Society 39: 1478.

Oda T, Kato T, Takahashi T, Shimizu K. 1998. Nitric oxide decomposition in air by using nonthermal plasma processing with additives and catalyst. IEEE Transactions Industry Applications 34(2):268-72.

Park P, Kung H, Kim D, Kung M. 1999. Characterization of $SnO_2/Al_2O_3$ lean $NO_x$ catalysts. J Catalysis 184: 440-54.

Parvulescu V, Centeno M, Grange P, Delmon B. 2000. NO decomposition over Cu-Sm-ZSM-5 zeolites containing low-exchanged copper. J Catalysis 191:445-55.

Pashaie B, Dhali S. Honea F. 1994. Electrical characteristics of a coaxial dielectric barrier discharge. J Phys D: Appl Phys 27: 2107-10.

Penetrante B. 1997. Effect of electrical parameters on chemical kinetics of plasma-based air pollution control. Application of electrostatics for control of gas phase air pollutants; 1997 Aug 22; Cincinnati, OH.

Penetrante B. 2000. Stationary source emission control using plasma-assisted catalysis. <http: //www. Energylan.sandia.gov/ngotp/projects/ngotp.cfm?ProjectID=UET-003>.

Penetrante B, Brusasco R, Merritt B, Pitz W, Vogtlin G, Kung M, Kung H, Wan C, Voss K. 1998. $NO_x$ conversion chemistry in plasma-assisted catalysis, Proceedings of the 1998 diesel engine emissions reduction workshop; 1998 July 6-9; Castine, ME. p177-86.

Penetrante B, Hsiao M, Merritt B, Vogtlin G, Wallman P. 1995. Comparison of electrical discharge techniques for nonthermal plasma processing of NO in $N_2$. IEEE Transactions Plasma Science 23(4): 679-87.

Person J, Ham D. 1988. Removal of $SO_2$ and $NO_x$ from stack gases by electron beam irradiation. Radiation Physics Chemistry 31(1-3):1-8.

Rosocha L, Anderson G., Bechtold L., Coogan J, Heck H, Kang M, McCulla W, Tennant R, Wantuck P. 1993. Treatment of hazardous organic wastes using silent discharge plasmas, In: Penetrante B and Schultheis S editors. Non-thermal plasma techniques for pollution control, Part B: electron beam and electrical discharge processing. Proceedings of the NATO advanced research workshop on non-thermal plasma techniques for pollution control; 1992 Sept 21-25; Cambridge, England. NATO ASI Series. p 281-308.

Sadhankar R, Lynch D. 1997. NO reduction by CO over a $Pt/Al_2O_3$ catalyst: reaction kinetics and experimental bifurcation behavior. Ind Eng Chem Res 36:4609-19.

Schluep M, Rosocha L. 2000. $NO_x$ removal via dielectric barrier discharge plasma. In: Topical conference proceedings of recent developments in air pollution control, AIChE spring national meeting; 2000 Mar 5-9; Atlanta, GA. p103-112.

Schmal M, Baldanza M, Vannice M. 1999. $Pd\text{-}xMo/Al_2O_3$ catalysts for NO reduction by CO. J Catalysis 185:138-51.

Sirdeshpande A, Lighty J. 2000. Kinetics of the selective catalytic reduction of NO with $NH_3$ over $CuO/\gamma\text{-}Al_2O_3$. Ind Eng Chem Res 39:1781-7.

Snyder H, Anderson G. 1998. Effect of air and oxygen content on the dielectric barrier discharge decomposition of chlorobenzene. IEEE Transactions Plasma Science 26(6): 1695-9.

Storch D, Kushner M. 1993. Destruction mechanisms for formaldehyde in atmospheric pressure low temperature plasmas. J Applied Physics 73(1): 51-5.

Subbotina I, Shelimov B, Kazansky V, Lisachenko A, Che M, Coluccia S. 1999. Selective photocatalytic reduction of nitric oxide by carbon monoxide over silica-supported molybdenum oxide catalysts. J Catalysis 184: 390-5.

Veldhuizen E, Zhou L, Rutgers W. 1998. Combined effects of pulsed discharge removal of NO, $SO_2$ and $NH_3$ from flue gas. Plasma Chemistry Plasma Processing 18(1): 91-111.

Visvanathan K. 1952. The decomposition of nitric oxide in the silent electric discharge, part I. J Indian Chem Soc 29(5): 307-16.

Visvanathan K. 1953. The decomposition of nitric oxide in the silent electric discharge, part II. J Indian Chem Soc 29(5): 836-40.

Wallin P. 1997. FTIR analysis of gaseous emissions – a report from the practice. Technical report. Olle Moberg AB, Sweden. <http://www.ollemo.se/Ftir.pdf>.

Yan J, Kung M, Sachtler W, Kung H. 1997. $Co/Al_2O_3$ lean $NO_x$ reduction catalyst. J Catalysis 172: 178-86.

## APPENDIX A

# Nonthermal Plasma for Gaseous Pollution Control

**Z. Chen and V. K. Mathur**

Department of Chemical Engineering, University of New Hampshire,
Durham, New Hampshire 03824

Reproduced with permission from

***Industrial & Engineering Chemistry Research***

# Nonthermal Plasma for Gaseous Pollution Control

**Z. Chen and V. K. Mathur***

*Department of Chemical Engineering, University of New Hampshire, Durham, New Hampshire 03824*

A nonthermal plasma technique in the form of dielectric barrier discharge has been studied on a laboratory scale for the removal of $NO_x$ and $SO_2$. The experimental parameters investigated are voltage, frequency, pollutant concentration, and energy density. Effect of $O_2$, $H_2O$, and $CO_2$ on $NO_x$ conversion is presented. The effect of chemical compounds such as CO, $CH_4$, and $C_2H_4$ on $NO_x$ conversion is also investigated. The chemistry of plasma reactions is discussed. Nonthermal plasma is found to be effective for the oxidization of NO into reactive $NO_2$ in the presence of $O_2$ and hydrocarbons. Conversions show wide variations in the presence of oxygen and moisture. Experimental results also show that nonthermal plasma can be used to convert $SO_2$ to $SO_3$. In addition, the effect of reactor geometry and dielectric materials on $SO_2$ conversion is also discussed.

## Introduction

During the past several years, control of $NO_x$ and $SO_x$ emissions has become a national priority. $NO_x$ and $SO_x$ emissions are a leading contributor to acid rain as well as contribute strongly to photochemical smog through the formation of ozone. Current state-of-the-art technologies for controlling $NO_x$ either pertain to the combustion zone in an effort to control the temperature, residence time and stoichiometry, thereby lowering the $NO_x$ formation, or provide a postcombustion reducing agent that consumes the oxygen in the $NO_x$ molecules producing nitrogen and water. $SO_2$ is mostly removed during combustion or by flue gas wet scrubbers. These approaches have essentially reached their maximum potential. One of the most promising classes of new technologies for the treatment of these pollutants is the use of nonthermal plasma to overcome some of the difficulties associated with current technologies.

Dielectric barrier discharges (DBD) are one of the electrical breakdowns that can be classified as nonequilibrium discharges also called nonthermal plasmas. An electrical discharge is a phenomenon wherein free electrons are produced and accelerated under the influence of an electric field. Through collisions with molecules in the gas, electrons cause excitation, ionization, electron multiplication, and the formation of atoms and metastable compounds. It is the formation of atoms and compounds that gives an electrical discharge its unique chemical environment and makes it useful for chemical processing.

Investigation of the electrical discharge-initiated reaction of nitrogen oxides was first undertaken by S. S. Joshi at the University College, London, in 1927.[1] Since then, particularly in the 1980s and 1990s, considerable work has been conducted for controlling $NO_x$ and $SO_2$ using corona,[2,3] pulse,[4,5] e-beam,[6,7] or dielectric barrier discharge.[8–10] The dielectric barrier discharge technique has also been used for the oxidation of chlorobenzene, trichloroethylene, formaldehyde, etc.[11–13] Some workers have investigated the use of dielectric barrier discharge for the conversion of methane and carbon dioxide to form more valuable chemicals.[14,15] The research and development of dielectric barrier discharge technique have been conducted at UNH for several years.[16–20] On the basis of this work, several efforts are in progress to commercialize this technique for $NO_x$ and $SO_2$ removal from utility boiler flue gas.

The present study[21] is focused on gaining an understanding of the electrical and chemical effects in the decomposition process of nitric oxide by a DBD technique. In addition, the effects of barrier (dielectric) materials and reactor geometry on $SO_2$ conversion are also investigated.

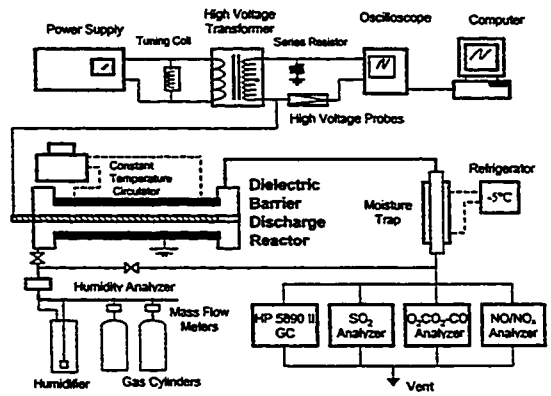


**Figure 1.** Schematic diagram of benchtop system.

## Experimental Apparatus and Procedure

A schematic diagram of the benchtop reactor system for NO conversion is shown in Figure 1. It includes the barrier discharge reactor, high voltage power supply and measurement, gas supply, and gas analytical instrumentation. Details can be found in earlier publications.[18,19]

**Dielectric Barrier Discharge Reactor.** The reactor geometry used to initiate a barrier discharge in a gas space containing oxides of nitrogen is two concentric stainless steel tubes. Each of these cylinders serves as an electrode while the outer cylinder also serves as the pressure boundary. A high voltage is applied between the electrodes, with the outer electrode (tube) at ground

* To whom correspondence should be addressed. Telephone: 603-862-1917. Fax: 603-862-3747, E-mail: vkm@cisunix.unh.edu.

10.1021/ie010459h CCC: $22.00 
Published on Web 04/06/2002

**Table 1. Specifications of Reactors**

| reactor geometry | cylindrical | rectangular A, B, C | square |
|---|---|---|---|
| electrode (high volt) | SS tube (o.d. 3) | SS wire (o.d. 0.5) | aluminum wire (o.d. 0.5) |
| electrode (grounded) | SS tube (i.d. 23) | copper strips | aluminum foil |
| barrier covering electrode (high volt) | quartz tube (i.d. 4 × 1 mm) | none | quartz tube (i.d. 1 × 1 mm) |
| barrier covering electrode (grounded) | quartz tube (i.d. 18 × 2) | plate A: quartz (3.2 thick)<br>plate B: soft glass (3.0 thick)<br>plate C: composite mica (2.4 thick) | soft glass (15 × 3.0 thick) |
| gas spacing, mm | 6 | 5 | 6 |
| cross-section area, $mm^2$ | 226 | 24 × 10 | 218 |
| length of reactor, mm | 300 | 200 | 280 |
| vol of reactor, $mm^3$ | 69 | 48 | 61 |

potential for safety reasons. The distance between the two electrodes is 10 mm. Two quartz tubes are installed adjacent to the electrodes for producing barrier discharge and the gas spacing between the two quartz tubes is 6 mm. The effective length of the reaction space is what both electrodes cover and generate microdischarges along. It is 305 mm.

Gas mixture enters the inlet plenum of the reactor and exits through the outlet plenum. The outer stainless steel electrode for the benchtop reactor is wrapped with copper tubing fed by a constant-temperature bath, cooling or heating the reactor as necessary for temperature control. Same apparatus is used for the study of $SO_2$ removal by barrier discharge. In addition, three rectangular reactors and one square reactor are also used to investigate the effect of reactor geometry as well as barrier (dielectric) materials. Specifications of all reactors are listed in Table 1.

**HV Power Measurement.** The high voltage supplied to the DBD reactor is monitored and measured by a Tektronix 2211 digital storage oscilloscope sampling at 20 MHz. The HV signal is first reduced with a Tektronix P6015 HV probe (1000×) in series with a Tektronix P6109 probe (10×) before being fed to channel 1 of the oscilloscope. The current in the secondary circuit of the HV transformer is indirectly measured using a resistor of 50 Ω and a Tektronix P6027 (1×) probe. This signal is fed to channel 2 of the oscilloscope.

Power consumption in the DBD reactor is calculated using the voltage and current traces recorded and stored by the oscilloscope. By multiplying the corresponding current and voltage values at the same phase angle, a curve of point power is obtained and is averaged to give the discharge power. An on-line computer reads the values recorded by the oscilloscope and calculates the discharge power. The voltage and current signals are taken from the second circuit of the transformer where there are some inefficiencies including transformer, inductors and resistances. However, these inefficiencies are negligible compared to discharge power consumption.

**Gas Analytical Instrumentation.** Several commercial gas analyzers are installed on-line. A Thermo-Electron model 10A/R Chemiluminescent NO–$NO_2$–$NO_x$ analyzer is used to measure the NO and $NO_x$ (NO and $NO_2$ collectively referred to $NO_x$). A Nova model 375 portable combustion analyzer is used to measure the $O_2$, $CO_2$ and CO concentrations in the gas stream. A Hewlett-Packard 5890 Series II gas chromatograph with a SUPELCO column packed with 60/80 Carboxen-1000 is used to analyze $CH_4$, $C_2H_4$, and $C_2H_2$ in the gas stream when a reducing agent such as $CH_4$ or $C_2H_4$ is added in the simulated gas mixture. The thermal conductivity detector installed in the GC is used with helium as carrier and reference gas. A Rosemount model 880 nondispersive infrared analyzer is used to measure $SO_2$ concentration in gas stream. In addition, a Nicolet 520 FTIR spectrometer is used to analyze the gas products particularly $N_2O$. This instrument is not installed on line. A gas cell is used to take samples. The path length of the gas cell is 10 cm.

## Results and Discussion

This study identifies the important variables in the barrier discharge process and their effects on the removal of $NO_x$ and $SO_2$ pollutants. Destruction of pollutants is measured in terms of inlet and outlet concentrations as follows:

$$\text{pollutant conversion (\%)} = \frac{C_{\text{inlet}} - C_{\text{outlet}}}{C_{\text{inlet}}} \times 100 \quad (1)$$

Accordingly, NO conversion can be referred to percentage of inlet NO converted to $NO_2$, $HNO_3$, $N_2O$, and/or $N_2$. $NO_x$ conversion is also calculated from eq 1. $C_{\text{inlet}}$ is $C_{NO}$ plus $C_{NO_2}$ in the inlet stream while $C_{\text{outlet}}$ is $C_{NO}$ plus $C_{NO_2}$ in the outlet stream. The term $NO_x$ conversion is the measurement of removal of both NO and $NO_2$. $NO_x$ conversion can be used to estimate inlet NO converted to $N_2$ when $HNO_3$ and $N_2O$ produced are considered to be negligible. Energy density is the power deposited into a liter of gas mixture at standard conditions (J/L), i.e., discharge power divided by total gas flow rate.

In this study effect of the following experimental parameters on pollutant conversion is studied:

| | |
|---|---|
| electric frequency | $CO_2$ concn in inlet gas |
| energy density | reducing compds: CO, $CH_4$, and $C_2H_4$ |
| pollutant concn in inlet gas | barrier (dielectric) materials |
| $O_2$ concn in inlet gas | reactor geom |
| $H_2O$ (g) concn in inlet gas | packing in reaction space |

The electrical variables, in a barrier discharge, affect the operation of the system in two major ways. First, the effective use of these parameters can enhance the efficiency of the discharge process as measured by the pollutant conversion, voltage and energy requirements, to achieve an optimal design. Second, the reaction path sequence and consequently the product slate can be controlled.

All of the experimental results are obtained using a mixture of a pollutant and other gases. The system is operated at atmospheric pressure and room temperature except high moist condition that is maintained at 65 °C. Chemical concentrations and discharge power are experimentally determined. The plasma startup usually needs 5–10 min to reach the steady state. A concentration reading is taken after it stays within acceptable range for 5 min. Discharge power is calculated by the

computer, and usually 3–5 readings of discharge power are taken to get one averaged data point.

### Electric Frequency Selection

In a barrier discharge system with ac power supply, the reactions are functions of electric energy deposited into gas passing through. An increase in voltage or frequency will result in increase in energy input. Total energy consumption is the sum of discharge power and other circuit consumption (transformer, inductors, etc.). The present study investigates the effects of frequency on total energy consumption and discharge power. It is found that the ratio of discharge power to total energy consumption reached the maximum at a frequency of 150 Hz for this barrier discharge system. Therefore, most of the experiments are conducted at a frequency of 150 Hz.

### Effects of Chemical Compounds Present in the Inlet Gas on $NO/NO_x$ Conversions

The makeup of the gas entering the barrier discharge reactor can significantly affect the performance of the reactor and thus the products of the discharge-initiated reactions. Exhaust gas from fossil fuel combustion generally contains several compounds including $N_2$, $H_2O$, $CO_2$, $O_2$, $NO_x$, and $SO_2$, among which $N_2$, $H_2O$, $CO_2$, and $O_2$ are present in large concentrations of 1–2 digital percentage while $NO_x$ and $SO_2$ are present in hundreds of parts per million levels. The amount of each compound varies depending on the fuel and the way it is burned as well as the amount of excess air used in the combustor.

**Effect of Oxygen.** Figure 2 shows the effect of oxygen concentration in a mixture of $NO/O_2/N_2$ on $NO/NO_x$ conversions. At low $O_2$ concentrations (<1%), a small increase in $O_2$ content results in a significant drop in $NO/NO_x$ conversions at 150 J/L. An increase in energy density to 320 J/L greatly enhances $NO/NO_x$ conversions. At higher $O_2$ concentrations (>1%), NO conversion increases as $O_2$ concentration is increased while $NO_x$ conversion decreases close to zero. An increase in $O_2$ concentration from 1% to 10% leads to a significant increase in $NO_2$ formation. There are several reactions proposed by McLarnon and Penetrante[22] to occur in the plasma as follows:

$$e + N_2 \rightarrow e + N + N \quad (2)$$

$$N + NO \rightarrow N_2 + O \quad (3)$$

$$e + O_2 \rightarrow e + O(^3P) + O(^3P) \quad (4)$$

$$e + O_2 \rightarrow e + O(^3P) + O(^1D) \quad (5)$$

$$O(^3P) + NO + M \rightarrow NO_2 + M \quad (6)$$

$$O + O_2 + M \rightarrow O_3 + M \quad (7)$$

$$O_3 + NO \rightarrow NO_2 + O_2 \quad (8)$$

Here, $O(^3P)$ and $O(^1D)$ are ground-state and metastable excited-state oxygen atoms, respectively, and M is either $N_2$ or $O_2$.

Variations in NO conversions at different energy densities are due to the competition between reaction 2 and reaction 6 or 8. At $O_2$ concentration less than 1%, the dominant reaction 3 mainly contributes to NO conversion into $N_2$ although the presence of $O_2$ competes for consuming electrons via reactions 4 and 5. At $O_2$ concentration greater than 1%, however, reaction 6 or 8 becomes dominant and more oxygen molecules compete for electrons, resulting in increasing amount of $NO_2$ formation while NO conversion via reaction 3 into $N_2$ decreases. Both reactions, reaction 6 at low energy density (<100 J/L) and reaction 8 at high energy density (>100 J/L), demonstrate dominance. Comparing NO conversions, when $O_2$ concentration is greater than 5%, an increase in energy density from 150 to 320 J/L does not help NO conversion because reaction 8 needs three oxygen atoms to convert one NO molecule while reaction 6 only needs one oxygen atom. This counterbalances the effect of reactions 4 and 5 at high energy density.

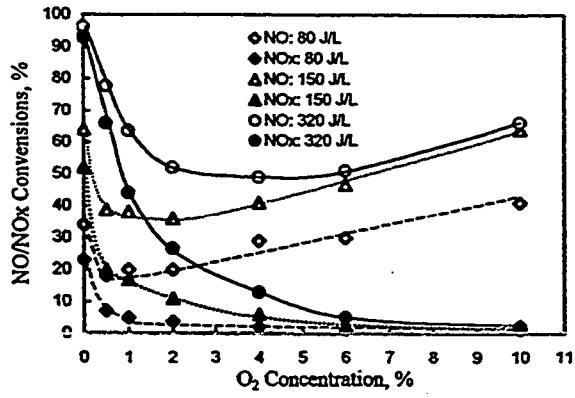


**Figure 2.** Effect of oxygen concentration on $NO/NO_x$ conversions. Conditions: total flow rate 1000 SCCM, 250 ppm of NO with $N_2$ balance, 150 Hz, room temperature.

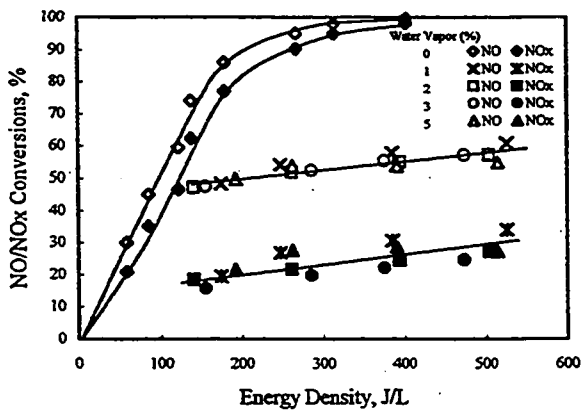


**Figure 3.** Effect of water vapor concentration on $NO/NO_x$ conversions. Conditions: frequency 150 Hz, total flow rate 1000 SCCM, 250 ppm of NO with $N_2$ balance, temperature 65 °C.

**Effect of Water Vapor.** In the absence of $O_2$ and $H_2O$, the dominant reaction is the reduction of NO to $N_2$ as shown in reaction 3 and Figure 3. However, both NO and $NO_x$ conversions significantly decrease with the addition of 1% $H_2O$. Electroimpact dissociation of $H_2O$ competes for electrons and accounts for the conversion drop as follows:

$$e + H_2O \rightarrow e + H + OH \quad (9)$$

$$OH + NO + M \rightarrow HNO_2 + M \quad (10)$$

As $H_2O$ concentration is increased from 1.to 5%, both NO and $NO_x$ conversions change little. Fewer electrons

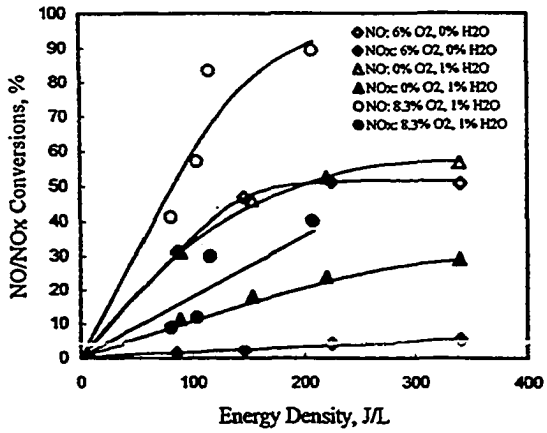


Figure 4. Effect of 1% water vapor and 8.3% $O_2$ on $NO/NO_x$ conversions. Conditions: frequency 150 Hz, total flow rate 1000 SCCM, 250 ppm of NO with $N_2$ balance, temperature 65 °C.

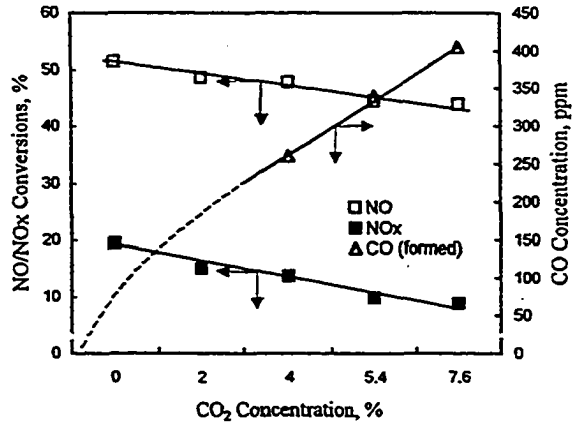


Figure 5. Effect of $CO_2$ concentration on $NO/NO_x$ conversions. Conditions: total flow rate 1000 SCCM, 250 ppm of NO, 3% $O_2$, and $N_2$ balance. Plasma: 320 J/L at room temperature.

are available for reaction 2 and thus less nitrogen atoms are available for reaction 3, leading to possibly lower NO and $NO_x$ conversions. However, reactions 9 and 10 enhance NO conversion which counterbalances the effect of reaction 3, resulting in little overall change in $NO/NO_x$ conversions. An increase in energy density helps N and OH formation but does not promote NO and $NO_x$ conversions significantly as shown in Figure 3.

**Effect of Water Vapor and Oxygen.** Experiments are conducted in the presence of 1% water vapor and 8.3% $O_2$ in the inlet $NO/N_2$ gas stream. Higher $NO/NO_x$ conversions are observed in the presence of combined $O_2$ and $H_2O$ than in the presence of either $O_2$ or $H_2O$ alone (Figure 4). The following reactions may provide an explanation:

$$O(^1D) + H_2O \rightarrow 2\,OH \quad (11)$$

$$NO_2 + OH + M \rightarrow HNO_3 + M \quad (12)$$

Reaction 11 contributes OH radicals in the presence of $O_2$. Reactions 10 and 12 account for much of the higher NO conversion because the presence of $O_2$ promotes $NO_2$ formation. $NO_x$ conversion increases in the presence of 1% water mainly because of reaction 12 rather than reaction 2.

**Effect of Carbon Dioxide.** Addition of $CO_2$ decreases NO and $NO_x$ conversions slightly as shown in Figure 5. A large CO formation is observed due to the electroimpact dissociation of $CO_2$ in a mixture of $NO/O_2/N_2/CO_2$ in a plasma system.

$$e + CO_2 \rightarrow e + O + CO \quad (13)$$

Reaction 13 competes for electrons leading to less electrons available for radicals formation such as N and O to convert NO into $N_2$ or $NO_2$.

### Effect of CO, $CH_4$, and $C_2H_4$ in the Inlet Gas Mixture on $NO/NO_x$ Conversions

Chemical compounds such as CO, $CH_4$, and $C_2H_4$ have played an important role in the catalytic reduction of $NO_x$. Experiments are conducted to study their effects in the presence of nonthermal plasma.

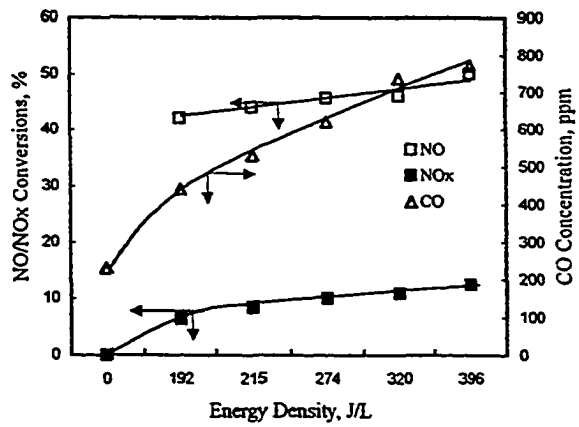


Figure 6. $NO/NO_x$ conversions and CO concentration vs energy density. Conditions: total flow rate 1000 SCCM. Inlet: 250 ppm of NO, 230 ppm of CO, 3% $O_2$, 7.6% $CO_2$, and $N_2$ balance.

**Effect of Carbon Monoxide.** Figure 6 shows that there is only a small increase in NO conversion when energy density is increased from 150 to about 400 J/L. However, there is a significant increase in CO formation. Reaction 13 suggests that CO is formed in the plasma process from $CO_2$ present in the gas mixture. The addition of small amount of CO probably has no significant effect on $NO/NO_x$ conversions since a large amount of CO is formed from $CO_2$ via reaction 13.

**Effect of Methane.** Methane is added to the mixture of $NO/O_2/CO_2/N_2$ to investigate its effect on $NO/NO_x$ conversions. Figure 7 shows that NO conversion slowly increases as methane concentration is increased while $NO_x$ conversion decreases a little. The following reactions are proposed to occur in the presence of nonthermal plasma:

$$CH_4 + e \rightarrow CH_3 + H + e \quad (14)$$

$$CH_4 + O \rightarrow CH_3 + OH \quad (15)$$

$$CH_4 + O(^1D) \rightarrow CH_3OH \quad (16)$$

$$HO_2 + NO \rightarrow NO_2 + OH \quad (17)$$

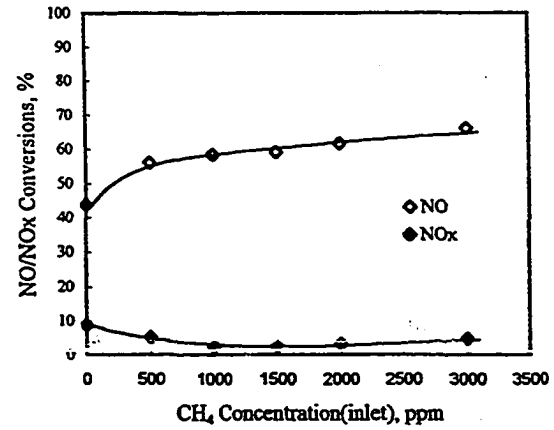


Figure 7. Effect of $CH_4$ concentration on $NO/NO_x$ conversions. Conditions: total flow rate 1000 SCCM. 250 ppm of NO, 3% $O_2$, 7.6% $CO_2$, and $N_2$ balance. Plasma: 320 J/L at room temperature.

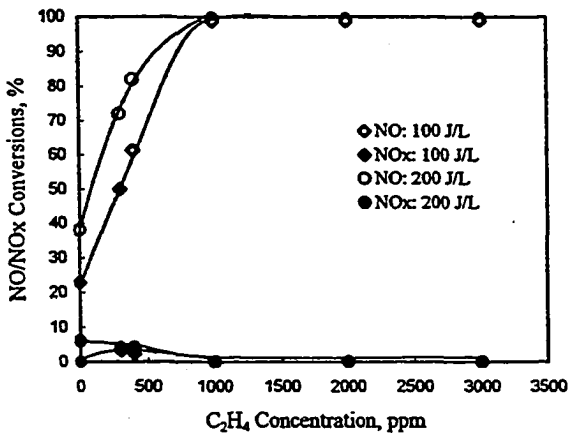


Figure 8. $C_2H_4$ concentration effect on $NO/NO_x$ conversions. Conditions: total flow rate 1000 SCCM. 250 ppm of NO, 3% $O_2$, 7.6% $CO_2$, and $N_2$ balance. Temperature 60 °C; frequency 150 Hz.

Here, $HO_2$ is formed mainly via the following reactions:[23]

$$H + O_2 \rightarrow HO_2 \quad (18)$$

$$CH_3OH + O_2 \rightarrow CH_3O + HO_2 \quad (19)$$

$$CH_3O + O_2 \rightarrow CH_2O + HO_2 \quad (20)$$

Saturated hydrocarbon methane can undergo electron-impact dissociation reaction 14 at a slow rate. Therefore, reactions 14 and 15 are limited and consequently $HO_2$ available for reaction 17 is limited, resulting in only a small increase in NO conversion from 56 to 66% as methane concentration is increased from 500 to 3000 ppm.

**Effect of Ethylene.** Figure 8 shows that $C_2H_4$ significantly enhances NO conversion to $NO_2$. The following two reactions are proposed to occur in the plasma process:

$$C_2H_4 + O \rightarrow CH_2CO + H + H \quad (21)$$

$$C_2H_4 + O + O \rightarrow HCO + HCO + H + H \quad (22)$$

Unsaturated hydrocarbon $C_2H_4$ consumes most of the O atoms via reactions 21 and 22 that might otherwise react with NO to form $NO_2$. As $C_2H_4$ concentration is increased, more $HO_2$ is produced via reactions 18 and 23:[23]

$$HCO + O_2 \rightarrow CO + HO_2 \quad (23)$$

$$HO_2 + NO \rightarrow NO_2 + OH \quad (17)$$

The reaction 17 becomes dominant, leading to almost 100% NO conversion to $NO_2$.

### Byproduct $N_2O$ Formation

Nitrous oxide ($N_2O$) is one of the six gases listed by the Kyoto Protocol. Literature review reveals that $N_2O$ may be formed during plasma process. The reaction

$$NO_2 + N \rightarrow N_2O + O \quad (24)$$

takes place and produces $N_2O$ as a stable product.[24] In the presence of $O_2$ and $H_2O$, up to 10 ppm of $N_2O$ is formed in a positive-pulsed corona discharge reactor.[25]

In this study, a series of experiments are conducted to investigate the possible $N_2O$ formation in the DBD reactor. The total flow rate is 1000 SCCM. Table 2 gives the summary of $NO/NO_x$ conversions and $N_2O$ formation. Then 19 ppm of $N_2O$ is formed when 250 ppm of NO in $N_2$ is passed through the DBD plasma reactor. In the presence of 3% oxygen, the concentration of $N_2O$ is 25 ppm. The increase of 6 ppm is attributed to the increase in energy density. However, no $N_2O$ is detected when 2% water vapor is added to the gas feed.

The effect of adding reducing agents such as $CH_4$ and $C_2H_4$ is investigated in the same reactor. Under dry conditions, addition of 3000 ppm of $CH_4$ does not reduce $N_2O$ formation whereas with 2% water vapor addition, a reduction in $N_2O$ formation from 20 to 5 ppm is observed.

### Effect of Packing in Plasma Reactor

The effects of reactor packing on discharge stability and $NO/NO_x$ conversion are investigated using an NO concentration of 250 ppm in inlet gas mixtures. Glass wool is packed in the space between the two concentric barriers (dielectric). The density of glass wool packing is 0.3 g/cm$^3$. It is found that a glass wool packing helps in stabilization of discharge.

Figure 9 shows that at energy density less than 225 J/L, $NO/NO_x$ conversions for packing are less than for no-packing experimental runs. At energy density greater than 225 J/L, however, $NO/NO_x$ conversions for packing are almost the same as for no packing. Electrical and hydrodynamic factors probably account for the lower conversions at low energy density (<225 J/L). The glass wool packing with higher dielectric constant increases the capacitance of the reactor, probably causing a decrease in discharge efficiency. Packing also considerably shortens the gas residence time in the reactor, resulting in lower $NO/NO_x$ conversions. At high energy density (>225 J/L), however, these factors appear to have little effect.

### Sulfur Dioxide Oxidation in Barrier Discharge

The nonthermal experimental system described earlier is used to investigate $SO_2$ oxidation. The experiments have been extended to study the effect of cylindrical, square and rectangular reactor geometries on

**Table 2. Summary of $N_2O$ Formations for Various Feeds**

| gas feed ($N_2$ balance) | energy density (J/L) | NO convn (%) | $NO_x$ convn (%) | $N_2O$ (ppm) |
|---|---|---|---|---|
| 250 ppm of NO | 323 | 99.6 | 99.4 | 19 |
| 250 ppm of NO + 3% $O_2$ | 344 | 72.8 | 32 | 25 |
| 250 ppm of NO + 3% $O_2$ + 2% $H_2O$ | 309 | 46 | 3.2 | 0 |
| 250 ppm of NO + 3% $O_2$ + 3000 ppm of $CH_4$ | 320 | 62 | 16.8 | 20 |
| 250 ppm of NO +3% $O_2$ + 3000 ppm of $CH_4$ + 3% $H_2O$ | 300 | 51.2 | 6.8 | 5 |

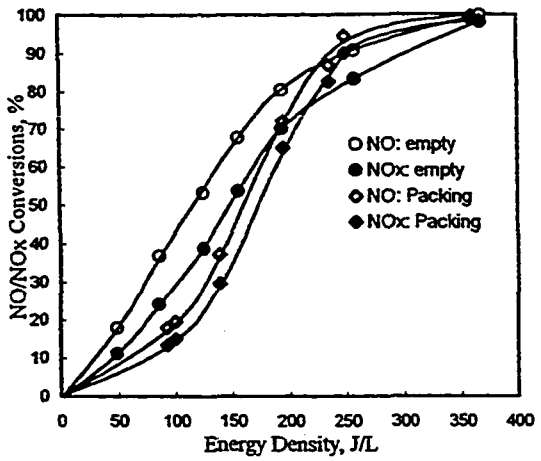


**Figure 9.** Effect of packing on $NO/NO_x$ conversions for NO/N2 gas mixture.

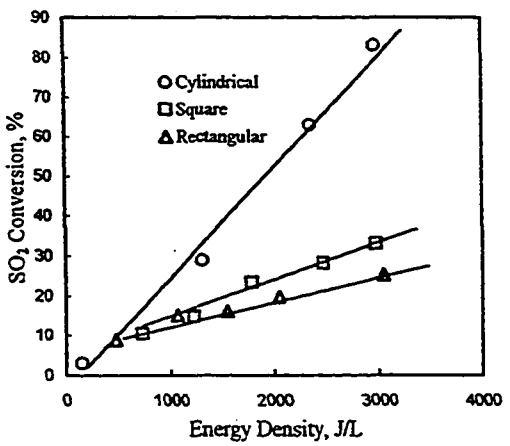


**Figure 10.** Effect of reactor geometry and energy density on $SO_2$ conversion.

$SO_2$ to $SO_3$ conversion.[26] A rectangular reactor is also used to compare effects of different barrier (dielectric) materials and their thickness on $SO_2$ conversion. Most of the experiments are conducted with an inlet gas mixture of 770 ppm of $SO_2$, 4000 ppm of $O_2$ and the balance $N_2$ at 400 Hz. The $SO_2$ concentration measurements are made by an infrared analyzer.

**Effect of Geometry on $SO_2$ Conversion.** Figure 10 shows that the energy requirements of cylindrical, square and rectangular reactors for the same conversion are in an increasing order under identical experimental conditions. For the same energy density of 3000 J/L, the $SO_2$ conversions are about 80, 33, and 22% for cylindrical, square and rectangular reactors, respectively.

**Effect of Barrier(Dielectric) Materials.** The barrier materials tested are composite mica, quartz and soft glass with dielectric constants of 2.3, 3.7, and 6.4, respectively. Reactor geometry used is rectangular.

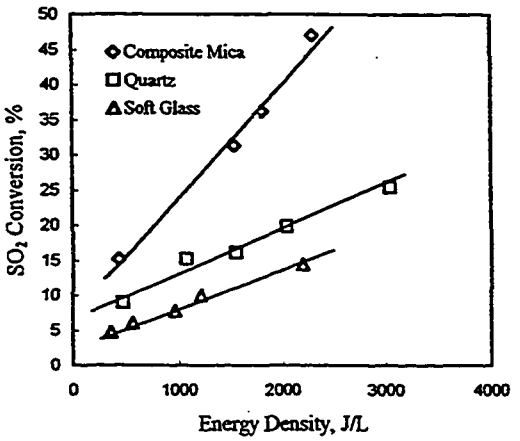


**Figure 11.** Effect of barrier materials and energy density on $SO_2$ conversion.

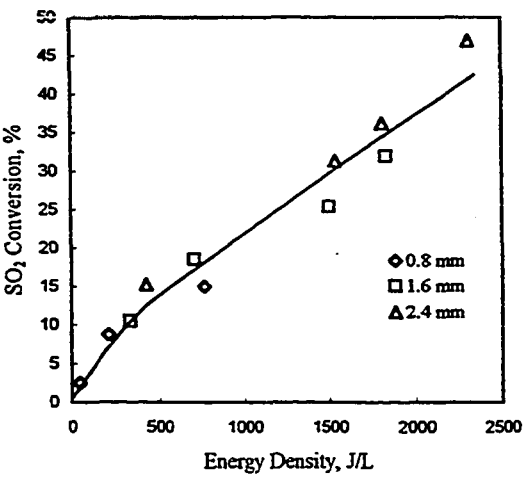


**Figure 12.** Effect of barrier thickness and energy density on $SO_2$ conversion.

Figure 11 shows that for the same energy density, reactor with composite mica as barrier material gives the highest conversion. It appears that lower dielectric constant may be helpful in achieving higher $SO_2$ conversion. The rough surface of composite mica may have caused local microsparking areas where more concentrated and higher energy electrons may have promoted $SO_2$ conversion.

**Effect of Barrier (Dielectric) Thickness on $SO_2$ Conversion.** Composite mica is selected to investigate barrier thickness effect on $SO_2$ conversion. For the convenience of fabrication, a rectangular reactor is used. One, two, and three layers of composite mica are used to obtain increases in thickness (0.8, 1.6, and 2.4 mm). Experimental results show that barrier thickness has little effect on $SO_2$ conversion (Figure 12). However, a thicker barrier could stand a greater discharge power, leading to higher $SO_2$ conversion. In each case, energy

density is increased until the experiment had to be discontinued due to excessive sparking.

## Commercialization Efforts

Our work on the removal of $NO_x$ and $SO_x$ has been extended from laboratory scale to commercialization at several companies. Powerspan, Inc., New Durham, NH, is currently conducting laboratory and field testing of a barrier discharge system for the $NO_x$ and $SO_x$ removal at a utility plant.[27] The test system consists of one dry ESP, two parallel barrier discharge reactors, and one wet ESP, processing up to 4000 cu ft/min of flue gas drawn from the exhaust of a 125 MW coal-fired power plant. The inlet flue gas contains $SO_2$ and $NO_x$ about 1700−1800 ppm and 240−400 ppm, respectively. The gas is at 300 °F. Conversion efficiencies of about 50 and 80% have been achieved for $SO_2$ and $NO_x$, respectively.

## Conclusions

A nonthermal plasma technique in the form of barrier discharge has been studied on a laboratory scale for the removal of $NO_x$ and $SO_2$. The $NO_x$ conversion is investigated in the presence of other gases such as $O_2$, $H_2O$, $CO_2$, CO, $CH_4$, and $C_2H_4$. NO undergoes chemical oxidization into $NO_2$ or reduction into $N_2$ depending upon the inlet gas composition. High $O_2$ content and energy density promote NO oxidization but when $O_2$ concentration is greater than 5%, an increase in energy density from 150 to 320 J/L does not help NO conversion. The presence of $H_2O$ has a strong effect on NO conversion. It is found that the effects of 1−5% $H_2O$ on NO/$NO_x$ conversions are the same. Addition of $C_2H_4$ significantly improves NO oxidization into $NO_2$. As $C_2H_4$ concentration is increased from 0 to 3000 ppm, almost 100% NO conversion to $NO_2$ is observed. The effect of $CH_4$ addition on NO oxidization is limited. Experimental results also show that passing a dry gas feed of 250 ppm NO through the DBD plasma reactor produces about 20 ppm of $N_2O$. In the presence of 2% water vapor, however, no $N_2O$ is detected.

Plasma reactor performance is also studied with respect to geometry and dielectric materials for $SO_2$ oxidation. Cylindrical reactor is of significant advantage over square and rectangular rectors in terms of $SO_2$ conversion. Barrier (dielectric) materials composite mica, quartz and soft glass with dielectric constants of 2.3, 3.7, and 6.4, respectively, are evaluated as barrier materials. Experimental results show that a lower dielectric constant material provides higher $SO_2$ conversion.

## Acknowledgment

Z.C. is thankful to the Department of Chemical Engineering, UNH, for financial support.

## Literature Cited

(1) Joshi, S. The Decomposition of Nitrous Oxide in the Silent Electric Discharge. *Trans. Faraday Soc.* **1927**, *23*, 227.

(2) Chang, J. Simultaneous Removal of $NO_x$ and $SO_x$ from a Combustion Flue Gas by Corona Discharge Radical Shower Systems. *Applications of Electrostatics Workshop*; University of Cincinnati: Cincinnati, OH, August 22, 1997.

(3) Matteson, M.; Stringer, H.; Busbee, W. Corona Discharge Oxidation of Sulphur Dioxide. *Environ. Sci. Technol.* **1972**, *6*, 895.

(4) Clements, J.; Mizuno, A.; Finney, W.; Davis, R. Combined Removal of $SO_2$, $NO_x$, and Fly Ash from Simulated Flue Gas Using Pulsed Streamer Corona. *IEEE Trans. Ind. Appl.* **1989**, *25* (1), 62.

(5) Veldhuizen, E.; Zhou, L.; Rutgers, W. Combined Effects of Pulsed Discharge Removal of NO, $SO_2$ and $NH_3$ from Flue Gas. *Plasma Chem. Plasma Process.* **1998**, *18* (1), 91.

(6) Maezawa, A.; Izutsu, M. Application of e-Beam Treatment to Flue Gas Cleanup in Japan. In *Non-Thermal Plasma Techniques for Pollution Control*, Penetrante, B. M., Schultheis, S. E., Eds.; NATO ASI Series, Volume 34, Part B: Electron Beam and Electrical Discharge Processing; Springer-Verlag: Berlin, 1993; pp 47−54.

(7) Frank, N.; Hirano, S. The History of Electron beam Processing for Environ. Pollut. Control and Work Performed in the United States. In *Non-Thermal Plasma Techniques for Pollution Control*; Penetrante, B. M.; Schultheis, S. E., Eds.; NATO ASI Series, Volume 34, Part B: Electron Beam and Electrical Discharge Processing; Springer-Verlag: Berlin, 1993; pp 1−26.

(8) Kogelschatz, U.; Eliasson, B.; Egli, W. Dielectric-Barrier Discharges Principle and Applications. printed plenary lecture, *International Conference on Phenomena in Ionized Gases (ICPIG XXXIII)*; Toulouse, France, July 17−22, 1997.

(9) Penetrante, B.; Hsiao, M.; Merritt, B.; Vogtlin, G.; Wallman, P. Pulsed Corona and Dielectric-Barrier Discharge Processing of NO in $N_2$. *Appl. Phys. Lett.* **1996**, *68*, 3719.

(10) Urashima, K.; Chang, J.; Ito, T. Reduction of $NO_x$ from Combustion Flue Gases by Superimposed Barrier Discharge Plasma Reactors. *IEEE Trans. Ind. Appl.* **1997**, *33* (4).

(11) Snyder, H.; Anderson, G. Effect of Air and Oxygen Content on the Dielectric Barrier Discharge Decomposition of Chlorobenzene. *IEEE Trans. Plasma Sci.* **1998**, *26*, 1695.

(12) Evans, D.; Rosocha, L.; Anderson, G.; Coogan, J.; Kushner, M. Plasma Remediation of Trichloroethylene in Silent Discharge Plasmas. *J. Appl. Phys.* **1993**, *74*, 5378.

(13) Storch, D.; Kushner, M. Destruction Mechanisms for Formaldehyde in Atmospheric Pressure Low-Temperature Plasmas. *J. Appl. Phys.* **1993**, *73*, 51.

(14) Eliasson, B.; Liu, C.; Kogelschatz, U. Direct Conversion of Methane and Carbon Dioxide to Higher Hydrocarbons Using Catalytic Dielectric-Barrier Discharges with Zeolites. *Ind. Eng. Chem. Res.* **2000**, *35*, 1221.

(15) Larkin, D.; Lobban, L.; Mallinson, R. Production of Organic Oxygenates in the Partial Oxidation of Methane in a Silent Electric Discharge Reactor, *Ind. Eng. Chem. Res.* **2001**, *40*, 1594.

(16) Mathur, V.; Breault, R.; McLarnon, C.; Medros, F. $NO_x$ Reduction by Sulfur Tolerant Corona-Catalytic Apparatus and Methodology. U.S. Patent 5,147,516, 1992.

(17) Breault, R.; McLarnon, C.; Mathur, V. Reaction Kinetics for Flue Gas Treatment of $NO_x$. In *Non-Thermal Plasma Techniques for Pollution Control.* Penetrante, B. M., Schultheis, S. E., Eds.; NATO ASI Series, Volume 34, Part B: Electron Beam and Electrical Discharge Processing; Springer-Verlag: Berlin, 1993; pp 239−256.

(18) McLarnon, C. Nitrogen Oxide Decomposition by Barrier Discharge. Ph.D. Dissertation, University of New Hampshire, Durham, NH, 1996.

(19) McLarnon, C.; Mathur, V. Nitrogen Oxide Decomposition by Barrier Discharge. *Ind. Eng. Chem. Res.* **2000**, *39*, 2779.

(20) Mathur, V.; Chen, Z.; Carlton, J.; McLarnon, C.; Golden, C. Barrier Discharge for Gaseous Pollution Control. *Proceedings of the 3rd Joint China/USA Chemical Engineering Conference*; Beijing, China, September 25−28, 2000.

(21) Chen, Z. Nitric Oxide and Sulphur Dioxide Remediation by Non-Thermal Plasma and Catalysis. Ph.D. Dissertation to be submitted, University of New Hampshire, Durham, NH, 2002.

(22) McLarnon, C.; Penetrante, B. Effect of Gas Composition on the $NO_x$ Conversion Chemistry in a Plasma. *SAE Technical Paper Series 982433*; SAE: San Francisco, CA, October, 1998.

(23) Penetrante, B.; Brusasco, R.; Merritt, B.; Pitz, W.; Vogtlin, G.; Kung, M.; Kung, H.; Wan, C.; Voss, K. $NO_x$ Conversion Chemistry in Plasma-Assisted Catalysis. *Proceedings of the 1998 Diesel Engine Emissions Reduction Workshop*; Maine Maritime Academy: Castine, ME, July 6−7, 1998.

(24) Matzing, H. Chemical Kinetics of Flue Gas Cleaning by Irradiation with Electrons. In *Advances in Chemical Physics*; Prigorgine, I., Stuart, A. R., Eds.; John Wiley & Sons: 1991; Vol 80.

(25) Mok, Y.; Kim J.; Nam, I.; Ham, S. Removal of NO and Formation of Byproducts in a Positive-Pulsed Corona Discharge Reactor. *Ind. Eng. Chem. Res.* **2000**, *39*, 3938.

(26) Mathur, V.; Chen, Z.; Carlton, J. Electrically Induced Chemical Reactions in a Barrier Discharge Reactor. Technical Report, Zero Emissions Technology, Inc., August, 1999.

(27) McLarnon, C.; Jones, M. Electro-Catalytic Oxidation Process for Multi-Pollutant Control at FirstEnergy's R. E. Burger Generating Station. *Proceedings of Electric Power 2000 Conference in Cincinnati*; 2000.

*Received for review* May 23, 2001
*Revised manuscript received* December 17, 2001
*Accepted* February 13, 2002

IE010459H

# APPENDIX B

## REACTION OF $CH_4$ AND $CO_2$ IN DBD REACTOR TO FORM VALUE-ADDED PRODUCTS

The objective of this study is to investigate the reaction of $CH_4$ and $CO_2$, two inexpensive gases, in a DBD reactor to explore the possibility of forming high-value products such as olefins, hydrogen, CO, etc. Converting $CO_2$ into valuable products has long been pursued especially since the "greenhouse effect" attracted worldwide attention. The present investigation includes three steps, namely methane dissociation, carbon dioxide dissociation, and reaction of methane with carbon dioxide in a DBD reactor. The apparatus used is the same as has been used for $NO_x$ and $SO_2$ studies. Experiments are carried out at atmospheric pressure and room temperature. A gas chromatograph equipped with thermal conductivity detector (TCD) and flame ionization detector (FID) is used for feed and product identification and quantitative analysis.

### Analysis Method

A suitable detection method for GC is essential for the identification and quantitative analysis of methane, carbon dioxide and related products. TCD and FID are used due to their wide responses to various gases. In addition to usual helium, nitrogen is used as a carrier and reference gas.

### Apparatus

Hewlett Packard 5890 Series II Gas Chromatograph with accessories:

- FID and TCD detectors
- SUPELCO column (Cat. No. 1-2390): 60/80 Carboxen-1000
- Hewlett Packard HP3396 Series II integrator
- Two sampling loops: small (original, 0.25ml) and large (self-made, 0.62 ml)

### TCD and Reference Gas Selection

Working of TCD is based on the difference of thermal conductivity coefficients, K for various gases. It can be described by the following equation:

$$K = (\text{density})(\text{velocity})(\text{mean free path})(\text{specific heat})/2$$

K is almost independent of pressure because the density and mean free path vary in the opposite directions with change in pressure (Mann and others 1994).

In general, a reference gas needs to be of much higher K so that the signal for the component to be detected can be large enough. Helium with a much greater K value is the best candidate to serve as a reference gas(see Table 1). In order to get a steady signal output, the same gas is used as both carrier and reference gas.

**Table 1**

**Gas Thermal Conductivity Coefficients (at 500 K)**

(Perry and Chilton 1973; Chang 1973) Unit: 100 w/mK

| **Gas** | Air | Ar | $CO_2$ | **He** | **$H_2$** | $CH_4$ | $N_2$ |
|---|---|---|---|---|---|---|---|
| **K** | 4.07 | 2.66 | 3.25 | **21.8** | **26.2** | 6.68 | 3.89 |
| **Gas** | $O_2$ | $H_2O$ | CO | $C_2H_6$ | $C_2H_4$ | $C_2H_2$ | |
| **K** | 4.12 | 3.58 | 3.80 | 5.2 | 5.0 | 4.4 | |

Some workers in this area used helium (instead of nitrogen) as balance gas in their simulated gas mixtures fed to DBD reactors. By doing so, they could measure nitrogen gas produced in the outlet stream from a DBD reactor. However, nitrogen accounts for up to 90% of flue gas from power plants and exhaust from engines. $N_2$ plays an important role in DBD process because of electron-impact dissociation of $N_2$. Therefore, using a simulated gas mixture without $N_2$ would make experimental reaction paths far different from the real situation.

In the present study, nitrogen is used as balance gas in the simulated gas feed. Hydrogen could be one of products from DBD reactor. The measurement of a small amount of hydrogen with TCD needs nitrogen as reference and carrier gas because hydrogen K is of the same magnitude as helium K. This arrangement has the advantage of avoiding large signal of balance nitrogen gas in the sample.

**Retention Time Used for Identification of a Gas Peak**

GC provides peak area and retention time (RT). Peak area is dependent on the amount of a gas component and is used to calculate the gas concentration. Peak RT is the time taken for a component band to pass through the column and reach the detector. Peak RT and its sequence can be used to identify products.

Figure 1 is a standard chromatogram of gases and $C_2$ hydrocarbons provided by SUPELCO (SUPELCO 1995) for the column used in this study. Calibration gases are used with 1% each in $N_2$ balance and helium serves as reference and carrier gas for the chromatogram. Every RT in Figure 1 may not been used to identify individual gas in this study because of different flow rate, carrier gas and oven temperature. However, the RT sequence can be used as a guide for identification of feed and product gases. As shown in Figure 1, carbon monoxide peak appears after but close to nitrogen peak. Methane

follows the carbon monoxide. Then comes the peak for carbon dioxide. RTs of acetylene, ethylene and ethane are in increasing order.

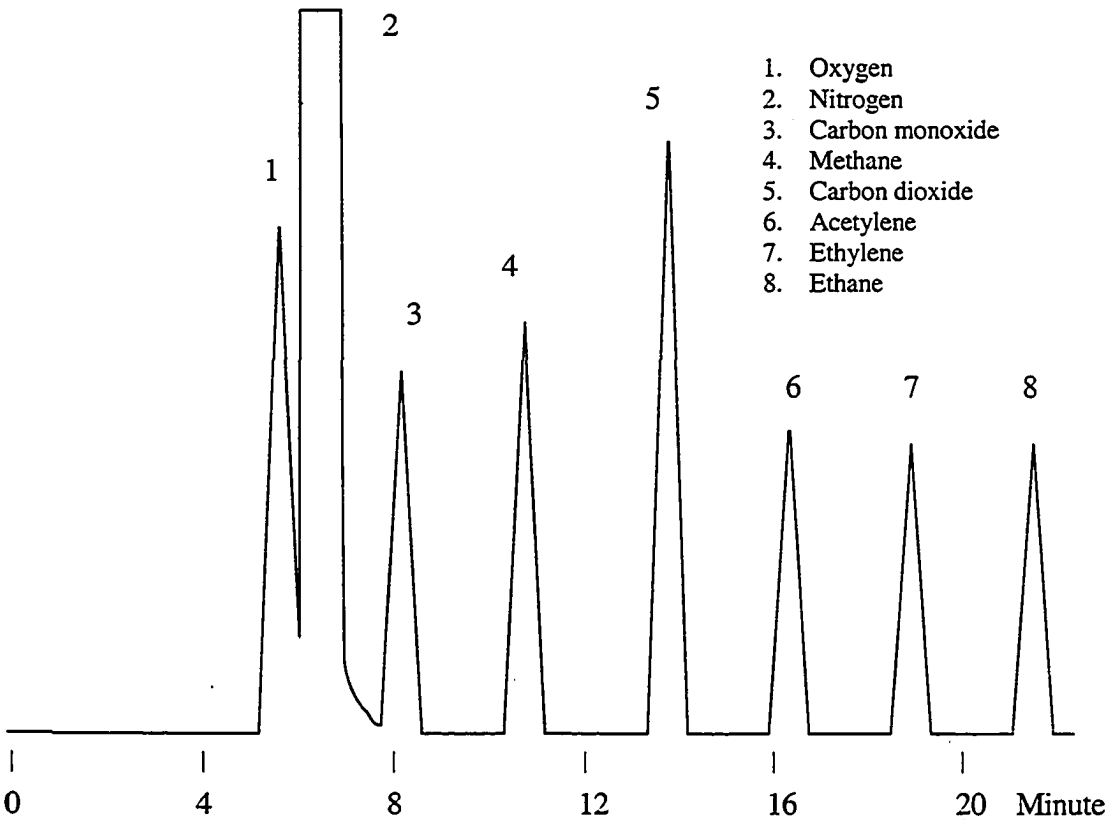


**Figure 1 Chromatogram of Calibration Gases and $C_2$ Hydrocarbons. Column:60/80 Carboxen-1000, TCD** (SUPELCO 1995)

**Dissociation of Methane**

The DBD reactor used in this study has limitation of power that can be applied, and therefore a low inlet $CH_4$ concentration to provide a high specific energy (kJ/mole-$CH_4$inlet) is used for the experiments. Dissociation of $CH_4$ is investigated at concentration of 100 and 5000 ppm levels.

Low Concentration Methane Dissociation(124 ppm)

A gas mixture of 124 ppm methane and balance $N_2$ is fed to the DBD reactor and subjected to various power inputs. The total flow rate is 1.86 SLM. A large sampling loop of 0.62 ml is used to enhance the peak signals of GC. Presented in Figure 2 and Table 2 are the results obtained using TCD that are in good agreement with those reported earlier with FID (Golden 1997). At an energy density of 593 J/L (peak voltage 26.4 kV), the conversion of methane is found to be 23.7%.

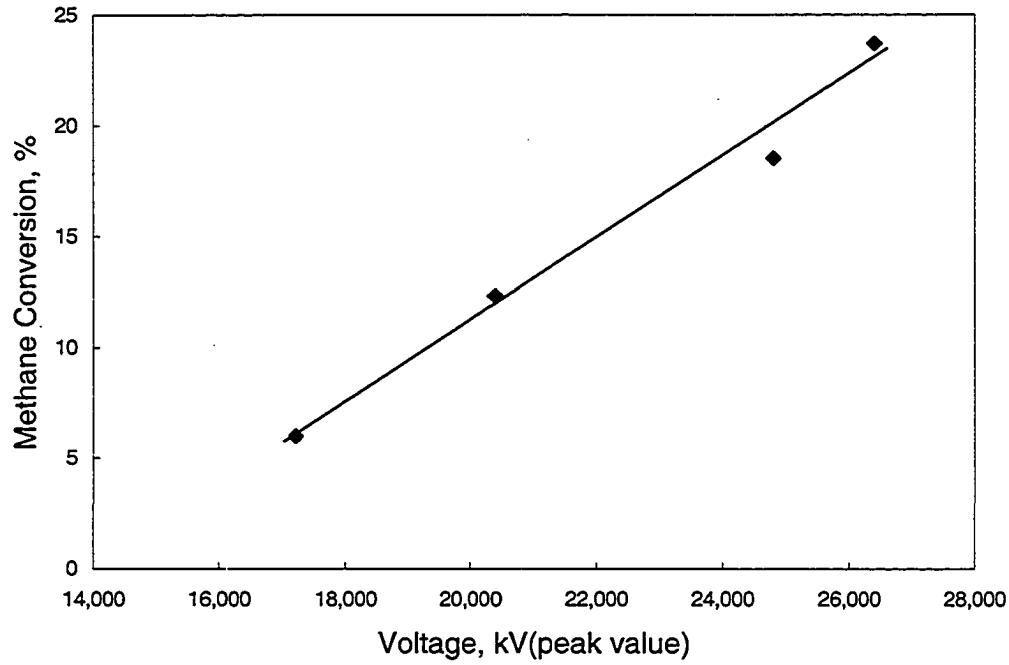


**Figure 2 Methane Conversion vs. Voltage.** Frequency is 400 Hz. Room temperature.

**Table 2**

**Methane Conversion Under Different Voltage Applied**

| Peak Voltage (V) | 17,202 | 20,403 | 24,804 | 26,403 |
|---|---|---|---|---|
| Energy Density (J/L) | 250 | 380 | 482 | 593 |
| Conversion (%) | 6.0 | 12.3 | 18.5 | 23.7 |

Identification and Quantification of Product $H_2$

Hydrogen molecule is regarded as the most likely product from methane dissociation. Since the thermal conductivity coefficient of hydrogen is higher than that of helium, nitrogen is used as a carrier and reference gas instead of helium for GC-TCD analysis. By injecting a calibration hydrogen gas, an RT of 1.528 minutes is obtained for the large sampling loop of 0.62 ml. Similarly, RTs of other gases are obtained by injecting calibration gases.

The chromatograms of the products of methane dissociation show that a new peak appears with RT of 1.50 minutes and the peak area increases as applied voltage is

increased. When this RT of 1.50 minutes is compared with calibration data of RT 1.528 minutes, the peak is found to be that of hydrogen.

Dissociation results of 124 ppm methane mixture are presented in Table 3. The experimental results show the ratio of $H_2$ produced to $CH_4$ converted is 1.5. Based on this ratio, the following reaction may be proposed:

$$2\,x\,CH_4 \rightarrow 3\,x\,H_2 + (2\,x\,H + 2\,x\,C) \qquad (1)$$

Where item ($2\,x\,H + 2\,x\,C$) is the mixture of possible products C, $C_2H_2$, $C_2H_4$ and/or $C_2H_6$. The stoichiometric theoretical ratio of $H_2/CH_4$ for Equation (1) is 1.5.

**Table 3**

**Methane Converted and Hydrogen Yields**

| Applied Vpeak | Methane Converted | Hydrogen Yield | Ratio of $H_2/CH_4$ |
|---|---|---|---|
| 24,804 v | 23.0 ppm | 33.4 ppm | 1.5 |
| 26,403 v | 29.4 ppm | 42.9 ppm | 1.5 |

Identification and Quantification of Product Hydrocarbons

Equation (1) suggests that other products may be hydrocarbons such as acetylene ($C_2H_2$), ethylene ($C_2H_4$), ethane ($C_2H_6$) or carbon (C).

To check if acetylene could be present in the products, an experiment is conducted to verify the stability of acetylene under DBD experimental conditions. A mixture of 2 ppm acetylene is passed through DBD reactor. Flame ionization detector (FID) is used to analyze acetylene and its plasma products. Presented in Table 4 are the results of acetylene dissociation under different applied voltages. Acetylene RT is found to be 14.4 minutes. As the power increases, acetylene concentration in the outlet stream decreases, dropping to zero at the power of 16.4 w. In addition, trace methane is identified in the product stream according to its RT of 4.2 minutes. It can be concluded

**Table 4**

**Acetylene Dissociation under Different Voltage (peak value)**

| Compounds in Product Stream | Peak Areas under Different Voltage | | | | |
|---|---|---|---|---|---|
| | No voltage | 27,149 V 1.1 w | 28,850 V 3.1 w | 35,073 V 10.7 w | 37,334 V 16.4 w |
| Acetylene | 2,766 (2.0 ppm) | 2,463 (1.8 ppm) | 320 (0.02 ppm) | 50 (0.003 ppm) | 0 (0 ppm) |
| Methane (product) | 0 ( 0 ppm) | 20 (0 ppm) | 202 (0.3 ppm) | 397 (0.7 ppm) | 529 (1 ppm) |

$C_2H_2$ scale: 0.00074 ppm/area; $CH_4$ scale: 0.0017 ppm/area.

that acetylene is easily dissociated in DBD and therefore it is probably not one of products of methane dissociation under the experimental conditions.

Similarly, ethane could be one of $C_2$ products. To check if ethane could be present in the products, a separate experiment is conducted with a mixture of $CH_4$ (130 ppm) and $N_2$. The total flow rate is maintained at 2 SLM with a peak voltage of 31.6 kV and power of 20.3 w. A conversion of 38% is achieved for methane. Results presented in Table 5 show that there is an unknown peak with an average RT of 19.341 minutes. By referring to the sequence of Figure 1, this unknown peak is probably ethylene peak.

**Table 5**

**Methane Dissociation under 31.6 kV**

| Compounds | Peak Areas | | | | |
|---|---|---|---|---|---|
| | No voltage | Run 127 | Run 128 | Run 129 | Average |
| Methane | 1,298 (130 ppm) | 812 | 808 | 779 | 800 (80 ppm) |
| Unknown Product | 0 | 124 (RT: 18.990) | 100 RT: 19.980) | 142 (RT: 19.052) | 122 (RT: 19.341) |

High Concentration Methane Dissociation(5298 ppm)

A mixture of 5298 ppm methane and 0.1% argon in $N_2$ balance is prepared with a standard methane source (5% methane mixture in balance argon, Airgas). The same GC TCD with $N_2$ as carrier and reference gas is used for analyzing gas composition. A calibration hydrogen gas gives a RT of 0.997 minutes for a small sampling loop used (0.25 ml). With nitrogen as reference and carrier gas, a negative peak of hydrogen in the product is clearly detected when a suitable voltage is applied to the reactor. Its retention time is 0.999-1.000 minutes matching the calibration hydrogen RT. Results are presented in Table 6.

**Table 6**

**Methane converted and Hydrogen Yields (methane feed: 5298 ppm)**

| Applied Voltage | Methane converted | Hydrogen yield | Ratio of $H_2/CH_4$ |
|---|---|---|---|
| 22,000 v | 304 ppm | 158 ppm | 0.52 |
| 24,900 v | 430 ppm | 223 ppm | 0.52 |

Based on the ratio of $H_2$ produced to $CH_4$ converted, i.e., 0.52, the following reaction may be proposed:

$$2x\ CH_4 \rightarrow x H_2 + (6x H + 2x C) \qquad (3)$$

Where (6 $x$ H + 2 $x$ C) is the mixture of products C, $C_2H_4$ and/or $C_2H_6$. The stoichiomistric theoretical ratio of $H_2/CH_4$ for Reaction (3) is 0.5. Hsieh *et al.* (1998) used FTIR and identified $C_2H_2$, $C_2H_4$ and $C_2H_6$ from a radio-frequency(RF) plasma system with a feed of 5-20% $CH_4$ in Ar.

Mechanism for Methane Dissociation in DBD

Specific Energy (SE) is used to compare the energy efficiency in the DBD process. SE is defined as the electric energy consumed per inlet mole of methane. Table 7 shows that under the same applied voltage, methane in low concentration with much greater SE undergoes higher decomposition of 18.5%. On the other hand, methane in high concentration shows a conversion of only 8.1%. In the DBD reactor, methane undergoes electron-impact dissociation:

$$CH_4 + e \rightarrow CH_3 + H + e \quad (4)$$

**Table 7**

**Comparison between Low and High Inlet Concentrations of Methane**

| Methane Inlet, ppm | Voltage V | Flow rate L/min | Specific Energy KJ/mol(inlet) | Conversion % | Products |
|---|---|---|---|---|---|
| 124 | 24,804 | 1.86 | 87,200 | 18.5 | $H_2$, $C_2H_4$* |
| 5298 | 24,900 | 2.00 | 1,663 | 8.1 | $H_2$, $C_2H_6$* |

* Compounds have not been identified due to instrumentation limit.

In the case of 124 ppm methane feed, a methane molecule get a higher probability to be dissociated as reaction (4) compared with in the case of 5298 ppm methane feed. Therefore, a higher methane conversion can be achieved for a feed of lower methane concentration. In addition, part of $CH_3$ radicals may undergo further electron-impact dissociation depending on the availability of energetic electrons:

$$CH_3 + e \rightarrow CH_2 + H + e \quad (5)$$
$$CH_2 + e \rightarrow CH + H + e \quad (6)$$
$$CH + e \rightarrow C + H + e \quad (7)$$

Meanwhile, part of $CH_3$ radicals form ethane as reaction (8) and hydrogen radicals form hydrogen molecule as reaction (9):

$$CH_3 + CH_3 \rightarrow C_2H_6 \quad (8)$$
$$H + H \rightarrow H_2 \quad (9)$$

The overall reaction for Reactions (4)-(9) could be described as follows:

$$CH_4 \rightarrow k\,H_2 + m\,C_2H_6 + n\,C \quad (10)$$

Reaction (10) is well comparable with Reaction (2), 50 $CH_4$ → 75 $H_2$ + 8.46 $C_2H_6$ + 33 C, which is proposed based on experimental results.

On the other hand, in the case of 5298 ppm methane feed under the same energy density as used for 124 ppm methane feed, most energetic electrons are consumed by Reaction (4), $CH_4 + e \rightarrow CH_3 + e$. No excess electrons are available for $CH_3$ radicals to undergo further dissociation. Accordingly, Reactions (8) $CH_3 + CH_3 \rightarrow C_2H_6$ and (9) $H + H \rightarrow H_2$ become dominant. The overall reaction can be described as

$$CH_4 \rightarrow m\,H_2 + n\,C_2H_6 \qquad (11)$$

Reaction (11) is the same as Reaction (3) proposed according to experimental results.

**Dissociation of Carbon Dioxide**

Experiments on $CO_2$ dissociation are conducted at 100 ppm and 10,000 ppm levels to check $CO_2$ conversion and the possible existence of carbon monoxide (CO) in product stream.

Low Concentration $CO_2$ Dissociation (100 ppm level)

Like methane, 100 ppm $CO_2$ is used to investigate $CO_2$ dissociation in the DBD reactor. Under 32,000 V(peak value), the conversion of $CO_2$ is about 3.2%. Based on the retention time of CO ( about 2.33 min), CO peak is observed although the peak is not well separated from nitrogen peak. The GC column fails to separate CO due to the presence of large component of $N_2$. CO peak probably can be separated if helium is used as balance gas.

High Concentration $CO_2$ Dissociation (10,000 ppm level)

In order to obtain a separate CO peak, a high inlet concentration (10,000 ppm) of $CO_2$ with $N_2$ balance is passed through the DBD reactor. Under the same peak voltage of 32,000 V, the area of CO peak obtained appears larger than that for a low concentration $CO_2$ dissociation. It shows that more CO is formed for the high concentration $CO_2$ feed. Unfortunately, the CO peak is not well separated from nitrogen peak. Peak area could not be measured for the estimation of product CO.

The mechanism for $CO_2$ dissociation in the DBD reactor is proposed as follows:

$$CO_2 + e \rightarrow CO + O + e \qquad (12)$$

**Reaction of Methane and Carbon Dioxide**

Experiments on the reaction of $CH_4$ and $CO_2$ are also conducted at two concentration levels of 100 ppm and 10,000 ppm with balance $N_2$.

Low Concentration(100 ppm each) of $CH_4$ + $CO_2$ in Nitrogen Mixture

A $CH_4$-$CO_2$ mixture (100 ppm each in nitrogen) is used to investigate reactions of $CH_4$+$CO_2$. Results are presented in Table 8. $CO_2$ conversion is found to be 10% compared to 3.2% in the absence of $CH_4$ under the same peak voltage of 31,600 V and flow rate of 1.8 SLM. The conversion of $CH_4$ in the presence of $CO_2$ is 26.3% compared with 38.4% when treated alone. An important finding is that the CO peak is clearer and larger than obtained for $CO_2$ dissociation alone. These results suggest that $CO_2$ reacts with $CH_4$ under the plasma conditions.

**Table 8**

**$CH_4$ and $CO_2$ Conversions for Different Feed Mixtures at Voltage of 31,600 V**

| Components | Feed Mixture | Conversion, % |
|---|---|---|
| $CH_4$ | 124 ppm $CH_4$ with balance $N_2$ | 38.4 |
| | 100 ppm $CH_4$ and 100 ppm $CO_2$ with balance $N_2$ | 26.3 |
| $CO_2$ | 100 ppm $CO_2$ with balance $N_2$ | 3.2 |
| | 100 ppm $CH_4$ and 100 ppm $CO_2$ with balance $N_2$ | 10.0 |

High Concentration(10,000 ppm each) $CH_4$+ $CO_2$ in Nitrogen Mixture

In order to obtain a separate and complete CO peak, the inlet concentrations of $CH_4$ and $CO_2$ are maintained about 10,000ppm each. Under the same power condition as for 100 ppm mixture, the area of CO peak in the product stream appears larger than that for the low concentration of $CH_4$ and $CO_2$ mixture. However, the CO peak is not well separated from nitrogen peak. No peak area could be measured for the estimation of product CO.

Proposed Mechanism for the Reaction of $CH_4$ and $CO_2$

Results in Table 8 show that the presence of $CH_4$ enhances $CO_2$ dissociation. On the other hand, $CH_4$ conversion decreases due to $CO_2$ competition for energy or energetic electrons. Hydrogen and CO are the main products. The mechanism for $CH_4$ reaction with $CO_2$ could be proposed as follows:

$$CH_4 + e \rightarrow CH_3 + H + e \quad (13)$$
$$CH_3 + e \rightarrow CH_2 + H + e \quad (14)$$
$$CH_2 + e \rightarrow CH + H + e \quad (15)$$
$$CO_2 + e \rightarrow CO + O + e \quad (16)$$
$$H + H \rightarrow H_2 \quad (17)$$
$$CH_3 + CH_3 \rightarrow C_2H_6 \quad (18)$$
$$CH_4 + O \rightarrow CH_3OH \quad (19)$$
$$CH + O \rightarrow CO + H \quad (20)$$
$$O + H \rightarrow OH \quad (21)$$
$$OH + H \rightarrow H_2O \quad (22)$$

Reactions(19)-(21) might account for more $CO_2$ dissociation by enhancing Reaction (16) and contributing additional CO formation via Reaction (20).

## Conclusions

The following conclusions are drawn from the investigation of methane and carbon dioxide reactions in the DBD plasma reactor:

1. 38.4% conversion of methane can be achieved when a mixture of $CH_4$ and $N_2$ is passed through the DBD reactor at 31.6 kV and 400 Hz (20 w). Hydrogen gas is one of the products. Ethane could be the main $C_2$ product.
2. Only 3.2 % conversion of carbon dioxide can be achieved when a mixture of $CO_2$ and $N_2$ is fed to the DBD reactor at 31.6 kV and 400 Hz ( 20 w). CO is one of the products.
3. Conversion of carbon dioxide is increased from 3.2 % to 10% when it is mixed with methane. Hydrogen gas and CO are amongst the products. The following reaction probably occurs in the DBD reactor:

$$CH_4 + CO_2 \rightarrow 2\,CO + 2\,H_2$$

This work was discontinued due to lack of analytical facilities such as a high sensitive pair of Dual-Module Microgas Chromatographs (Eliasson and others 2000).

## References


Chang H. 1973. Thermal conductivities of gases at atmospheric pressure. Chemical Engineering April, 16.

Eliasson B, Liu C, Kogelschatz U. 2000. Direct conversion of methane and carbon dioxide to higher hydrocarbons using catalytic dielectric-barrier discharges with zeolites. Ind Eng Chem Res 39:1221-7.

Golden C. 1997. Decomposition of refrigerants R12, R-22 and R-50 by barrier discharge [ master thesis]. Durham(NH): University of New Hampshire.

Mann C, Vickers T, Gulick W. 1994. Instrumental analysis. Harper & Row, Publishers. p183.

Perry P, Chilton C. 1973. Chemical engineers' handbook. 5th ed. McGraw-Hill Book Company. p 3-215.

SUPELCO. 1995. Chromatography products. Supelco, Inc. p 768.

## APPENDIX C

## KINETICS AND MODELING OF NO CONVERSION UNDER NON-THERMAL PLAMSA CONDITIONS

Development of correlations for

(1) Kinetic equation for dry NO oxidation
(2) Correlation of NO conversion in the presence of moisture

### Kinetic Equation for Dry NO Oxidation

The reactions for dry NO oxidation can be simplified as follows:

Overall reaction: $NO + \frac{1}{2}O_2 \rightarrow NO_2$ (1)

The rate equation for reaction (1) can be expressed as follows

$$\mathbf{r} = -d[NO]/dt = k_p [NO]^{\alpha}[O_2]^{\beta} \quad (2)$$

Reaction orders $\alpha$ and $\beta$. Experiments have been conducted by varying inlet NO and $O_2$ concentrations at a constant energy density of 100 J/L. [NO] is estimated by averaging inlet and outlet NO concentrations. $[O_2]$ is assumed constant (3% or 5%) due to its large excess. This technique has been used earlier for other reactions (Seigneur and others 1994). The logarithmic form of equation (2) is

$$\ln(\mathbf{r}) = \ln(k_p) + \alpha \ln([NO]) + \beta \ln([O_2]) \quad (3)$$

Where $\mathbf{r} = d \times c$ and $\ln(\mathbf{r}) = \ln(d) + \ln(c)$. $d$ is the amount of NO converted (ppm) and c is a conversion factor. The equation (3) can be rewritten as

$$\ln(d) = \alpha \ln([NO]) + \ln(k_p) + \beta \ln([O_2]) - \ln(c) \quad (4)$$

Where $\ln(k_p)$, $\beta \ln([O_2])$ and $\ln(c)$ are constant. The regression analysis of two sets of data yields slopes, 0.62 and 0.35 of the fitting straight lines (Table 1& Figure 1, Table 2 & Figure 2). Therefore, the value of $\alpha$ is taken as ½.

**Table 1** Data Set 1

| NO inlet | NO outlet | Converted, *d* | Avg.[NO] | ln([NO]) | ln(*d*) |
|---|---|---|---|---|---|
| ppm | ppm | ppm | ppm | | |
| 250 | 186 | 64 | 218 | 5.38 | 4.16 |
| 309 | 217 | 92 | 263 | 5.57 | 4.52 |
| 358 | 258 | 100 | 308 | 5.73 | 4.61 |
| 458 | 360 | 98 | 409 | 6.01 | 4.58 |

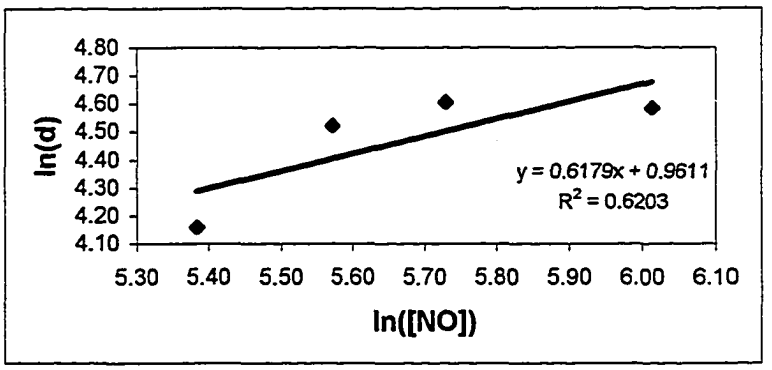


**Figure 1 Data Set 1**

**Table 2** Data Set 2

| NO inlet | Outlet | Converted, *d* | Avg.[NO] | ln([NO]) | ln(*d*) |
|---|---|---|---|---|---|
| ppm | ppm | ppm | ppm | | |
| 100 | 56 | 44 | 78 | 4.36 | 3.78 |
| 250 | 180 | 70 | 215 | 5.37 | 4.25 |
| 300 | 222 | 78 | 261 | 5.56 | 4.36 |
| 350 | 280 | 70 | 315 | 5.75 | 4.25 |
| 450 | 372 | 78 | 411 | 6.02 | 4.36 |

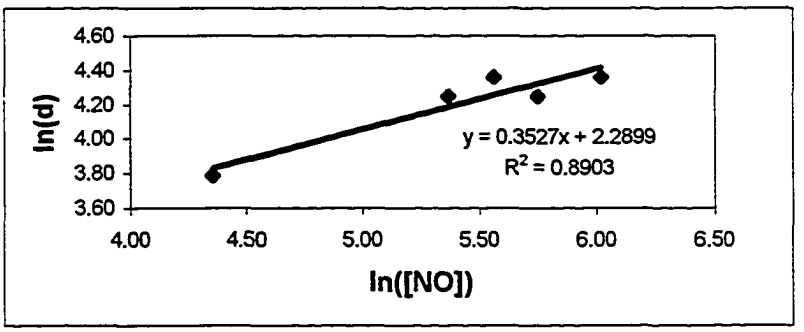


**Figure 2 Data Set 2**

Similarly, $\beta$ value is estimated by varying $O_2$ concentration while keeping the inlet NO concentration constant. The values for $\beta$ are 0.70, 0.32, 0.44 and 0.35. Therefore, $\beta$ can be assumed to be ½. The rate equation becomes:

$$r_{NO} = - d[NO]/dt = k_p [NO]^{½} [O_2]^{½} \quad (5)$$

In the present study, the rate constant correlation is proposed as follows:

$$k_p = A_p e^{-Ea/E_d} \quad (6)$$

Where $E_a$ is effective activation energy (J/mol of NO) and $E_d$ is discharge power or energy density (J/mol of gas mixture). $A_p$ is frequency factor under plasma conditions.

Derivation of correlation between $k_p$ and conversion rate $x$:

Assumption: ideal plug-flow reactor for the DBD reactor
Reactor volume (V): 69 $cm^3$
Total gas flow rate (Q): 1 liter/min
$C_{NOo}$: inlet concentration of NO, ppm
$x = (C_{NOo} - C_{NO})/ C_{NOo}$
$C_{NO} = C_{NOo}(1 - x)$

For ideal plug-flow reactor, we have the following equation:

$$V/(Q\, C_{NOo}) = \int_0^x (1/\mathbf{r}_{NO})\, dx \qquad (7)$$

Substitution of $C_{NOo}$ and $\mathbf{r}_{NO}$ expressions into equation (7) and integration yield

$$k_p = V/Q\, (C_{O2}/C_{NOo})^{1/2} / (2 - 2(1 - x)^{1/2}) \qquad (8)$$

By defining

$V/Q = t$, residence time in the reactor
$C_{O2}/C_{NOo} = m$, ratio of $O_2$ concentration to inlet NO concentration

equation (8) is written as:

$$x = k_p\, t\, m^{1/2} - 1/4\, m k_p^2\, t^2 \qquad (9)$$

Check: 1) At $t = 0$ ( inlet point):
$x = 0$ ( no conversion)
2) At $k_p \rightarrow 0$ (extremely low energy density or high activation energy):
$x = 0$ ( no conversion)

Equation (8) is used to calculate the values of $k$ as shown in the following table. The logarithmic form of equation (6) is $\ln(k_p) = E_a\, (-1/24.4E_d) + \ln A_p$, where $E_d$ is expressed as J/L.

**Table 3**

| | | Inlet NO | $O_2$ | | | |
|---|---|---|---|---|---|---|
| | | 258 | 4% | | | |
| Ed | Out NO | $NO_x$ | x, NO conv | $k_p$ | ln(k) | -1/(24.4Ed) |
| J/L | ppm | ppm | | | | mole/J |
| 288 | 132 | 228 | 0.49 | 1.10E-02 | -4.506 | -0.00014 |
| 432 | 125 | 216 | 0.52 | 1.18E-02 | -4.440 | -9.5E-05 |
| 540 | 121 | 207 | 0.53 | 1.22E-02 | -4.404 | -7.6E-05 |
| 678 | 114 | 195 | 0.56 | 1.30E-02 | -4.342 | -6E-05 |

From Figure 3, $E_a$ and $A_p$ are found to be 1865 J/mol and 0.0143, respectively.

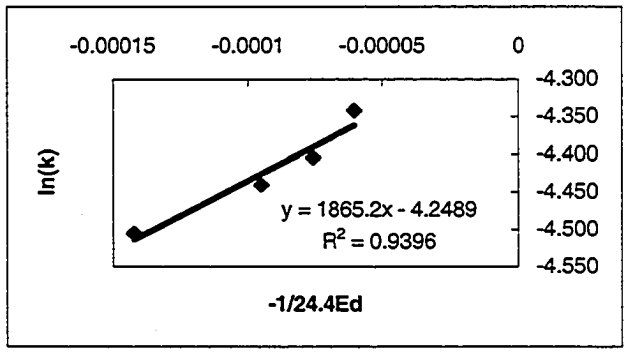


**Figure 3**

## Correlation of NO Conversion in the Presence of Moisture

The following equation has been proposed:

$$[X]/[X]_0 = \exp\{-(E_d - E_i)/\gamma\} \quad (10)$$

The logarithmic form of equation (6) is

$$E_d = \gamma(-\ln([X]/[X]_0)) + E_i \quad (11)$$

Regression analysis of present experimental data yields the values of $\gamma$ and $E_i$, 61 J/L and 45 J/L, respectively (Table 4 & Figure 4).

**Table 4**

| 250 ppm NO/8.3%$O_2$/1%$H_2O$/$N_2$ | | | | |
|---|---|---|---|---|
| | Conversion | | | -ln([X]/[X]$_0$)= |
| Ed | NO% | NOx% | Ed | -ln(1-NO%) |
| 81 | 41.3 | 8.9 | 81 | 0.532 |
| 104 | 57.4 | 11.9 | 104 | 0.853 |
| 116 | 83.4 | 30 | 116 | 1.795 |
| 208 | 89.4 | 40 | 208 | 2.244 |

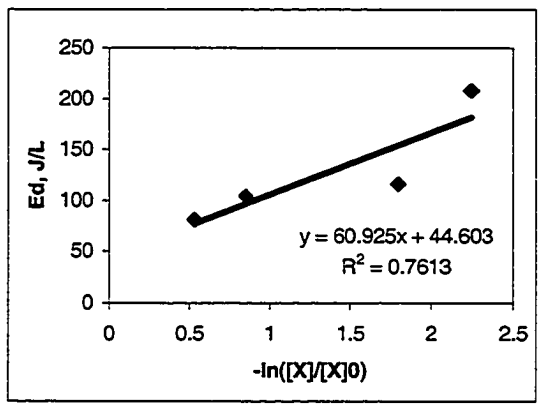


**Figure 4**

Regression analysis of experimental data from an early study (Mclamon 1996) yields the values of $\gamma$ and $E_i$, 133 J/L and 14 J/L, respectively (Table 4 & Figure 4).

**Table 5**

| | | -ln([X]/[X]0) |
|---|---|---|
| NOx% | Ed, J/L | -ln(1-NOx%) |
| 66.5 | 154 | 1.09 |
| 74 | 206 | 1.35 |
| 84.5 | 248 | 1.86 |
| 88 | 304 | 2.12 |

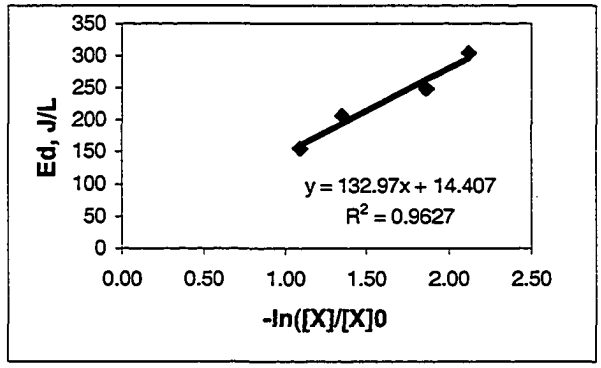


**Figure 4**

**References:**

McLamon C. 1996. Nitrogen oxide decomposition by barrier discharge [dissertation]. Durham (NH):University of New Hampshire. p 87.

Seigneur C, Wrobel J, Constantinou E. 1994. A chemical kinetic mechanism for atmospheric inorganic mercury. Environ Sci Technol 28:1589-97.

# APPENDIX D

## MEASUREMENT OF DIELECTRIC CONSTANTS

The objective of this study is to determine the dielectric constants of barrier materials used for fabricating dielectric barrier discharge reactors. A dielectric constant can not be directly measured. An indirect measurement method is developed and the effects of two parameters on the measurement are investigated. The two parameters are the thickness of the dielectric material and the area of the electrodes used to measure capacitance across the dielectric material.

### Principle of Dielectric Constant Measurement

The dielectric constant of a material, K, is used to quantitatively describe the property of the dielectric material that increases the capacitance between a pair of plates (conductors) as follows:

$$K = C/C_0 \tag{1}$$

where C is the capacitance across the dielectric material, and $C_0$ is the capacitance across the same distance in a vacuum. Since the difference between air and a vacuum is negligible in electrostatics, $C_0$ may be approximated by the capacitance across the same distance of air.

A capacitance meter connected to a pair of parallel plates may be used to measure the capacitances.

$$C_0 = \varepsilon_0 A/d \tag{2}$$
$$C = K\varepsilon_0 A/d \tag{3}$$

where $\varepsilon_0$ is the permitivity of free space, $8.854 \times 10^{-12}$ F/m. A is the area of each conductor, and d is the distance between the two plates. Equation (3) shows that the capacitance is a function of dielectric constant of a dielectric material measured, plate area and plate separation. The reliability of measurement thus depends on meter quality and geometrical factor, A/d for the case of parallel plates.

### Factors Affecting the Measurement

The measured capacitance may need to be corrected to account for edge capacitance and ground capacitance. Edge capacitance is an excess reading due to the perimeter of the plates, and, for equal circular plates which are smaller than the dielectric material, is given by:

$$C_e = P[-0.225 + 0.050K + 0.153 \log(P/t)] \quad (pF) \tag{4}$$

where P is the perimeter of the plates, measured in inches. Ground capacitance is an excess reading due to charge passing to ground, and, for equal circular plates, is given by:

$$C_g = 0.105d^2/h + 0.65t \quad (pF) \tag{5}$$

where h is the height above surrounding grounds. The corrected capacitance then becomes:

$$C_{corr} = C_{meas} - C_e - C_g \tag{6}$$

where $C_{meas}$ is the measured capacitance (Hippel and Robert 1954).

It should be noted that the plate separation d would have a significant effect on capacitance measurement for the case of a thin sample used. Typically, the measured dielectric constant of a thin sheet of material is less than the actual. An increase in thickness of the material leads to the measured value closer to the actual. This difference might result from the existence of space between plate and sample due to incomplete contact. It may be described as follows:

$$1/C_{meas} = 1/C_{air} + 1/C_{actual} \tag{7}$$

Substitution of equations (2) and (3) gives:

$$1/C_{meas} = 1/(\varepsilon_0 A)\,(\,d_{air} + d/K\,) \tag{8}$$

The item $d_{air}$ contributes to the increase in $1/C_{meas}$, i.e., lower $C_{meas}$. It suggests that a greater distance between plates is good to achieving better measurements. Therefore, if a sample of a given dielectric material available is too thin, an indirect measurement may be conducted by using the thin sample together with a thick sample of another material. The capacitance across two dielectric materials in series follows the relation:

$$1/C_{tot} = 1/C_{thin} + 1/C_{thick} \tag{9}$$

where $C_{tot}$ and $C_{thick}$ can be measured individually. $C_{thin}$ may be calculated using equation (9).

**Apparatus for Capacitance Measurement**

The equipment used to measure capacitance includes an Electro Scientific Industries Impedance Meter 253 and a pair of circular aluminum parallel plates (conductors). A series of paired thin disks of aluminum foil with varying diameters are also prepared to allow a study of observed capacitance in relation to electrode diameter. The aluminum foil disks are lightly pasted onto thick sheets of composite mica to provide flatness, strength, and insulation. The thickness of the dielectric samples is measured using a Lufkin micrometer. Figure 1 is the schematic diagram of capacitance measurement.

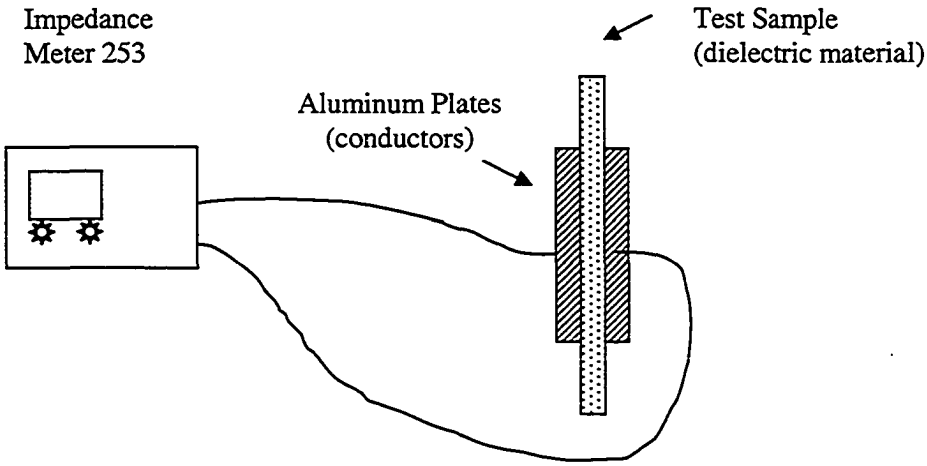


**Figure 1 Schematic Diagram of Capacitance Measurement**

## Dielectric Materials

Several dielectric materials are used in this study to measure their dielectric constants. They are soft glass, composite mica, natural mica (S & J 1998) and quartz (QSI 1998) with different thickness (Table 1).

**Table 1 Thickness of Several Dielectric Materials**

| Dielectric Material | Thick Soft Glass | Thin Soft Glass | Composite Mica | Natural Mica | Quartz |
|---|---|---|---|---|---|
| Thickness (mm) | 4.0 | 3.0 | 0.8 | 0.2 | 4.0 |

## Results of Dielectric Constant Measurement

Large conductors are used to measure the capacitances since the edge effect could be reduced significantly. Dielectric constants are calculated via equation (1): $K = C/C_0$. Presented in Table 2 are the measured dielectric constants of several materials as well as their literature values available.

**Table 2 Dielectric Constants of Several Dielectric Materials**

| Dielectric Material | Thick Soft Glass | Thin Soft Glass | Composite Mica | Natural Mica | Quartz |
|---|---|---|---|---|---|
| Measured K | 6.4 | 6.0 | 2.3 | 5.8 | 3.7 |
| Literature Value | 5-9 (O'Dwyer 1990) | 5-9 (O'Dwyer 1990) | n.a. | 6-7 (S&J 1998) | 3.75 (QSI 1998) |

**References:**

O'Dwyer J. 1990. College physics. 3rd ed. Brooks/Cole Publishing Company. P 476.

QSI (Quartz Scientific, Inc.). 1998. Public release of physical properties of products.

S & J Trading Inc. 1998. Public release of physical properties of products.

Hippel V, Robert A. (ed). 1954. Dielectric materials and applications. MIT Press, Cambridge, MA.